Article title: A simple and quick sensitivity analysis method for methane isotopologues detection with GOSAT-TANSO-FTS

Authors: Edward Malina[1], Jan-Peter Muller[2], David Walton[3]
Affiliations: Imaging Group, Mullard Space Science Laboratory, Department of Space and Climate Physics, University College London, Holmbury St. Mary, Dorking, Surrey, RH5 6NT, UK.[1]
Orcid ids: 0000-0002-1055-4598[1]
Contact e-mail: edward.malina.13@ucl.ac.uk

Preprint statement: This article is a preprint and has not been peer-reviewed, under consideration and submitted to UCL Open: Environment Preprint for open peer review.
DOI: 10.14324/111.444/000019.v2
Preprint first posted online: 13 December 2020
Keywords: Methane, Radiative transfer, GOSAT, Isotopologue, SWIR, Education, Outreach, Climate

12/12/2020

Subject: Revision requests for UCL Open Environment manuscript "A simple and quick sensitivity analysis method for methane isotopologues detection with GOSAT-TANSO-FTS"

Dear Dr Brierley, Professor Dobson and Dr Luo,

Thank you for handling and reviewing this manuscript; please find attached to this cover letter direct comments to the reviews, a marked up version of the manuscript, highlighting changes and a non-marked up version of the proposed new manuscript.

The original review comments are kept in black, our responses are in blue, and changes to the manuscript are in underline blue.

With best regards

Ed Malina

Review 1 – Professor Dobson

This is a welcome review of how satellite observations can be used to differentiate between methane from biogenic and industrial sources from the isotope signatures in infra-red absorption. The study is based mainly on the Japanese GOSAT data and it is a good introduction to students about Radiation Transfer Modelling, but with the proviso that the students are already very familiar with infra-red adsorption and light scattering physics.

Thank you for these positive general comments, we expand further below.

The paper would have much wider appeal if there were explanatory diagrams about the mechanisms of light scattering/adsorption in an introductory section. For example a simple diagram to explain what the GOSAT-TANSO-FTS actually measures would make a large difference to the understanding of the work and give this much more general appeal.

Thank you for this point, in order to address this we have taken the following action.

The original 'Introduction' section has been split into two, part one discusses the global context of measurements of methane and why it is important we do so. Part two 'GOSAT and measuring radiance' provides a brief introduction to the operations of GOSAT-TANSO-FTS with a diagram showing the concept of solar backscatter. The 'Beer-Lambert' law is introduced, in order to give an overview of the physics of absorption.

The data permits detection of $^{13}CH_4$, and the ratio of $^{13}CH_4$ and $^{12}CH_4$ known as $\delta\,^{13}C$. This subject has a lot of acronyms, and an explanatory box listing these would also be very helpful.

We have added a new section (number 8) titled “Glossary” to identify key terms and acronyms. This section includes Table 6, populated by these terms.

Generally the attention to detail about the modelling is clear, but a reader new to the subject would like to know more about the real utility of this approach. For example it would be useful to see if the methodology has been able to pick out geographical regions where the biogenic methane dominates the industrial methane, so a spatial map of $\delta^{13}C$ would be useful.

In order to address this comment we have included a brief section where we apply the data to GOSAT L1B data downloaded from the GOSAT data archive. The following changes have been made.

Section 4.4.3. has been added, describing a method used for matching the simulated spectra with GOSAT-TANSO-FTS L1B data for a short study.

Section 5.4. has been added, indicating the results of the short study proposed in section 4.4.3, with Figure 10 included in this section, generally indicating the challenge of the task with small radiance changes.

Finally some comment about the methane released from methane clathrates should be included in the paper. These may assume increasing importance as the Arctic and Antarctic regions warm and release such methane.
Thank you, we have inserted the following section into the introduction in order to address these comments.

Melting of the permafrost is a topic of particular concern, with the Arctic warming faster than any other part of the Earth. The Arctic, currently a minor source of methane could become a major source over the coming century due to this warming (Nisbet et al., 2019). Methane emissions from the Arctic is a particularly complex issue, with up to 33% of the world’s organic carbon stored within the Arctic permafrost (Schuur et al., 2015), and vast reserves of methane stored in crystalline clathrate structures (Myhre et al., 2016). Yet there is no consensus on how and when these carbon reserves will enter the atmosphere; new data and methods are required to address these uncertainties.

Review 2 – Dr Luo

This paper introduces a quick method to detect the methane isotopologues using Radiative Transfer Models. As described by authors, this is just a first step and the retrieval algorithm needs further development. The authors have also investigated the spectral distribution of the methane, and the potential error sources such as from water vapor and SCIATRAN. Overall, it is a clear and well-organized structure. I would recommend accept after only a few minor corrections listed as follows.

Thank you for your general positive comments.

Page 1 Line 40 :
"the feasibility" should be "the feasibility of"

Thank you, this has been changed.

Page 2 Line 18:
"ethane" should be "methane"

Thank you, however we do mean ethane here. The paper by Aydin et al (2011) used global variations of ethane as a proxy for methane variations.

Page 3 Line 19-21
The abbreviation "GOSAT21-TANSO-FTS" has been defined at Page 1 Line 43-44. Only define the abbreviation at the first time when it is used in the text.

Thank you, this has been changed.

Page 5 Line 16 :
"has significant pedigree " should be "has a significant pedigree"

Thank you, this has been changed.

Page 9 Line 14:
Remove the extra Kuze et al

Thank you, this has been changed.

Page 11 Line 41:
"which take three" should be "which takes three"

Thank you, this has been changed.

Page 14 Line 33 :
would to be?

Thank you, this has been changed to is to.

In addition at this point in the manuscript, we have removed the following section:

"We believe that a study using TCCON data should be a study in its own right, and does not fit in the context of the demonstration of the quick and simple methods we use in this paper.
".

This has been changed to:

This work has been shown in a separate study, indicating that even with the improved SNR of the TCCON instruments, there are still significant challenges with retrievals of methane isotopologues (Malina et al., 2020).

A simple and quick sensitivity analysis method for methane isotopologues detection with GOSAT-TANSO-FTS

Edward Malina[1*], Jan-Peter Muller[1], David Walton[1]
[1]Imaging Group, Mullard Space Science Laboratory, Department of Space and Climate Physics, University College London, Holmbury St. Mary, Dorking, Surrey, RH5 6NT, UK.
** Currently at ESA/ESTEC, Noordwijk, The Netherlands.*

Keywords: Methane; Radiative transfer; GOSAT; Isotopologue; SWIR; Education; Outreach

1. Abstract

Measurements of methane isotopologues can differentiate between different source types, be they biogenic (e.g. marsh lands) or abiogenic (e.g. industry). Global measurements of these isotopologues would greatly benefit the current disconnect between "top-down" (knowledge from Chemistry Transport Models (CTMs) and satellite measurements) and "bottom-up" (in situ measurement inventories) methane measurements. However, current measurements of these isotopologues are limited to a small number of in situ studies and airborne studies. In this paper we investigate the potential for detecting the second most common isotopologue of methane ($^{13}CH_4$) from space using the Japanese Greenhouse Gases Observation Satellite (GOSAT) applying a quick and simple residual radiance analysis technique. The method allows for a rapid analysis of spectral regions, and can be used to teach University students or advanced school students about radiative transfer analysis. Using this method we find limited sensitivity to $^{13}CH_4$, with detections limited to total column methane enhancements of >6%, assuming a desert surface albedo of >0.3.

2. Statement of Robustness

The potential impact of methane and other greenhouse gases (GHGs) on the global environment is recognised at the highest levels of government, shown in the recent signing of the COP21 in Paris. Atmospheric methane is composed of differing isotopic concentrations, with $^{12}CH_4$ and $^{13}CH_4$ representing ~99% of total methane concentration. Previous studies have shown that the ratio of these two main 'isotopologues' can indicate if the measurement is from a biological or non-biological source. Therefore the exploitation of this known ratio using new measurement techniques on current GHG measuring satellites is timely as well as necessary; potentially allowing for source apportionment on a global scale. This paper demonstrates a unique assessment towards determining the feasibility of retrieving the main methane isotopologues concentrations in the Earth's atmosphere, using the nadir-sounding instrument Greenhouse Gases Observing Satellite – Thermal and near Infrared Sensor for Carbon Observations – Fourier Transform Spectrometer (GOSAT-TANSO-FTS). The methods used in this paper are designed so that advanced school students or

early University students can easily apply the methods, which is important in the context of science outreach and citizen engagement.

3. Introduction

3.1. Global context

Formatted: Font color: Auto

Formatted: Heading 3

The impact of methane on the environment and its potential for global warming is well documented (IPCC, 2014). Wuebbles and Hayhoe (2002) state that the increasing levels of methane in the atmosphere significantly affects levels of ozone, water vapour (in the stratosphere), hydroxyl radicals, and numerous other compounds in the atmosphere which result from the oxidation of methane (Bréas et al., 2001). All of these occurrences lead to detrimental effects on the chemistry of the atmosphere (for example the formation of tropospheric ozone, and the depletion of atmospheric methane sinks), as well as the absorption of Infra-red (IR) radiation causing atmospheric heating (Bréas et al., 2001). The total global methane budget is not currently well understood, exemplified by multiple contrasting theories for the stall of the global methane concentration between 2000 and 2006 after a century of increase, and then a subsequent rise from 2014 (Nisbet et al., 2016). Aydin et al. (2011) suggest that the drop in global methane output is due to a reduction in the fossil fuel sources of methane, through observations of global concentrations of ethane, which can be used as a global indicator of anthropogenic methane. However in a completely contrasting view, Kai et al. (2011) assert that the reduction in global methane output is in fact due to a reduction in microbial methane from the northern hemisphere; while Mcnorton et al. (2016); Rigby et al. (2012); Turner et al. (2017) suggest that fluctuating hydroxyl radical concentrations is a potential cause of global methane variations. It is therefore important to understand how and where methane is released, and to develop more sophisticated methods of methane detection that will allow for greater understanding of the processes behind methane generation, and how they will affect the global environment.

Methane gas may be formed through multiple natural and anthropogenic processes, including microorganism decomposition of cellulose in sediments under reducing conditions, the breakdown of gas hydrates including clathrates, and thawing permafrost in arctic and subarctic conditions. Melting of the permafrost is a topic of particular concern, with the Arctic warming faster than any other part of the Earth. The Arctic, currently a minor source of methane, could become a major source over the coming century due to warming (Nisbet et al., 2019). Methane emissions from the Arctic is a particularly complex issue, with up to 33% of the world's organic carbon stored within the Arctic permafrost (Schuur et al., 2015), and vast reserves of methane stored in crystalline clathrate structures (Myhre et al., 2016). Yet there is no consensus on how and when these carbon reserves will enter the atmosphere; new data and methods are required to address these uncertainties. Other important processes include, geological processes in the Earth's crust reaching the surface through features such as mud volcanoes or soil exhalation, catagenesis, metamorphism of coal and dispersed organic matter, as well as during petroleum maturation. Anthropogenic sources such as industry bi-products (e.g. leaks from gas plants) and agriculture (e.g. livestock or rice paddy fields) must also be considered as highly significant (Archer et al., 2009; Bréas et al., 2001). Industrial bi-products imply that fossil fuels can be detected by the type of

methane gas given off by their formation and exploitation (Kort et al., 2014; Rella et al., 2013). Towards this end many satellite missions have been focused on trying to measure fossil fuel sources by their methane emissions, including the Japanese Greenhouse Gases Observation Satellite (Kuze et al., 2009; Turner et al., 2015), which was designed specifically for this purpose.

Atmospheric methane consists of a number of different isotopologues (molecules that vary according to their isotopic composition), the main four being $^{12}CH_4$ accounting for roughly 98% of atmospheric methane, $^{13}CH_4$ making up roughly 1.1% of atmospheric methane and CH_3D, present in very small concentrations (roughly 0.06%), with all the other isotopologues present in tiny amounts. The ability to distinguish spectroscopically between the isotopologues of methane can potentially allow the determination of the nature of the source of methane emissions (either biogenic, thermogenic or abiogenic), by taking the ratio of the concentration of $^{12}CH_4$ and $^{13}CH_4$ isotopologues (Etiope and Ciccioli, 2009; Nisbet et al., 2016; Schwietzke et al., 2016). This method has been used effectively for *in situ* terrestrial studies previously and it is this relationship that is the focus of this study. Currently there are limited global measurements of separated methane isotopologues, the majority of measurement sites falling under the National Oceanic and Atmospheric Administration (NOAA) *(www.esrl.noaa.gov/gmd/ccgg/trends_ch4/)* as well as a small number of other independent organisations (Nisbet et al., 2016). Based on this limited spread of measurement sites, the existence of a satellite instrument that can differentiate between methane isotopologues would expand the global knowledge of methane distributions. It has been achieved in the upper troposphere and lower stratosphere with solar occultation limb viewing instruments (Buzan et al., 2016; Irion et al., 1996), and is hoped to be achieved with dedicated potential future instruments (Weidmann et al., 2017).

3.2. GOSAT and measuring radiance

GOSAT-TANSO-FTS measures solar backscatter radiance, such that solar irradiance passes through the atmosphere, is reflected off the surface of the Earth, and passes back through the atmosphere where GOSAT-TANSO-FTS measures the radiance (i.e light magnitude). As this light passes through the atmosphere, it is absorbed at specific frequencies determined by the gases the light passes through. Absorbing this light causing the atoms of the specific gas to change energy levels, these jumps are characterised by spectral lines of finite width. Knowledge of the position of spectral lines for methane (or other gases), means it is possible to calculate how much energy was absorbed by these gases, and therefore how much of this gas is in the path the light travelled through the atmosphere (Tennyson, 2005).

The radiance received at the instrument due to absorption in the Sun-Earth-GOSAT light path is determined by the following equation, known as the 'Beer-Lambert' law (Swinehart, 1962).

$$I(\lambda) = I_0(\lambda)e^{-\sigma C(\lambda)x}. \quad (1)$$

Formatted: Heading 3, Outline numbered + Level: 2 + Numbering Style: 1, 2, 3, … + Start at: 1 + Alignment: Left + Aligned at: 0" + Indent at: 0.5"

Formatted: Centered

Where I refers to the intensity of the incident radiation at wavelength λ, given an optical path of thickness x, and I_0 is the intensity of the initial incident light or radiation, C is the density of the light path (or concentration of molecules) and σ is the absorption cross section (or the likelihood of absorption by a given molecule).

A representation of the standard operations of GOSAT is identified in Figure 1, where $I(\lambda)$ is what is received at GOSAT-TANSO-FTS, and σ in the case of this paper refers to methane spectral lines. However, Equation 1 is not directly applicable to what GOSAT-TANSO-FTS measures, since Equation 1 assumes a constant density across the light path. The density of the atmosphere (C) is not constant, meaning Equation 1 must be separately applied for multiple atmospheric layers, in order to accurately measure absorption over a long distance. Larger particles in the atmosphere (e.g. aerosols) can scatter radiation away from the main light path, meaning the difference between I and I_0 is not purely due to absorption. These absorption and scattering properties vary depending on what region of the electromagnetic spectrum is observed. Meaning that prior to attempting to measure the concentration of trace gases in the atmosphere, the most optimum portion of the electromagnetic spectrum must be identified.

The aim of this paper is to identify spectral regions where the main methane isotopologues ($^{12}CH_4$ and $^{13}CH_4$) can be detected with the existing GOSAT-TANSO-FTS. Such studies are typically performed using the Information Content (IC) analysis method described in (Rodgers, 2000), examples of which are also reported in (Herbin et al., 2013; Malina et al., 2018; Yoshida et al., 2011). IC analysis is a powerful tool, but has several significant challenges associated with its use. Firstly, on its own the IC analysis cannot be used to estimate atmospheric trace gas concentration since it is an analysis method and not a full retrieval algorithm (such as (Parker et al., 2011; Schepers et al., 2012; Yoshida et al., 2011)). Secondly, there is a substantial step in effort required to convert the IC analysis method into a retrieval tool capable of trace gas estimation (in terms of computation, analysis methods etc). The current algorithms used to produce trace gas concentrations from instruments such as GOSAT-TANSO-FTS or the recently launched Sentinel-5P/Tropospheric Monitoring Instrument (TROPOMI) are the results of multi-year efforts, built on experience with older instruments (e.g. the SCanning Imaging Absorption SpectroMeter for Atmospheric CHartographY (SCIAMACHY) or similar). Therefore, new research into satellite trace gas retrieval must rely on one of these well-established algorithms, or embark on an expensive development program.

In this paper we propose to use a simple residual radiance analysis technique to identify the suitability of GOSAT-TANSO-FTS for detecting $^{13}CH_4$, and the ratio of $^{13}CH_4$ and $^{12}CH_4$ known as $\delta^{13}C$, which is based on the IC analysis method. Although the residual radiance analysis technique is not as sophisticated as the Optimal Estimation Method (OEM) of (Rodgers, 2000), it remains relevant in the context of trace gas detection/retrieval for its ease of use, and quick applicability. Fundamentally, the residual radiance technique is an excellent starting point for getting familiar with the OEM, and could be an important aspect of advanced school students or University students.

This paper is structured as follows:

- Section 1-3 – Abstract and Introduction.
- Section 4 – Describes the tools and methods used in this study.
- Section 5 – Outlines the results.

Deleted: GOSAT Thermal and Near Infrared Sensor for carbon Observation Fourier Transform Spectrometer (

Deleted:)

Deleted:

Deleted: 2

Deleted: 3

- Section 6 – Discusses the results and methods from sections 2 and 3.
- Section 7 – Concludes the findings.

4. Experimental Design and Starting Assumptions

4.1. Methane Source Isotopologue Composition

The isotopic composition of atmospheric background methane and methane sources has been studied at some length (Chanton, 2005; Nisbet et al., 2016; Rigby et al., 2012; Röckmann et al., 2011), especially the four key isotopologues $^{12}CH_4$, $^{13}CH_4$, $^{12}CH_3D$ and $^{13}CH_3D$. These papers effectively describe how the ratios of methane isotopologues (often referred to as "δ" values) can be used to identify the nature of the source. Normally the metrics $\delta^{13}C$ and δD are used to define the ratio of isotopologues at the source. The $\delta^{13}C$ ratio is defined as:

$$\boldsymbol{\delta^{13}C = \left(\frac{\left(\frac{13C}{12C}\right)sample}{\left(\frac{13C}{12C}\right)standard} - 1\right) \times 1000‰} \quad \textbf{(2)}$$

$\delta^{13}C$ is generated by taking the ratio C13:C12 of the gas sample under investigation, and dividing it by a base ratio (or standard ratio) taken from the established literature known as the Vienna Pee Dee Belemnite, which then determines how far the sample in question deviates from the standard (Craig, 1957). A large negative value indicates that the sample is depleted in C13. Large negative values tend to be associated with biogenic sources of methane, while values closer to 0 are largely from industrial sources.
The methane to deuterium based methane ratio is known as δD is calculated using a similar method to the calculation of $\delta^{13}C$, this ratio divided by an established base ratio taken from the established literature known as the Vienna Standard Ocean Water. However as stated earlier, deuterium based methane is very rare in the atmosphere, and we decided early on to focus solely on $^{13}CH_4$ as opposed to CH_3D.

The main reason for the depletion of the heavier isotopologues in biogenic sources is due to the observation that microorganism formation of methane tends to discriminate against ^{13}C due to Kinetic Isotope Effects (KIEs), accounting for the low $\delta^{13}C$ values. Different forms of microorganisms will have different rates of KIEs, thus changing the $\delta^{13}C$ values with respect to the exact source, however the precise nature of these KIEs is still poorly understood. In addition, specific plants will vary in their ^{13}C signature due to differing photosynthetic enzymes, partially accounting for the range in $\delta^{13}C$ values noted in microbial sources (Schweizer et al., 1999; Whiticar, 1999).

4.2. Radiative Transfer Models – SCIATRAN and ORFM

Radiative Transfer Models (RTMs) are a fundamental aspect of this work, and a key aspect of this study is focused on providing trace gas investigation methods for independent research. It is difficult to perform trace gas research without the use of an

Deleted: 4
Deleted: 5
Deleted:
Deleted: 1

RTM. Developing an RTM from scratch for this project fulfils neither of the quick or simple goals, and we therefore decided to use an open source RTM.

In this study we use the SCIATRAN (Rozanov et al., 2014) RTM, developed by the SCIATRAN working group at the Institute of Environmental Physics and the University of Bremen, available from http://www.iup.uni-bremen.de/sciatran/index.html. SCIATRAN is an RTM capable of solving the radiative transfer equation using multiple numerical methods. SCIATRAN can simulate satellite solar backscatter radiative transfer in both clear-sky and aerosol loaded conditions. SCIATRAN is versatile and can simulate numerous atmospheric effects such as clouds, fluorescence, advanced bidirectional reflectance distribution functions and others for multiple geometry types. For this study the simulations from SCIATRAN are run at a spectral resolution of 0.01 cm^{-1} and are convolved with a TANSO-FTS type Gaussian Instrument Line Shape Function (ILSF) of 0.27 cm^{-1} full width half max (Kuze et al., 2009). All simulations include multiple scattering effects, where all Mie scattering effects assume spherical particles. SCIATRAN has a significant pedigree with previous instruments such as SCIAMACHY, and has been previously used in studies relating to GOSAT previously e.g. (Reuter et al., 2012).

SCIATRAN uses a climatological database derived from a 2D CTM described in (Sinnhuber et al., 2009). All gases, temperatures and pressures are provided in the altitude range 1-95 km for 10° latitudinal bins for all months in a given year. The isotopologue profiles in SCIATRAN are identical to the CH_4 profile included in the simulated atmosphere. The difference in abundance between CH_4 and $^{12/13}CH_4$ is accounted for in the HITRAN2016 database, which scales the isotopologue line strengths by abundance figures provided by (Biévre et al., 1984). The advantage of this method is that the complexity of adding an additional trace gas profile to the forward model is reduced, the disadvantage is that this scaling assumes that this abundance ratio is true for the whole globe (which is unlikely to be true).

Deleted: chemistry transport model (

Deleted:)

Scattering is considered in SCIATRAN, both through Rayleigh scattering and aerosol induced Mie scattering. Rayleigh scattering is not considered in this study as it is minor in the SWIR. For aerosol related scattering SCIATRAN draws upon the LOWTRAN database (Kneizys et al., 1988), which can simulate multiple different aerosol types for different layers of the atmosphere. In this study we assume the standard SCIATRAN/LOWTRAN settings for aerosol loading in SCIATRAN.

The spectral line database used in this study is HITRAN2016 (Gordon et al., 2017). HITRAN2016 builds upon the HITRAN2012 database, but includes an increase in the number of assigned $^{13}CH_4$ spectral lines, with Brown et al (Brown et al., 2013) indicating a significant jump in the number of and accuracy of $^{13}CH_4$ (and $^{12}CH_4$) spectral lines in comparison to the previous HITRAN iteration (HITRAN 2008; (Rothman et al., 2009)). HITRAN2016 includes data from recent studies such as (Starikova et al., 2016), which contain numerous additional line assignments in the spectral range of GOSAT-TANSO-FTS band 2. However it is not suggested that there are any updates to the $^{13}CH_4$ line lists in band 4 of TANSO-FTS.

In addition to SCIATRAN, we also employ the Oxford Reference Forward Model (ORFM; (Dudhia, 2017)), developed at the University of Oxford, and available at http://eodg.atm.ox.ac.uk/RFM/. We do not use the ORFM in the residual radiance

calculations described in the sections below, but rather to simulate atmospheric transmittance and optical depth. This is because the ORFM allows for quick and easy transmission (and absorption) calculations in all of the wavelengths of interest in this study. ORFM is not used for the residual radiance study since a 'sun' is not included in the radiance calculations, and scattering is not included.

4.3. GOSAT-TANSO-FTS

The Japanese Aerospace Exploration Agency (JAXA) launched GOSAT in 2009; GOSAT was the first satellite specifically designed to measure GHG emissions around the globe. The GOSAT project is a joint effort between the Ministry of the Environment (MOE), the National Institute for Environmental Studies (NIES), and JAXA (Kuze et al., 2009; Yokota et al., 2009). GOSAT originally had a 6 year lifespan, but has since been extended. Its replacement was GOSAT-2 was launched in October of 2018, but data is as yet unavailable.

The key instrument on GOSAT is the TANSO-FTS, which measures the radiance of sunlight reflected from the Earth's surface through the atmosphere in three separate bands: the main band of interest in this study is band 2 which measures radiance in the wavenumber range 5814-6410 cm^{-1} (1.56-1.72 μm), with a sampling interval of 0.2 cm^{-1}. GOSAT-TANSO-FTS has a fourth band that measures emissions spectra in the Thermal Infrared (TIR) between 699 – 1799 cm^{-1} (5.56-14.3 μm) (Kuze et al., 2009; Yokota et al., 2009).

GOSAT has a history of providing reliable estimates of the global distributions of methane and carbon dioxide (Parker et al., 2015, 2016; Schepers et al., 2012; Yoshida et al., 2013) since its launch. With its high spectral resolution and high SNR, GOSAT was judged to be a good candidate for detecting methane isotopologues, and therefore prompted this investigation. There are other instruments for measuring methane isotopologues from orbit e.g. SCIAMACHY and TROPOMI. SCIAMACHY has a significantly lower spectral resolution (1.5 cm^{-1}) and has been found to have poor single sounding precision. Buchwitz et al (Buchwitz et al., 2017) state that SCIAMACHY registers a maximum single sounding measurement precision of 30 ppbv, which is unlikely to be sufficient for the retrieval of $^{13}CH_4$, where the total column concentration of $^{13}CH_4$ is roughly 20 ppbv. The recently launched TROPOMI is a possible candidate for methane isotopologues measurements, TROPOMI contains a push-broom spectrometer and sacrifices spectral resolution (0.45 cm^{-1}) for much increased SNR. TROPOMI is likely to be investigated in the future for methane isotopologue detection.

4.4. Study Structure and Methods

The following subsection discusses the structure of the research study. The key aims are to show the following under realistic atmospheric conditions:

a) The optimal regions in bands 2 and 4 of the GOSAT-TANSO-FTS for $^{13}CH_4$ detection.
b) Measurable changes in $^{13}CH_4$ spectral lines over and above the background contaminating gases, and GOSAT-TANSO-FTS instrument noise.

c) The effects of background contaminate gases on any measurable changes.

4.4.1. Spectral Region Identification

The first step of this study is to make an initial assessment as to where the least contaminated regions for $^{13}CH_4$ may be found in the SWIR and TIR. The strongest absorption lines for methane in the SWIR are present within the wavebands at 1.6 μm and 2.3 μm (Brown et al., 2013). However the GOSAT-TANSO-FTS sensitivity to methane is limited to 1.6 μm, in band 2. In the TIR region there is a broadband methane absorption feature at 7.7 μm, which is covered by band 4 of TANSO-FTS. We therefore set-up a simulation scenario with ORFM in order to pick out the maximum absorption points for the $^{13}CH_4$, outlined in Table 1.

The atmospheric model used in this assessment provides a high number of vertical levels and gas concentrations at more recent magnitudes (2002) than the standard mid-latitude model atmospheres (which were designed in the 1970's), and was originally designed to aid in Michelson Interferometer for Passive Atmospheric Sounding (MIPAS) retrievals (Remedios et al., 2007). An example of the atmospheric profiles of three gases from this model is shown in Figure 2.

Deleted: FASCODE

Deleted: 1

GOSAT-TANSO-FTS measures the column average density of methane and carbon dioxide (XCH_4, XCO_2); therefore, using the pressure profiles captured in the UoL MIPAS profile, the column-averaged densities can be calculated.

The strongest absorption regions of the methane isotopologues are then investigated in order to gain further insight into the influence of contaminant gases on the isotopologues. The ORFM includes the options to simulate absorption as well as radiance, thus giving some insight into the presence of spectral lines of interest. The conditions required to calculate a typical $^{13}CH_4$ atmospheric absorption profile are specified in Table 1.

4.4.2. Detecting Changes in $^{13}CH_4$ Signal

Background simulated radiance values (containing radiance from the main contaminating gases,) are subtracted from the radiances generated from a scenario with elevated concentrations of methane. If this calculated residual difference is greater than the noise radiance known as the Noise Equivalent Delta Radiance (NEDL) then it suggests that GOSAT-TANSO-FTS could detect this change in methane concentration. This is known as the residual radiance technique, and has been demonstrated by both Roberts et al and Leifer et al (Leifer et al., 2006; Roberts et al., 2010) as an effective technique for assessing whether changes in concentrations of trace gases can be detected. Roberts et al (Roberts et al., 2010) states that spectral residuals are often the first step in full atmospheric inversions. Following the method proposed by (Roberts et al., 2010), the residual radiance technique is used to determine the atmospheric conditions when isotopologue retrieval may be possible. The key question to answer is which combination(s) of methane concentration, water vapour concentration and

surface reflectance allow for a residual radiance greater than the instrumental noise. This can be determined from the equation below.

$$F_d = |L_b(A, \lambda_m) - L_e(A, \lambda_m)| - NEDL, \quad (3)$$

where F_d is the detection factor, where any value above 0 suggests that some signal is detectable above the noise limit, and therefore constitutes a detection. L_b is the background radiance at the wavelength of the maximum radiance λ_m given reflectance A, L_e is the atmospheric radiance with elevated methane concentrations (see Table 3) at the wavelength of the maximum radiance λ_m given reflectance A and NEDL.

Typically NEDL can be calculated from knowledge of instrument parameters (dark current etc), however these parameters are often kept secret by instrument manufacturers. According to the GOSAT-TANSO-FTS instrument manufacturers at JAXA the GOSAT-TANSO-FTS L1B product (interferograms (L1A data) are converted into radiance spectra via a Fourier transform, including some data screening routines). They contain two separate elements: real spectra (equivalent to the radiance spectra of interest in trace gas retrieval), and imaginary spectra which are equivalent to noise from FTS theory. The implication of this is that the noise from the spectrum of a particular retrieval can be extracted from the L1B spectra. Therefore, we generate a relationship where the noise profile of GOSAT-TANSO-FTS is estimated given a radiance output from real spectra. The steps for generating this profile are as follows: Extract the real and imaginary spectra from several L1B data GOSAT-TANSO-FTS band 2 products, in order to get variation in radiance output based on the location and surface characteristics of the retrieval. Calculate the Root Mean Square (RMS) of the off-band imaginary spectrum radiance (where off band is the region where the Indium Gallium Arsenide detector is not sensitive to the incident radiation due to an optical band pass filter present in the instrument). This is equivalent to the inherent instrument noise, and the RMS of the on-band (which is where the detector is sensitive to measured radiance) real spectrum for multiple retrievals. This builds up a profile of how instrument noise varies with received radiance at the detector (dominated by shot noise). The square of the RMS imagery spectrum radiance values are then plotted against the RMS of the real spectrum radiance values; this builds up a profile of how the noise is dependent on the spectral radiance, as well as highlighting what the basic instrument noise is. This allows for a mathematical relationship to be generated, meaning that for any given particular retrieval radiance, a specific noise value can be attributed to it. Using a random selection of 400 GOSAT L1b spectra downloaded from the GOSAT Data Archive Service (https://data2.gosat.nies.go.jp/index_en.html), the following relationship was calculated.

$$\text{NEDL} = \sqrt{(1.76e^{-8}\text{L} + 1.358e^{-11})} \times C, \quad (4)$$

where, L is the received radiance (in W/cm^2/str/cm^{-1}) and C is a conversion factor from internal GOSAT units into radiance units. The value of C is available on the GOSAT data archive website in the TANSO-FTS Radiometric Conversion for Band 1-3 document (https://data2.gosat.nies.go.jp/doc/document.html#Document). In this study the NEDL is assumed to be a constant value over the whole spectral range, and we assume that the GOSAT spectra are captured under high gain conditions.

Deleted: 2

Deleted: 3

Equation 3 is based on using individual measurements, which will most likely suffer significantly from noise levels. However as suggested by (Roberts et al., 2010) the NEDL can be reduced by averaging multiple spectral measurements focusing on the spectral positions with the most $^{13}CH_4$ information. In such a case the NEDL reduces with √n, where n is the number of spectral sampling points, described by Equation 5 (modified from (Roberts et al., 2010)), below.

$$F_d = \frac{\sum_{\lambda=b}^{\lambda=a}(L_b(A,\lambda_m) - L_e(A,\lambda_m))}{n} - \frac{NEDL}{\sqrt{n}}, \quad (5)$$

where Fd is the detection factor over an averaged number of spectral bands, n is the number of spectral bands for combination, between wavelengths a and b. In the normal operation of GOSAT there is no oversampling of measurement points, until the satellite returns to the same orbital path (i.e. only one spectrum is captured per sample point). In this case the method proposed in Equation 5 cannot be used, since repeat measurements are captured under different conditions. However, Kuze et al. (2012) describe non-standard operational modes, one of which includes 3 repeat measurements of the same point for "sun glint and limited calibration and validation site observations". Although not all GOSAT data will be captured in this way, for simulation purposes, it is justified to investigate the effects of averaging 3 concurrently captured spectra. Indeed, GOSAT has a 'targeted observations' mode, where registered researchers can request observations of specific sites, implying that a large number of concurrently captured spectra could be obtained with this method. The exact details of this mode are not published, and are therefore not modelled in this study. Note that the method described in Equation (5) assumes that errors between spectral points are uncorrelated.

The sensitivity of any $^{12}CH_4$ and $^{13}CH_4$ absorption bands to interfering trace gases and different reflectance conditions must also be considered; the methane absorption windows in the SWIR are typically heavily influenced by water vapour, and therefore any absorption by $^{13}CH_4$ is likely to be affected. The influence of water vapour on specific $^{13}CH_4$ absorption peaks can be determined from the simple ratio factor as described below (modified from (Roberts et al., 2010)).

$$S_f = \frac{\frac{\sum_{\lambda=b}^{\lambda=a} L_{res}(W_s,A)}{n}}{\frac{\sum_{\lambda=b}^{\lambda=a} L_{res}(W_e,A)}{n}}. \quad (6)$$

Where S_f is the sensitivity factor, $L_{res}(W_s,A)$ is the residual radiance between background and elevated methane conditions at standard atmospheric conditions between wavelengths, a and b, $L_{res}(W_e,A)$ is the residual radiance between background and elevated methane conditions with elevated water vapour concentrations between the wavelengths, a and b, and n is the number of spectral measurements considered. Note that this method applies to any desired target and interfering species.

It is important to define appropriate atmospheric scenarios in order to determine feasible detection factors, with the key factors being methane concentration in the atmospheric profile and surface reflectance. Numerous total column retrieval methods

Deleted: 2

Deleted: 4

Deleted: 4

Deleted: 4

Deleted: Kuze et al

Deleted: (

Deleted: .,

Deleted: (Kuze et al., 2012).

Deleted: 4

Deleted: 5

are based on the 'scale' method, where the total column concentration is scaled rather than individual atmospheric layer concentrations modified. Therefore, a range of total column scale factors on which to calculate residuals are specified, appropriate to real world scenarios. The maximum total column XCH_4 values observed from GOSAT tend to be roughly 1900 ppb (Parker et al., 2016), equating to a column scaling of 10% (w.r.t to the MIPAS profile). Very large methane values (>1900 ppb) have been observed by GOSAT in fire affected regions (Parker et al., 2016), suggesting that although >1900 ppb values are possible, they will be found in unique circumstances.

The second key factor, reflectance, can be determined using the online database created by UCL and Noveltis under contract to ESA called "A surface reflectance Database for ESA's earth observation Missions (ADAM)" available at http://adam.noveltis.com/ (Muller et al., 2013). ADAM predicts that the expected Earth surface reflectance values at 1600 nm range from 0.1 for densely vegetated areas, to 0.6 for desert regions (e.g. in the USA or the Sahara).

Based on this range of values, a series of simulation conditions and scenarios were generated as specified in Table 2.

4.4.3. Applying to GOSAT-TANSO-FTS L1B Spectra

The final step in this process is to determine whether or not the changes shown in the results from section 4.4.2 are observable in real L1B spectra. Towards that end, GOSAT L1B spectra were downloaded from the GOSAT Data Archive Service (https://data2.gosat.nies.go.jp/index_en.html), and compared against synthetic spectra, in order to determine what levels of $^{13}CH_4$ variation can be expected over real scenes as opposed to synthetic scenes. Unlike in section 4.4.2, direct comparisons of L1B spectra and synthetic spectra are not quite as simple, since all L1B spectra are captured under a wide range of atmospheric, surface reflectance and instrument geometry conditions. But close conditions are required in order to make any comparisons valid. Therefore, we matched the conditions in real spectra as closely as possibly by 1) Using solar zenith angles and instrument angles identified in the L1B data. 2) Using the geolocation of data capture to inform as to which UoL MIPAS model atmosphere to use. 3) Identify surface reflectance values by fitting reflectance values in 0.001 steps linearly to the synthetic spectra sections until the RMSE difference between the synthetic spectra and the L1B spectra were at a minimum. 4) Convolved the synthetic spectra with the GOSAT instrument line shape model available on the data archive service, and resampled to a 0.2 cm^{-1} grid using a 'Matlab' spline interpolation function. 5) Applied a linear shift to the x axis of the L1B spectra, since the wavenumber axis on TANSO-FTS is variable. The magnitude of the linear shift is defined by wavelength differences between large spectral peaks found in both simulated and measured spectra.

Based on these conditions, direct comparisons between synthetic spectra and L1B spectra were made over known regions of $^{13}CH_4$ activity in the SWIR spectrum. Several hundred L1B data points from June in 2016 were used in order to provide a wide range of atmospheric and surface conditions.

5. Results

5.1. Absorption Assessment

5.1.1. SWIR

Using the atmospheric conditions specified in Table 1, ORFM was used to focus on the 1600-1700nm region. Figure 3 indicates that it will be challenging to resolve $^{13}CH_4$ absorption lines in this spectral region, suggesting that pinpointing $^{13}CH_4$ absorption above background gases will be difficult. The strongest/most dense $^{13}CH_4$ lines appear to be at 1658-1659nm and 1670-1671nm. Focusing on these two spectral regions, the optical depth is explored to determine the effect of background absorbers at these specific wavelengths. Figure 4 makes clear that both of the $^{13}CH_4$ spectral regions indicated have similar optical depth values to those of all of the remaining gases, implying that the majority of absorption in these spectral regions is due to $^{13}CH_4$. However, the spectral line in the 1658-1659nm wavelength range clearly shows the least interference from background contaminating gases, therefore suggesting that it is more suited for retrieval. In spite of this, it is obvious that the optical depth of the $^{13}CH_4$ lines in this region is very low, and it will therefore be challenging to detect any changes to $^{13}CH_4$ in this wavelength range.

5.1.2. TIR

Focusing on the TIR band of GOSAT, we perform a repeat analysis of 4.1.1. Comparing the strength of $^{13}CH_4$ absorption in the TANSO-FTS TIR wavelength range shown in Figure 5 against that in the SWIR shows a number of striking differences, primarily in the magnitude of the absorption. With the strongest of the $^{13}CH_4$ TIR lines having absorption strengths x40 of their SWIR equivalents. Despite this, background interference is still strong, dominated by water vapour continuum absorption. We now focus on the optical depth of two regions, the 7700-7800 nm region due to the strength of $^{13}CH_4$ absorption in this region, and the 8050-8150 nm range due to the lower background absorbance.

The optical depth survey shown in Figure 6 demonstrates magnitudes far in excess of the SWIR optical depth in Figure 4 (especially Figure 6(a), where the atmosphere is opaque), but as shown in Figures 5 and 6, the background interference on the $^{13}CH_4$ signal is significant, with only minor impacts from the $^{13}CH_4$ spectral lines. This leaves us with the unenviable position of small optical depth but low background interference in the SWIR, and high optical depth but high levels of interference in the TIR.

Formatted: No bullets or numbering

Formatted: Heading 4

Deleted: 2

Deleted: 3

Deleted: 4

Deleted: 5

Deleted: 3

Deleted: 5

Deleted: 4

Deleted: 5

Figure 6 suggests that $^{12}CH_4$ and other background gases will dominate the residual radiance method for the TIR. Therefore for this reason, and that measurements in the TIR are often more uncertain than SWIR measurements, exemplified in multiple studies (Holl et al., 2016; Ohyama et al., 2013, 2017), we decided to focus on the SWIR in this study. In addition it has been shown that the SNR on the methane absorption regions in GOSAT are significantly lower than in the SWIR (Holl et al., 2016; Zou et al., 2016), suggesting that the TIR is not ideal for methane retrieval with GOSAT. TIR instruments are heavily based on measuring thermal contrast between atmospheric layers, and because of the lack of such contrast in the lower troposphere, therefore have limited sensitivity near the surface (Clerbaux et al., 2009; Worden et al., 2015). This suggests that measurements in the SWIR are far more likely to capture methane fractionation at the surface than in the TIR. There are cases with global scenes with high thermal contrast, which will allow for sensitivity to the surface for TIR instruments, however we believe that the low SNR of TANSO-FTS band 4 is the more important issue, as opposed to surface sensitivity.

5.2. $^{13}CH_4$ Detectability under Standard Conditions

Based on the simulation conditions specified in Table 2, consideration is given as to whether or not the individual peaks highlighted in Figure 4 will exceed the NEDL. Figures 5 and 8 show example results for two different surface albedos, for all the proposed methane concentration levels.

The results in Figures 7 and 8 suggest that detecting changes in concentration of $^{13}CH_4$ using individual peaks is unlikely to succeed, with only the highest methane concentrations at the highest albedo levels giving a positive detection and all other residual radiance calculations falling below the NEDL line. However, if we assume the GOSAT sampling pattern which takes three concurrent measurements of the same area (Kuze et al., 2012), by applying Equation 5, and using the mean of $^{13}CH_4$ residual radiance peaks, the NEDL is reduced by $\sqrt{3}$. These are summarised in Table 3.

Considering the results outlined in Table 3 it is clear that the feasibility of detecting any change in $^{13}CH_4$ concentration above the NEDL is going to be difficult. The results indicate that the minimum requirements for measuring $^{13}CH_4$ concentration with any certainty are a methane source of at least 10% higher concentration than background total column value, with a high surface albedo of 0.3. Although such a combination of conditions is possible, it would likely be limited to wildfire regions such as (Parker et al., 2016). Note that the detection factors between the two regions of interest are very similar.

We note in section 3.2 that HITRAN2016 includes an intensity adjustment for methane isotopologues that accounts for natural atmospheric abundance. We now investigate if the detection factors indicated in Table 3 change, if we assume the standard $\delta^{13}C$ value is -70‰ as opposed to 0‰. To achieve this, we modified the isotopologues intensity in HITRAN2016, by assuming Vienna Pee Dee Belemnite is 0.0010326 as opposed to

Deleted: 5

Deleted: 3

Deleted: 6

Deleted: 7

Deleted: 6

Deleted: 7

Deleted: 4

0.0011031. Then we reran the scenarios shown in Table 2; the results for the albedo = 0.3 case are shown in Figure 9,

Figure 9 is interesting because it shows that the $^{13}CH_4$ peak at 1658.6 nm is highly sensitive to changes in the assumed $\delta^{13}C$ value, to the point where changes of the methane column concentration has practically no impact on the residual radiance. While the spectral lines at 1670.4 is not as sensitive to the change in $\delta^{13}C$ value, and as indicated in Table 4, actually shows an increase in the magnitude of the detection factors.

The HITRAN2016 database suggests that the $^{13}CH_4$ spectral lines in the 1670.2-1670.6 nm are made up of a number of different transitions, which exhibit a range of lower state energy values. A number of which are of similar magnitude to those for the main methane isotopologue $^{12}CH_4$. While the lower state energy levels for $^{12}CH_4$ are significantly larger than those for the $^{13}CH_4$ lines in the 1658 – 1659 nm range, which explains this difference in reactions to changes in the standard $\delta^{13}C$ values.

In addition to the simulations for the $\delta^{13}C$ values of 0‰ and -70‰, we also performed an analysis for $\delta^{13}C$ values of -35‰. Based on the detection factors for the range of $\delta^{13}C$ value shown in this study, we can plot these variables and determine the conditions where GOSAT can detect differences in $\delta^{13}C$ values.

Based on the detection values indicated in Tables 3, and 4, and given similar results from an analysis of $\delta^{13}C$ values of -35‰. We can plot a relationship between the detection values and the surface albedo for a given $\delta^{13}C$ value.

Figure 10 is interesting since it shows that the 1658 nm band has more sensitivity to changes in surface reflectance, and total column methane concentration than the 1670 nm band. But only in the case where $\delta^{13}C$ is assumed to be equal to zero. For the other $\delta^{13}C$ cases shown in Figure 10, there are no examples where the detection factor is greater than 0. For the 1670 nm band, although the detection factors are lower in magnitude, the sensitivity to changes in the $\delta^{13}C$ are minor. These results imply (focusing on the 1670 nm band), that given a significant enhancement in the total methane column, and a high enough surface reflectance, it may be possible to detect changes in the $\delta^{13}C$ of the measurement. Since the detection factor can be related back to a total methane column value, $\delta^{13}C$ values could be directly estimated. Assuming some knowledge of $^{12}CH_4$. Figure 10 suggests that the lowest possible surface albedo of 0.35, requires an enormous methane enhancement of 8% in order to achieve a detection of $^{!3}CH_4$, while the highest surface albedo of 0.6 requires an enhancement of 5 or 6%.

The required surface conditions to achieve the above values are not common. Using the aforementioned ADAM dataset (http://adam.noveltis.com/), we can indicate how much of the Earth's land surface has surface albedo values of at least 0.3. The database suggests that a significant proportion of the Earth has >0.3 surface albedo. Significantly the biomass burning regions indicated in (Parker et al., 2016) have the required surface albedo, thus suggesting that in the scenarios observed in (Parker et al., 2016) it would be possible to detect $^{13}CH_4$ signals with GOSAT using the methods described in this paper.

Deleted: 8

Deleted: 8

Deleted: 9

Deleted: 9

Deleted: 9

5.3. $^{13}CH_4$ Detectability under High Water Vapour Conditions

Using Equation 6 we can interpret the potential effects of varying water vapour concentration on the spectral averaging factor, given the high water vapour concentration conditions specified in Table 3. Based on the sensitivity factors indicated in Table 5, it is clear that both of the spectral bands we investigate in this paper are affected by the increase in loading of water vapour to some degree. The 1658 nm band is affected to a far less extent than the 1670 nm band (~10%). Most likely because the 1658 nm band is narrower than the 1670 nm band. For both bands the scaling of the methane column has a negligible effect, meaning that the high methane scenarios required to detect $^{13}CH_4$ will not be subject to water vapour errors, any more than high surface albedo scenarios. The loading of the water vapour column by 100% is not an unreasonable scenario when considering the difference between mid-latitude scenes and tropical scenes.

5.4. Comparisons with GOSAT-TANSO-FTS L1B Data

The assessments outlined above are predominately based on using synthetic data; it is therefore important to determine if variations in $^{13}CH_4$ can occur in real measured GOSAT-TANSO-FTS L1B spectra. Based on the method described in section 4.4.3, direct comparisons can be made between the synthetic data and L1B data. Figure 11 represents an interesting counter perspective to the results shown in the previous sections. Figure 11(a) shows largely good agreement between the ORFM and L1B spectra, aside from two spectral line absorption points in the L1B data, not present in the ORFM simulation (highlighted in Figure 11(b)), possibly due to residuals not captured in the ORFM simulations. Despite this, there is very little difference between the radiances of the ORFM and L1B spectra in the highlighted portion. However, considering Figure 11(c), the closely matching spectra indicate a reasonable fit from the method discussed in section 2.4.3. Focusing on the highlighted region in Figure 11(c) and (d) show a variation in the radiance of the $^{13}CH_4$ region, suggesting potential for GOSAT measuring changes in $^{13}CH_4$ over background concentrations. An important point to consider is the water vapour spectral line peak at 1670.68 nm; the ORFM simulations suggest a higher concentration of water vapour in the atmosphere based on the depth of the spectral line than the L1B data. Section 3.3 shows that the methane isotopologue spectral lines are heavily influenced by water vapour; therefore the lower concentrations of water vapour in the L1B spectrum, combined with the high reflectance value may allow for variation in the $^{13}CH_4$ concentration to become more obvious than suggested in the simulation studies. Therefore, in some scenarios, a high surface reflectance of at least 0.6 may not be necessary.

6. Discussion

The range of scenarios where $^{13}CH_4$ can be detected is very small. We acknowledge that this method is not as sophisticated or as accurate as a full sensitivity analysis using

Deleted: 5

Deleted: ¶

Rodgers optimal estimation method. However we argue that the benefits of the method shown in this study is its simplicity, such that a quick analysis can be performed by a lay person interested in the subject area, or it could be used to teach advanced school students, or early year University students. Indeed scientists interested in quickly determining the sensitivity of a trace gas species could use this method as a quick first step, before committing to further analysis. The most complex part of this study is the RTM, and here we use two well established RTMs to achieve the goals of this study. RTM development is a far more complex task than developing a retrieval algorithm, and independently developing an RTM would no longer make this study simple or quick. There are significantly more open source RTMs available than retrieval algorithms, this variety in RTMs mean that there should be sufficient ranges in solutions and methods that allow for characterisation of any errors in the forward models.

The detection analysis outlined in section 4.4.2 is based on the total column of methane detection of $\delta^{13}C$, this method is potentially limiting to a degree since this does not take into account KIEs in the upper troposphere and lower stratosphere due to the destruction of methane. However, since $^{13}CH_4$ concentration is low, and the KIE factors are less than those at the surface, such factors are unlikely to have a significant impact on the results. In addition atmospheric air currents interfere with the total column and thus will dampen the signal of $\delta^{13}C$ in the total column, as opposed to in situ measurements. There are currently no studies that investigate this effect, but we can assume that the $\delta^{13}C$ differences between source types will be even smaller.

Other error sources include the spectroscopy and the forward model. The HITRAN2016 database in combination with the SCIATRAN forward model assumes a Voigt profile for all methane lines in the GOSAT spectral sensitivity ranges. The Voigt profile has been generally assumed for methane spectral regions in the past, however this shape is now acknowledged to be no longer sufficient (Gordon et al., 2017). The current HITRAN2016 database does not include the parameters necessary to estimate non-Voigt line shapes for methane; however it is anticipated that future updates will include these. We therefore accept that there will be spectroscopic errors present in this study. Following on from the HITRAN database, the next largest error sources are likely to arise from SCIATRAN, generated from inaccuracies in recreating the absorption or radiance spectra from a given set of atmospheric inputs.

The metrics F_d and S_f give a useful indication of the feasibility of detecting $^{13}CH_4$, and can be used to further inform a user about the feasibility of detection over a wider variety of atmospheric and surface conditions than shown in this study. However, caution must be applied since as highlighted in Table 5, the influence of water vapour on the $^{13}CH_4$ peaks might well lead to false positive values of F_d, and therefore create an incorrect inference of isotopologues detection.

Although we briefly looked at methane isotopologues absorption in the GOSAT TIR band, we did not investigate this in depth. This is despite the fact that the isotopologues indicated much larger optical depth than their equivalent in the SWIR. However there is significant evidence to suggest that the spectroscopy of methane in the TIR is not nearly as advanced as that in the SWIR (De Lange and Landgraf, 2018), which is important given the short wavebands used in this study. In addition to the high levels of background interference on the $^{13}CH_4$ spectral lines observed in Figure 6,

Deleted: 3

Deleted: 5

An obvious next or alternative step would is to perform retrievals of the methane isotopologues using the Total Column Carbon Observing Network (TCCON, (Wunch et al., 2011)). TCCON relies on solar occultation measurements as opposed to solar backscatter, and operates at a much higher SNR and spectral resolution than GOSAT. The key disadvantage to TCCON is that it is limited to a small number of sites all over the globe, and cannot be as beneficial to global studies as satellites such as GOSAT. This work has been shown in a separate study, indicating that even with the improved SNR of the TCCON instruments, there are still significant challenges with retrievals of methane isotopologues (Malina et al., 2020).

Deleted: to be

Deleted: We believe that a study using TCCON data should be a study in its own right, and does not fit in the context of the demonstration of the quick and simple methods we use in this paper.¶

7. Conclusions

In this paper we investigated the potential to detect the second most common methane isotopologue ($^{13}CH_4$) using the GOSAT-TANSO-FTS instrument. The ratio of the main methane isotopologues has been shown to be able to differentiate between different methane source types, and could be a useful tool in linking global bottom-up emissions with top-down emissions.

We use a simple and quick residual radiance method in order to investigate the benefit of such techniques, in the wider context of the more sophisticated methods based on Rodgers' optimal estimation techniques. We argue that the residual radiance technique is useful as a simple and quick method for analysing spectral regions for sensitivity to specific trace gases.

The results of this study generally suggest that detecting the second most important methane isotopologue is difficult in most circumstances, apart from unique circumstances such as large biomass burning events. Using these techniques we find that detections of $^{13}CH_4$ with GOSAT can only occur with surface albedos of >0.3, assuming at least an 8% enhancement in the methane total column. This total column requirement is reduced with increasing surface albedo. In the context of a world where El Nino events are likely to become more frequent, it is possible that the required conditions for $^{13}CH_4$ detection using this technique, may become more common.

We perform the assessment using the general assumption of $\delta^{13}C = 0$ globally as this is built into the HITRAN databases. However we also investigate the effects of detecting the $^{13}CH_4$ isotopologue using different values of $\delta^{13}C$, ranging up to -70‰. We find that the spectral lines in the 1670 nm waveband are unaffected by the change in $\delta^{13}C$, while other spectral regions are significantly affected by this change.

We also assess the suitability of the TIR region for methane isotopologues, and find that although the optical depth of $^{13}CH_4$ is greater than that in the SWIR region, the dominance of background trace gases, and the unknowns in the spectroscopy of the region make this region less attractive than the SWIR.

Acknowledgments
We would also like to acknowledge Anu Dudhia at Oxford University for the ORFM, the SCIATRAN working group at the Institute of Environmental Physics at the University of

Bremen for SCIATRAN, HITRAN for HITRAN2016 and JAXA/NIES/MOE for GOSAT-TANSO-FTS L1B data.

Funding Statement
This research has been funded under a PhD grant (award number 157550) from the National Centre for Earth Observation (NCEO) through the Natural Environment Research Council (NERC) based in the UK.

Data Accessibility

HITRAN2016 data is available from https://hitran.org/. The OFRM is available through the website http://eodg.atm.ox.ac.uk/RFM/. SCIATRAN is available through http://www.iup.uni-bremen.de/sciatran/index.html. The GOSAT L1B data is available through the GOSAT Data Archive Service https://data2.gosat.nies.go.jp/index_en.html.

The ORFM and SCIATRAN simulations used in this paper are fully reproducible given the input parameters provided in this paper.

Competing Interests
'There are no competing interests.'

Authors' Contributions
E.M., J-P. M. and D.W. conceived and designed the experiments; E.M. performed the experiments, analysed the data and wrote the paper; D.W. contributed code for initial HITRAN line survey analysis. JPM contributed the reflectance analysis.

8. Glossary

This section provides a table of key terms and acronyms.

Deleted: ¶
¶

9. References

Archer, D., Buffett, B., Brovkin, V. and Schellnhuber, H. J.: Ocean methane hydrates as a slow tipping point in the global carbon cycle, PNAS, 106(49), 20596–20601, doi:10.1073/pnas.0800885105, 2009.
Aydin, M., Verhulst, K. R., Saltzman, E. S., Battle, M. O., Montzka, S. A., Blake, D. R., Tang, Q. and Prather, M. J.: Recent decreases in fossil-fuel emissions of ethane and methane derived from firn air, Nature, 476(7359), 198–201, doi:10.1038/nature10352, 2011.
Biévre, P., Gallet, M., Holden, N. E. and Barnes, I. L.: Isotopic Abundances and Atomic Weights of the Elements, J. Phys. Chem. Ref. Data, 13(3), 809–891, doi:10.1063/1.555720, 1984.
Bréas, O., Guillou, C., Reniero, F. and Wada, E.: The Global Methane Cycle: Isotopes and Mixing Ratios, Sources and Sinks, Isotopes Environ. Health Stud., 37(4), 257–379,

doi:10.1080/10256010108033302, 2001.
Brown, L. R., Sung, K., Benner, D. C., Devi, V. M., Boudon, V., Gabard, T., Wenger, C., Campargue, A., Leshchishina, O., Kassi, S., Mondelain, D., Wang, L., Daumont, L., Régalia, L., Rey, M., Thomas, X., Tyuterev, V. G., Lyulin, O. M., Nikitin, A. V, Niederer, H. M., Albert, S., Bauerecker, S., Quack, M., O'Brien, J. J., Gordon, I. E., Rothman, L. S., Sasada, H., Coustenis, A., Smith, M. A. H., Carrington, T., Wang, X. G., Mantz, A. W. and Spickler, P. T.: Methane line parameters in the HITRAN2012 database, J. Quant. Spectrosc. Radiat. Transf., 130, 201–219, doi:10.1016/j.jqsrt.2013.06.020, 2013.
Buchwitz, M., Schneising, O., Reuter, M., Heymann, J., Krautwurst, S., Bovensmann, H., Burrows, J. P., Boesch, H., Parker, R. J., Somkuti, P., Detmers, R. G., Hasekamp, O. P., Aben, I., Butz, A., Frankenberg, C. and Turner, A. J.: Satellite-derived methane hotspot emission estimates using a fast data-driven method, Atmos. Chem. Phys., 17(9), 5751–5774, doi:10.5194/acp-17-5751-2017, 2017.
Buzan, E. M., Beale, C. A., Boone, C. D. and Bernath, P. F.: Global stratospheric measurements of the isotopologues of methane from the Atmospheric Chemistry Experiment Fourier transform spectrometer, Atmos. Meas. Tech, 9, 1095–1111, doi:10.5194/amt-9-1095-2016, 2016.
Chanton, J. P.: The effect of gas transport on the isotope signature of methane in wetlands, , doi:10.1016/j.orggeochem.2004.10.007, 2005.
Clerbaux, C., Boynard, A., Clarisse, L., George, M., Hadji-Lazaro, J., Herbin, H., Hurtmans, D., Pommier, M., Razavi, A., Turquety, S., Wespes, C. and Coheur, P. F.: Monitoring of atmospheric composition using the thermal infrared IASI/MetOp sounder, Atmos. Chem. Phys., 9(16), 6041–6054, doi:10.5194/acp-9-6041-2009, 2009.
Craig, H.: Isotopic standards for carbon and oxygen and correction factors for mass-spectrometric analysis of carbon dioxide, Geochim. Cosmochim. Acta, 12(1–2), 133–149, doi:10.1016/0016-7037(57)90024-8, 1957.
Dudhia, A.: The Reference Forward Model (RFM), J. Quant. Spectrosc. Radiat. Transf., 186, 243–253, doi:10.1016/j.jqsrt.2016.06.018, 2017.
Etiope, G. and Ciccioli, P.: Earth's Degassing: A Missing Ethane and Propane Source, Science (80-.)., 323(5913), 478–478, doi:10.1126/science.1165904, 2009.
Gordon, I. E., Rothman, L. S., Hill, C., Kochanov, R. V., Tan, Y., Bernath, P. F., Birk, M., Boudon, V., Campargue, A., Chance, K. V., Drouin, B. J., Flaud, J.-M., Gamache, R. R., Hodges, J. T., Jacquemart, D., Perevalov, V. I., Perrin, A., Shine, K. P., Smith, M.-A. H., Tennyson, J., Toon, G. C., Tran, H., Tyuterev, V. G., Barbe, A., Császár, A. G., Devi, V. M., Furtenbacher, T., Harrison, J. J., Hartmann, J.-M., Jolly, A., Johnson, T. J., Karman, T., Kleiner, I., Kyuberis, A. A., Loos, J., Lyulin, O. M., Massie, S. T., Mikhailenko, S. N., Moazzen-Ahmadi, N., Müller, H. S. P., Naumenko, O. V., Nikitin, A. V., Polyansky, O. L., Rey, M., Rotger, M., Sharpe, S. W., Sung, K., Starikova, E., Tashkun, S. A., Auwera, J. Vander, Wagner, G., Wilzewski, J., Wcisło, P., Yu, S. and Zak, E. J.: The HITRAN2016 Molecular Spectroscopic Database, J. Quant. Spectrosc. Radiat. Transf., doi:10.1016/j.jqsrt.2017.06.038, 2017.
Herbin, H., -Labonnote, L. C. and Dubuisson, P.: Multispectral information from TANSO-FTS instrument – Part 1: Application to greenhouse gases (CO 2 and CH 4) in clear sky conditions, Atmos. Meas. Tech, 6, 3301–3311, doi:10.5194/amt-6-3301-2013, 2013.
Holl, G., Walker, K. A., Conway, S., Saitoh, N., Boone, C. D., Strong, K. and Drummond, J. R.: Methane cross-validation between three Fourier transform spectrometers: SCISAT ACE-FTS, GOSAT TANSO-FTS, and ground-based FTS measurements in the Canadian high Arctic, Atmos. Meas. Tech., 9(5), 1961–1980, doi:10.5194/amt-9-1961-2016, 2016.
IPCC: Fifth Assessment Report - Impacts, Adaptation and Vulnerability, [online]

Available from: http://www.ipcc.ch/report/ar5/wg2/ (Accessed 12 June 2017), 2014.
Irion, F. W., Moyer, E. J., Gunson, M. R., Rinsland, C. P., Yung, Y. L., Michelsen, H. A., Salawitch, R. J., Chang, A. Y., Newchurch, M. J., Abbas, M. M., Abrams, M. C. and Zander, R.: Stratospheric observations of CH_3D and HDO from ATMOS infrared solar spectra: Enrichments of deuterium in methane and implications for HD, Geophys. Res. Lett., 23(17), 2381–2384, doi:10.1029/96GL01402, 1996.
Kai, F. M., Tyler, S. C., Randerson, J. T. and Blake, D. R.: Reduced methane growth rate explained by decreased Northern Hemisphere microbial sources, Nature, 476(7359), 194–197, doi:10.1038/nature10259, 2011.
Kneizys, F. X., Anderson, G. P., Shettle, E. P., Gallery, W. O., Abreu, L. W., Selby, J. E. A., Chetwynd, J. H. and Clough, S. A.: Users guide to LOWTRAN 7. [online] Available from: https://apps.dtic.mil/dtic/tr/fulltext/u2/a206773.pdf (Accessed 12 January 2019), 1988.
Kort, E. A., Frankenberg, C., Costigan, K. R., Lindenmaier, R., Dubey, M. K. and Wunch, D.: Four corners: The largest US methane anomaly viewed from space, Geophys. Res. Lett., 41(19), 6898–6903, doi:10.1002/2014GL061503, 2014.
Kuze, A., Suto, H., Nakajima, M. and Hamazaki, T.: Thermal and near infrared sensor for carbon observation Fourier-transform spectrometer on the Greenhouse Gases Observing Satellite for greenhouse gases monitoring, Appl. Opt., 48(35), 6716, doi:10.1364/AO.48.006716, 2009.
Kuze, A., Suto, H., Shiomi, K., Urabe, T., Nakajima, M., Yoshida, J., Kawashima, T., Yamamoto, Y., Kataoka, F. and Buijs, H.: Level 1 algorithms for TANSO on GOSAT: processing and on-orbit calibrations, Atmos. Meas. Tech, 5, 2447–2467, doi:10.5194/amt-5-2447-2012, 2012.
De Lange, A. and Landgraf, J.: Methane profiles from GOSAT thermal infrared spectra, Atmos. Meas. Tech., 11(6), 3815–3828, doi:10.5194/amt-11-3815-2018, 2018.
Leifer, I., Roberts, D., Margolis, J. and Kinnaman, F.: In situ sensing of methane emissions from natural marine hydrocarbon seeps: A potential remote sensing technology, Earth Planet. Sci. Lett., 245(3–4), 509–522, doi:10.1016/j.epsl.2006.01.047, 2006.
Malina, E., Yoshida, Y., Matsunaga, T. and Muller, J. P.: Information content analysis: The potential for methane isotopologue retrieval from GOSAT-2, Atmos. Meas. Tech., 11(2), 1159–1179, doi:10.5194/amt-11-1159-2018, 2018.
Malina, E., Veihelmann, B., Feist, D. and Morino, I.: On the consistency of methane isotopologue retrievals using TCCON and multiple spectroscopic databases, Atmos. Meas. Tech. Discuss., 1–44, doi:10.5194/amt-2020-86, 2020.
Mcnorton, J., Chipperfield, M. P., Gloor, M., Wilson, C., Feng, W., Hayman, G. D., Rigby, M., Krummel, P. B., O 'doherty, S., Prinn, R. G., Weiss, R. F., Young, D., Dlugokencky, E. and Montzka, S. A.: Role of OH variability in the stalling of the global atmospheric CH 4 growth rate from 1999 to 2006, Atmos. Chem. Phys, 16, 7943–7956, doi:10.5194/acp-16-7943-2016, 2016.
Muller, J.-P., Lewis, P., Bréon, F.-M., Bacour, C., Price, I., Chaumat, L., Prunet, P., Gonzales, L., Schlundt, C., Vountas, M., Burrows, J., von Hoyningen-Huene, W., Guanter, L., Fischer, J., North, P., Heckel, A. and Straume-Lindner, A. G.: A Surface Reflectance Database for ESA's Earth Observation Missions (ADAM), ESA Living Planet Symposium , Edinburgh. [online] Available from: http://www.livingplanet2013.org/abstracts/849688.htm (Accessed 13 June 2017), 2013.
Myhre, C. L., Ferré, B., Platt, S. M., Silyakova, A., Hermansen, O., Allen, G., Pisso, I., Schmidbauer, N., Stohl, A., Pitt, J., Jansson, P., Greinert, J., Percival, C., Fjaeraa, A. M., O'Shea, S. J., Gallagher, M., Le Breton, M., Bower, K. N., Bauguitte, S. J. B., Dalsøren, S.,

Vadakkepuliyambatta, S., Fisher, R. E., Nisbet, E. G., Lowry, D., Myhre, G., Pyle, J. A., Cain, M. and Mienert, J.: Extensive release of methane from Arctic seabed west of Svalbard during summer 2014 does not influence the atmosphere, Geophys. Res. Lett., 43(9), 4624–4631, doi:10.1002/2016GL068999, 2016.
Nisbet, E. G., Dlugokencky, E. J., Manning, M. R., Lowry, D., Fisher, R. E., France, J. L., Michel, S. E., Miller, J. B., White, J. W. C., Vaughn, B., Bousquet, P., Pyle, J. A., Warwick, N. J., Cain, M., Brownlow, R., Zazzeri, G., Lanoisellé, M., Manning, A. C., Gloor, E., Worthy, D. E. J., Brunke, E.-G., Labuschagne, C., Wolff, E. W. and Ganesan, A. L.: Rising atmospheric methane: 2007-2014 growth and isotopic shift, Global Biogeochem. Cycles, 30(9), 1356–1370, doi:10.1002/2016GB005406, 2016.
Nisbet, E. G., Manning, M. R., Dlugokencky, E. J., Fisher, R. E., Lowry, D., Michel, S. E., Myhre, C. L., Platt, S. M., Allen, G., Bousquet, P., Brownlow, R., Cain, M., France, J. L., Hermansen, O., Hossaini, R., Jones, A. E., Levin, I., Manning, A. C., Myhre, G., Pyle, J. A., Vaughn, B. H., Warwick, N. J. and White, J. W. C.: Very Strong Atmospheric Methane Growth in the 4 Years 2014–2017: Implications for the Paris Agreement, Global Biogeochem. Cycles, 33(3), 318–342, doi:10.1029/2018GB006009, 2019.
Ohyama, H., Kawakami, S., Shiomi, K., Morino, I. and Uchino, O.: Atmospheric Temperature and Water Vapor Retrievals from GOSAT Thermal Infrared Spectra and Initial Validation with Coincident Radiosonde Measurements, SOLA, 9(0), 143–147, doi:10.2151/sola.2013-032, 2013.
Ohyama, H., Kawakami, S., Shiomi, K., Morino, I. and Uchino, O.: Intercomparison of XH2O data from the GOSAT TANSO-FTS (TIR and SWIR) and ground-based FTS measurements: Impact of the spatial variability of XH2O on the intercomparison, Remote Sens., 9(1), 64, doi:10.3390/rs9010064, 2017.
Parker, R., Boesch, H., Cogan, A., Fraser, A., Feng, L., Palmer, P. I., Messerschmidt, J., Deutscher, N., Griffith, D. W. T., Notholt, J., Wennberg, P. O. and Wunch, D.: Methane observations from the Greenhouse Gases Observing SATellite: Comparison to ground-based TCCON data and model calculations, Geophys. Res. Lett., 38(15), doi:10.1029/2011GL047871, 2011.
Parker, R. J., Boesch, H., Byckling, K., Webb, A. J., Palmer, P. I., Feng, L., Bergamaschi, P., Chevallier, F., Notholt, J., Deutscher, N., Warneke, T., Hase, F., Sussmann, R., Kawakami, S., Kivi, R., Griffith, D. W. T. and Velazco, V.: Assessing 5 years of GOSAT Proxy XCH 4 data and associated uncertainties, Atmos. Meas. Tech, 8, 4785–4801, doi:10.5194/amt-8-4785-2015, 2015.
Parker, R. J., Boesch, H., Wooster, M. J., Moore, D. P., Webb, A. J., Gaveau, D., Murdiyarso, D. and Parker, R.: Atmospheric CH 4 and CO 2 enhancements and biomass burning emission ratios derived from satellite observations of the 2015 Indonesian fire plumes, Atmos. Chem. Phys, 16, 10111–10131, doi:10.5194/acp-16-10111-2016, 2016.
Rella, C. W., Crosson, E., Jacobson, G., Karion, A., Petron, G. and Sweeney, C.: Quantifying the relative contribution of natural gas fugitive emissions to total methane emissions in Colorado and Utah using mobile d 13 CH 4 analysis, pp. 12–1, EGU, Vienna. [online] Available from: https://www.picarro.com/sites/default/files/Rella IG4 - S4.12 - BG1.4 - 20130411 - 0845.pdf (Accessed 12 June 2017), 2013.
Remedios, J. J., Leigh, R. J., Waterfall, A. M., Moore, D. P., Sembhi, H., Parkes, I., Greenhough, J., Chipperfield, M. P. and Hauglustaine, D.: MIPAS reference atmospheres and comparisons to V4.61/V4.62 MIPAS level 2 geophysical data sets, Atmos. Chem. Phys. Discuss. Eur. Geosci. Union, 7(4), 9973–10017, doi:10.5194/acpd-7-9973-2007, 2007.
Reuter, M., Bovensmann, H., Buchwitz, M., Burrows, J. P., Deutscher, N. M., Heymann, J.,

Rozanov, A., Schneising, O., Suto, H., Toon, G. C. and Warneke, T.: On the potential of the 2041-2047nm spectral region for remote sensing of atmospheric CO 2 isotopologues, J. Quant. Spectrosc. Radiat. Transf., 113(16), 2009–2017, doi:10.1016/j.jqsrt.2012.07.013, 2012.
Rigby, M., Manning, A. J. and Prinn, R. G.: The value of high-frequency, high-precision methane isotopologue measurements for source and sink estimation, J. Geophys. Res. Atmos., 117(12), doi:10.1029/2011JD017384, 2012.
Roberts, D. A., Bradley, E. S., Cheung, R., Leifer, I., Dennison, P. E. and Margolis, J. S.: Mapping methane emissions from a marine geological seep source using imaging spectrometry, Remote Sens. Environ., 114(3), 592–606, doi:10.1016/j.rse.2009.10.015, 2010.
Röckmann, T., Brass, M., Borchers, R. and Engel, A.: The isotopic composition of methane in the stratosphere: High-altitude balloon sample measurements, Atmos. Chem. Phys., 11(24), 13287–13304, doi:10.5194/acp-11-13287-2011, 2011.
Rodgers, C. D.: Inverse Methods for Atmospheric Sounding - Theory and Practice, World Scientific., 2000.
Rothman, L. S., Gordon, I. E., Barbe, A., Benner, D. C., Bernath, P. F., Birk, M., Boudon, V., Brown, L. R., Campargue, A., Champion, J.-P., Chance, K., Coudert, L. H., Dana, V., Devi, V. M., Fally, S., Flaud, J.-M., Gamache, R. R., Goldman, A., Jacquemart, D., Kleiner, I., Lacome, N., Lafferty, W. J., Mandin, J.-Y., Massie, S. T., Mikhailenko, S. N., Miller, C. E., Moazzen-Ahmadi, N., Naumenko, O. V., Nikitin, A. V., Orphal, J., Perevalov, V. I., Perrin, A., Predoi-Cross, A., Rinsland, C. P., Rotger, M., Šimečková, M., Smith, M. A. H., Sung, K., Tashkun, S. A., Tennyson, J., Toth, R. A., Vandaele, A. C. and Vander Auwera, J.: The HITRAN 2008 molecular spectroscopic database, J. Quant. Spectrosc. Radiat. Transf., 110(9–10), 533–572, doi:10.1016/j.jqsrt.2009.02.013, 2009.
Rozanov, V. V., Rozanov, A. V., Kokhanovsky, A. A. and Burrows, J. P.: Radiative transfer through terrestrial atmosphere and ocean: Software package SCIATRAN, J. Quant. Spectrosc. Radiat. Transf., 133, 13–71, doi:10.1016/j.jqsrt.2013.07.004, 2014.
Schepers, D., Guerlet, S., Butz, A., Landgraf, J., Frankenberg, C., Hasekamp, O., Blavier, J. F., Deutscher, N. M., Griffith, D. W. T., Hase, F., Kyro, E., Morino, I., Sherlock, V., Sussmann, R. and Aben, I.: Methane retrievals from Greenhouse Gases Observing Satellite (GOSAT) shortwave infrared measurements: Performance comparison of proxy and physics retrieval algorithms, J. Geophys. Res. Atmos., 117(10), doi:10.1029/2012JD017549, 2012.
Schuur, E. A. G., McGuire, A. D., Schädel, C., Grosse, G., Harden, J. W., Hayes, D. J., Hugelius, G., Koven, C. D., Kuhry, P., Lawrence, D. M., Natali, S. M., Olefeldt, D., Romanovsky, V. E., Schaefer, K., Turetsky, M. R., Treat, C. C. and Vonk, J. E.: Climate change and the permafrost carbon feedback, Nature, 520(7546), 171–179, doi:10.1038/nature14338, 2015.
Schweizer, M., Fear, J. and Cadisch, G.: Isotopic (13C) fractionation during plant residue decomposition and its implications for soil organic matter studies, Rapid Commun. Mass Spectrom., 13(13), 1284–1290, doi:10.1002/(SICI)1097-0231(19990715)13:13<1284::AID-RCM578>3.0.CO;2-0, 1999.
Schwietzke, S., Sherwood, O. A., Bruhwiler, L. M. P., Miller, J. B., Etiope, G., Dlugokencky, E. J., Michel, S. E., Arling, V. A., Vaughn, B. H., White, J. W. C. and Tans, P. P.: Upward revision of global fossil fuel methane emissions based on isotope database, Nature, 538(7623), 88–91, doi:10.1038/nature19797, 2016.
Sinnhuber, B. M., Sheode, N., Sinnhuber, M., Chipperfield, M. P. and Feng, W.: The contribution of anthropogenic bromine emissions to past stratospheric ozone trends: A

modelling study, Atmos. Chem. Phys., 9(8), 2863–2871, doi:10.5194/acp-9-2863-2009, 2009.
Starikova, E., Nikitin, A. V., Rey, M., Tashkun, S. A., Mondelain, D., Kassi, S., Campargue, A. and Tyuterev, V. G.: Assignment and modeling of the absorption spectrum of13CH4at 80 K in the region of the 2ν3band (5853-6201 cm-1), J. Quant. Spectrosc. Radiat. Transf., 177, 170–180, doi:10.1016/j.jqsrt.2015.12.023, 2016.
Swinehart, D. F.: The Beer-Lambert Law, J. Chem. Educ., 39(7), 333, doi:10.1021/ed039p333, 1962.
Tennyson, J.: Astronomical spectroscopy : an introduction to the atomic and molecular physics of astronomical spectra, Imperial College Press. [online] Available from: https://books.google.co.uk/books/about/Astronomical_Spectroscopy.html?id=A4BBfuJPqOAC&redir_esc=y (Accessed 13 June 2017), 2005.
Turner, A. J., Jacob, D. J., Wecht, K. J., Maasakkers, J. D., Lundgren, E., Andrews, A. E., Biraud, S. C., Boesch, H., Bowman, K. W., Deutscher, N. M., Dubey, M. K., Griffith, D. W. T., Hase, F., Kuze, A., Notholt, J., Ohyama, H., Parker, R., Payne, V. H., Sussmann, R., Sweeney, C., Velazco, V. A., Warneke, T., Wennberg, P. O. and Wunch, D.: Estimating global and North American methane emissions with high spatial resolution using GOSAT satellite data, Atmos. Chem. Phys., 15(12), 7049–7069, doi:10.5194/acp-15-7049-2015, 2015.
Turner, A. J., Frankenberg, C., Wennberg, P. O. and Jacob, D. J.: Ambiguity in the causes for decadal trends in atmospheric methane and hydroxyl., Proc. Natl. Acad. Sci. U. S. A., 114(21), 5367–5372, doi:10.1073/pnas.1616020114, 2017.
Weidmann, D., Hoffmann, A., Macleod, N., Middleton, K., Kurtz, J., Barraclough, S. and Griffin, D.: The Methane Isotopologues by Solar Occultation (MISO) Nanosatellite Mission: Spectral Channel Optimization and Early Performance Analysis, Remote Sens., 9(10), 1073, doi:10.3390/rs9101073, 2017.
Whiticar, M. J.: Carbon and hydrogen isotope systematics of bacterial formation and oxidation of methane, Chem. Geol., 161(1–3), 291–314, doi:10.1016/S0009-2541(99)00092-3, 1999.
Worden, J. R., Turner, A. J., Bloom, A., Kulawik, S. S., Liu, J., Lee, M., Weidner, R., Bowman, K., Frankenberg, C., Parker, R. and Payne, V. H.: Quantifying lower tropospheric methane concentrations using GOSAT near-IR and TES thermal IR measurements, Atmos. Meas. Tech, 8, 3433–3445, doi:10.5194/amt-8-3433-2015, 2015.
Wuebbles, D. and Hayhoe, K.: Atmospheric methane and global change, Earth-Science Rev., 57(3–4), 177–210, doi:10.1016/S0012-8252(01)00062-9, 2002.
Wunch, D., Toon, G. C., Blavier, J.-F. L., Washenfelder, R. A., Notholt, J., Connor, B. J., Griffith, D. W. T., Sherlock, V. and Wennberg, P. O.: The Total Carbon Column Observing Network, Phil. Trans. R. Soc. A, 369, 2087–2112, doi:10.1098/rsta.2010.0240, 2011.
Yokota, T., Yoshida, Y., Eguchi, N., Ota, Y., Tanaka, T., Watanabe, H. and Maksyutov, S.: Global Concentrations of CO2 and CH4 Retrieved from GOSAT: First Preliminary Results, SOLA, 5, 160–163, doi:10.2151/sola.2009-041, 2009.
Yoshida, Y., Ota, Y., Eguchi, N., Kikuchi, N., Nobuta, K., Tran, H., Morino, I. and Yokota, T.: Retrieval algorithm for CO 2 and CH 4 column abundances from short-wavelength infrared spectral observations by the Greenhouse gases observing satellite, Atmos. Meas. Tech, 4, 717–734, doi:10.5194/amt-4-717-2011, 2011.
Yoshida, Y., Kikuchi, N., Morino, I., Uchino, O., Oshchepkov, S., Bril, A., Saeki, T., Schutgens, N., Toon, G. C., Wunch, D., Roehl, C. M., Wennberg, P. O., Griffith, D. W. T., Deutscher, N. M., Warneke, T., Notholt, J., Robinson, J., Sherlock, V., Connor, B., Rettinger, M., Sussmann, R., Ahonen, P., Heikkinen, P., Kyrö, E., Mendonca, J., Strong, K., Hase, F., Dohe, S. and Yokota, T.: Improvement of the retrieval algorithm for GOSAT SWIR XCO2 and XCH4 and their

validation using TCCON data, Atmos. Meas. Tech., 6(6), 1533–1547, doi:10.5194/amt-6-1533-2013, 2013.
Zou, M., Xiong, X., Saitoh, N., Warner, J., Zhang, Y., Chen, L., Weng, F. and Fan, M.: Satellite observation of atmospheric methane: intercomparison between AIRS and GOSAT TANSO-FTS retrievals, Atmos. Meas. Tech, 9, 3567–3576, doi:10.5194/amt-9-3567-2016, 2016.

Tables

Table 1. The conditions used by ORFM in generating SWIR Absorption from an assumed GOSAT-TANSO-FTS like instrument. All conditions are taken from MIPAS Model atmospheres (Remedios et al., 2007)**.**

Condition Variables	Value
Wavelength Range	1600-1700 nm 7600 – 8300 nm
Background Gases	H_2O, CO_2 and N_2O at standard model concentrations
Instrument Altitude	666km
Solar Zenith Angle	30°
Atmospheric Model	University of Leicester MIPAS Model
Spectral Line Database	HITRAN 2016
Spectral Resolution	0.01cm^{-1}
Viewing Profile	Nadir

Table 2. SCIATRAN Simulation conditions for detection study.

Sensor	Surface/Atmosphere	Notes
Solar Zenith: 30° Altitude: 666 km	Background Conditions	
	Reflectance: 0.1, 0.3 - 0.6	
	H_2O: As SCIATRAN CTM (November, Latitude 45°)	
	CH_4: As SCIATRAN CTM (November, Latitude 45°)	
	Aerosols: As LOWTRAN SCIATRAN standard settings	Maritime/tropospheric in the boundary layer. Background in the stratosphere.
	Elevated Conditions	
	Reflectance: 0.1, 0.3, 0.6	Vegetation to Desert.
	H_2O: As background x2	Not necessarily realistic, but indicates sensitivity to water vapour.
	CH_4 Scale Factor: 1.02, 1.04, 1.06, 1.08, 1.10	XCH_4 values, minimum 1.78 ppm, maximum 1.94 ppm.

Table 3. Spectral average F_d (Equation 5) values summarised for the standard conditions expressed Table 2. The F_d values are shown for each CH_4 scale given the range of reflectances indicated in Table 1.

Deleted: 4

CH_4 Total Column Scale Factor	F_d Albedo = 0.1 (x10^{-10})	F_d Albedo = 0.3 (x10^{-10})	F_d Albedo = 0.4 (x10^{-10})	F_d Albedo = 0.5 (x10^{-10})	F_d Albedo = 0.6 (x10^{-10})
1658.6 – 1658.65 nm					
x1.02	-1.41	-1.19	-1.08	-0.975	-0.864
x1.04	-1.30	-0.87	-0.652	-0.432	-0.211
x1.06	-1.19	-0.546	-0.219	0.110	0.444
x1.08	-1.08	-0.223	0.213	0.652	1.10
x1.10	-0.974	0.0999	0.644	1.19	1.75

1670.35 – 1670.55 nm					
x1.02	-1.42	-1.23	-1.13	-1.03	-0.931
x1.04	-1.32	-0.938	-0.742	-0.545	-0.346
x1.06	-1.23	-0.648	-0.355	-0.0582	0.241
x1.08	-1.13	-0.358	0.0327	0.428	0.827
x1.10	-1.03	-0.0688	0.420	0.913	1.41

Table 4. Spectral average F_d (Equation 5) values summarised for the standard conditions expressed Table 2, assuming a global standard $\delta^{13}C$ value of -70. The F_d values are shown for each CH_4 scale given the range of reflectances indicated in Table 2.

Deleted: 4

CH_4 Total Column Scale Factor	F_d Albedo = 0.1 ($x10^{-10}$)	F_d Albedo = 0.3 ($x10^{-10}$)	F_d Albedo = 0.4 ($x10^{-10}$)	F_d Albedo = 0.5 ($x10^{-10}$)	F_d Albedo = 0.6 ($x10^{-10}$)
1658.6 – 1658.65 nm					
x1.02	-1.51	-1.49	-1.47	-1.46	-1.45
x1.04	-1.50	-1.45	-1.43	-1.41	-1.39
x1.06	-1.48	-1.42	-1.39	-1.35	-1.32
x1.08	-1.47	-1.39	-1/34	-1.30	-1.25
x1.10	-1.46	-1.36	-1.30	-1.25	-1.19
1670.35 – 1670.55 nm					
x1.02	-1.42	-1.22	-1.12	-1.03	-0.924
x1.04	-1.32	-0.93	-0.733	-0.535	-0.330
x1.06	-1.22	-0.636	-0.341	-0.043	0.263
x1.08	-1.12	-0.343	0.0512	0.448	0.857
x1.10	-1.02	-0.0494	0.443	0.939	1.450

Table 5. Sensitivity factor for the 1658 nm and 1670 nm wavebands, assuming the low and high water vapour conditions, and a surface albedo of 0.3 specified in Table 2.

Waveband/Methane scale	Scale = 2%	Scale = 4%	Scale = 6%	Scale = 8%	Scale = 10%
1658.6 nm S_f	1.00121	1.00126	1.00127	1.00125	1.00125
1670.35 nm S_f	1.0113	1.00113	1.0113	1.0112	1.0112

Table 6. Glossary of key terms and acronyms used in this paper.

Formatted: Font: Times New Roman, 9 pt

Term	Details
ADAM	A surface reflectance Database for ESA's earth observation Missions; Database of surface reflectance.
CTM	Chemistry Transport Model; Mathematical model simulating the transport of trace gases in the atmosphere.
$\delta^{13}C$	Ratio of $^{13}CH_4$ to $^{12}CH_4$ compared to the Vienna Pee Dee Belemnite standard.
ESA	European Space Agency
FTS	Fourier Transform Spectrometer; Sensor on GOSAT designed to measure trace gases.
GHG	Greenhouse Gas(es)
GOSAT	Greenhouse Gases Observing Satellite; Satellite launched in 2009.
HITRAN	High Resolution Transmission; Database of spectroscopic parameters.
L1B	Level 1B data; first stage processed data from the instrument, representing the spectral response.
IC	Information Content; Mathematical technique to assess quality of trace gas retrievals.
Isotopologue	Molecule with at least one atom containing non-periodic table number of neutrons.
JAXA	Japanese Aerospace Exploration Agency.
KIE	Kinetic Isotope Effects; Determines the rate of reactions based on isotopic make up of molecule.
MIPAS	Michelson Interferometer for Passive Atmospheric Sounding; Instrument on ENVISAT.
NEDL	Noise Equivalent Radiance; Instrument noise represented as radiance values.
NIES	National Institute for Environmental Studies.
ORFM	Oxford Reference Forward Model; Radiative transfer model developed at the University of Oxford.
RTM	Radiative Transfer Model; Model designed to simulate radiation transfer through a medium.
SCIAMACHY	SCanning Imaging Absorption SpectroMeter for Atmospheric CHartographY; Instrument on ENVISAT.

SCIATRAN	Name of radiative transfer model developed at the University of Bremen.
SNR	Signal to Noise Ratio.
SWIR	Shortwave Infrared; Portion of the electromagnetic spectrum ~1-3 µm.
TANSO	Thermal and near Infrared Sensor for Carbon Observations; Instrument onboard GOSAT.
TCCON	Total Column Carbon Observing Network; Series of upwards viewing FTSs located around the world.
TIR	Thermal Infrared; Portion of the electromagnetic spectrum ~>5 µm to microwave.
TROPOMI	Tropospheric Monitoring Instrument; Instrument based on Sentinel-5P.

Figures

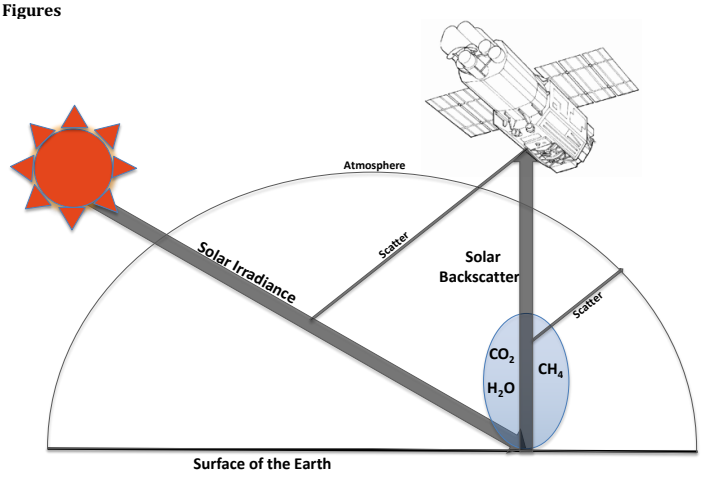

Figure 1. Schematic representation of GOSAT measuring solar backscatter light.

Formatted: Caption

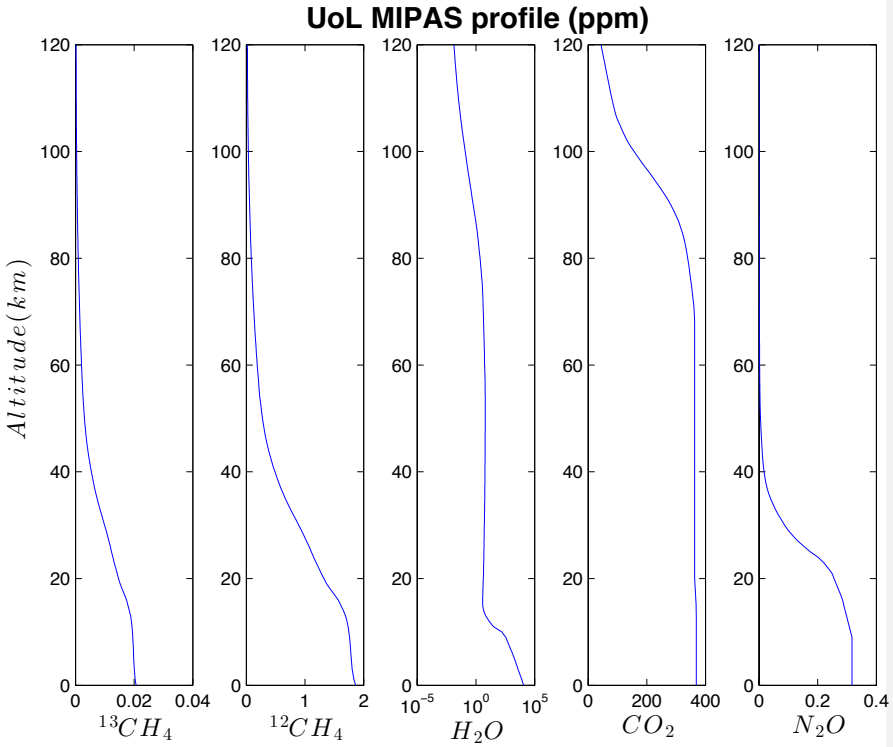

Figure 2. Volume Mixing Ratio profiles of the main gases of interest CH_4, H_2O and CO_2 in ppm from 0-120km altitude, (Remedios et al., 2007), adapted from (Malina et al., 2018).

Deleted: 1

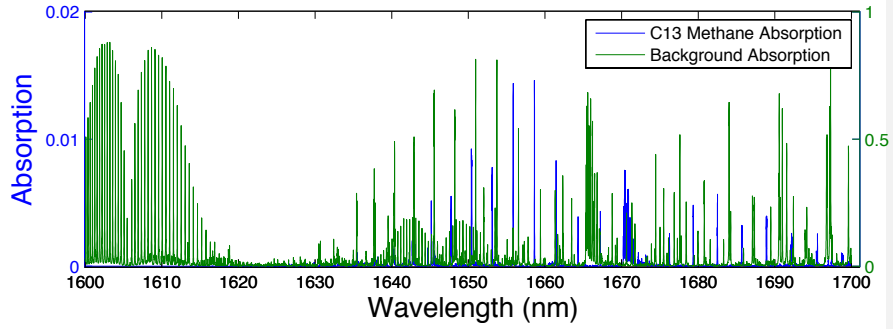

Figure 3. Simulated absorption spectrum from ORFM in the wavelength range 1600-1700nm, the y scale represents the fraction of radiation absorbed by the molecules under investigation. The blue line represents absorption by $^{13}CH_4$ (left hand scale) and green represents all other key absorbing background gases (CO_2, H_2O and $^{12}CH_4$) (right hand scale).

Deleted: 2

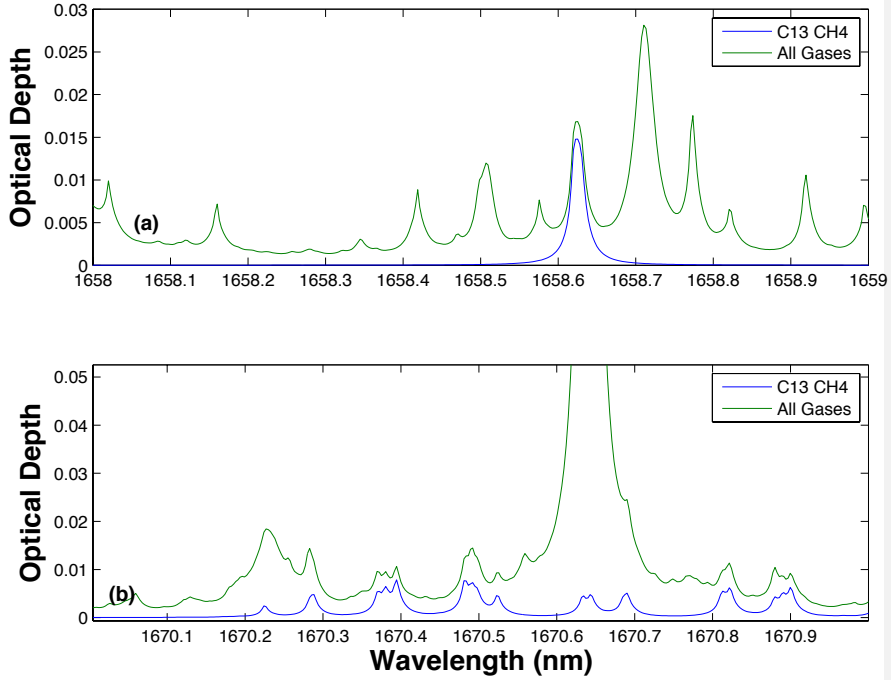

Figure 4. Optical depth covering $^{13}CH_4$ absorption points of interest, the green line represents optical depth of all gases present in this portion of the spectrum (CH_4, CO_2 and H_2O), whilst the blue line shows optical depth of purely the methane isotopologue $^{13}CH_4$: (a) indicates optical depth in the wavelength range 1658-1659nm; (b) shows optical depth in the wavelength range 1670-1671nm. This figure is as figure 5 in (Malina et al., 2018), but has been updated to reflect the use of HITRAN2016.

Deleted: 3

Deleted: 5

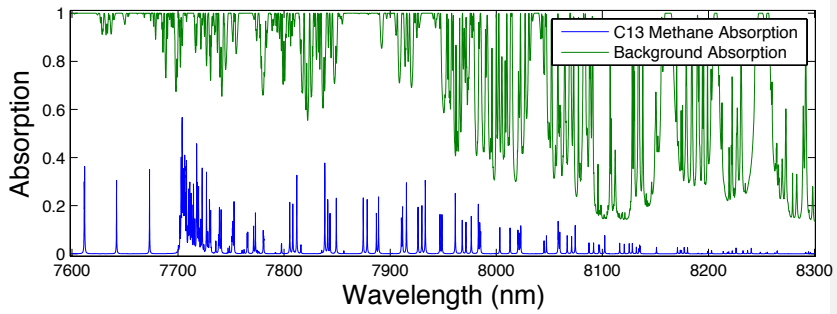

Figure 5. Simulated absorption spectrum from ORFM in the wavelength range 7600-8300 nm, the y scale represents the fraction of radiation absorbed by the molecules under investigation. The blue line represents absorption by $^{13}CH_4$ and green represents all other key absorbing background gases (CO_2, H_2O, N_2O and $^{12}CH_4$).

Deleted: 4

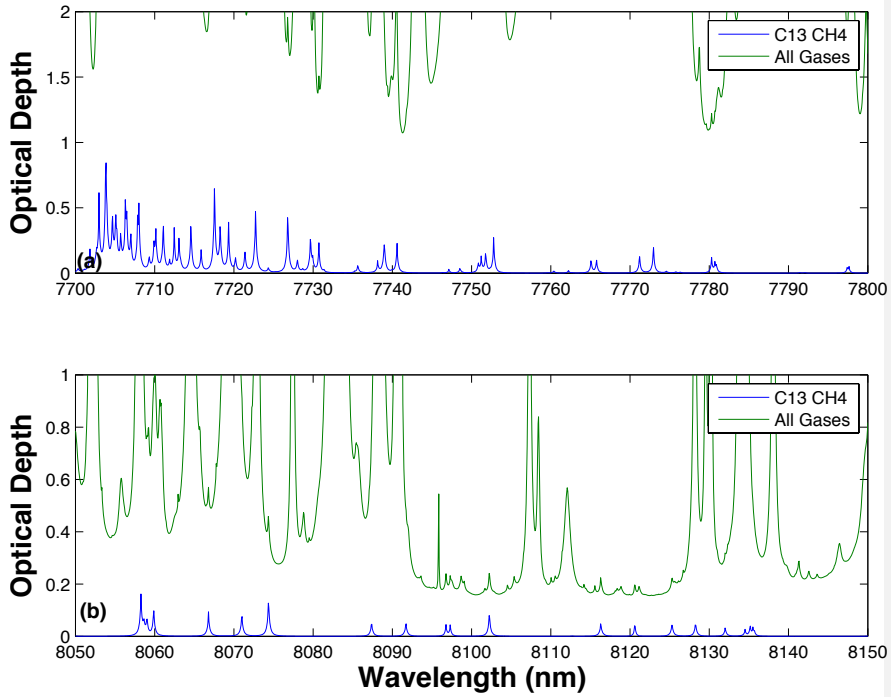

Figure 6. As figure 4 but focused on the wavelength ranges 7700-7800 nm and 8050-8150 nm.

Deleted: 5

Deleted: 3

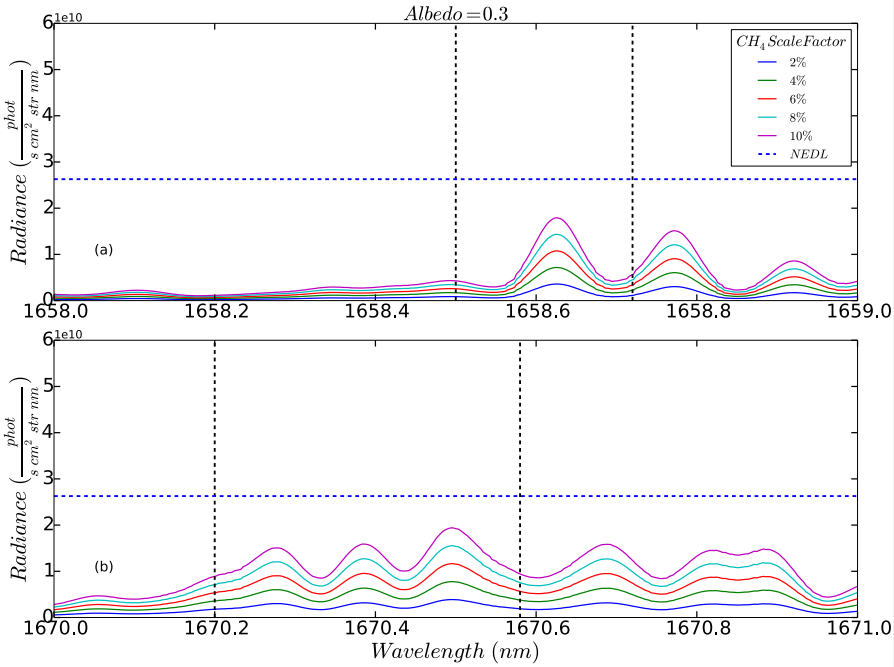

Figure 7. Residual Radiance plots based on the simulation conditions highlighted in Table 3, where simulated radiance from the background conditions under the standard 'day' scene with a reflectance of 0.3 are subtracted from elevated methane conditions. The residual radiance values are represented by the lines indicated in the legend. The Blue dashed line represents the NEDL. The solid vertical dashed lines identify the regions where $^{13}CH_4$ spectral lines are prevalent: (a) highlights the $^{13}CH_4$ spectral line in the 1658-1659 nm range; (b) focuses on the $^{13}CH_4$ spectral line in the 1670-1671 nm range.

Deleted: 6

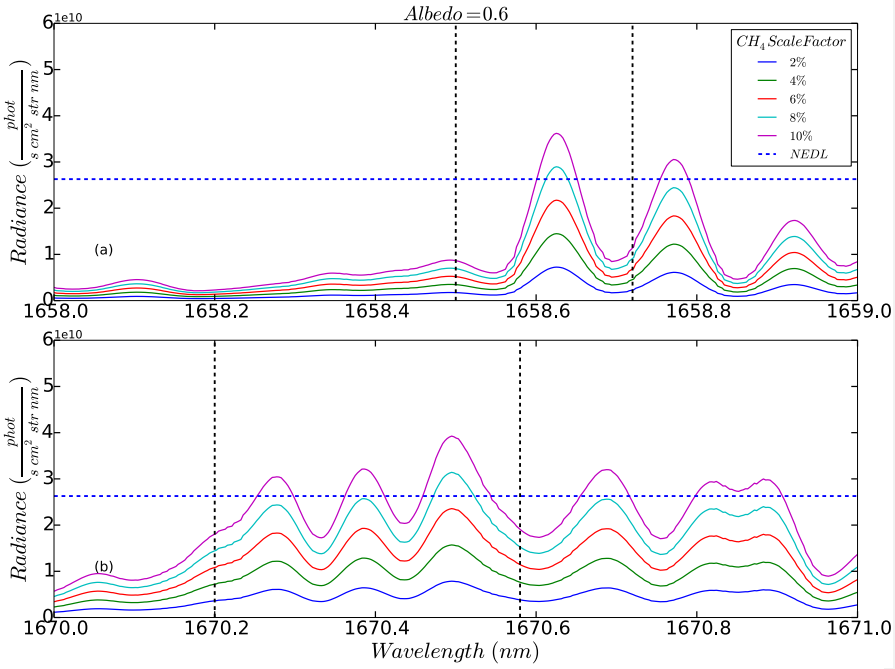

Figure 8. As Figure 7, with surface albedo increased to 0.6.

Deleted: 7

Deleted: 6

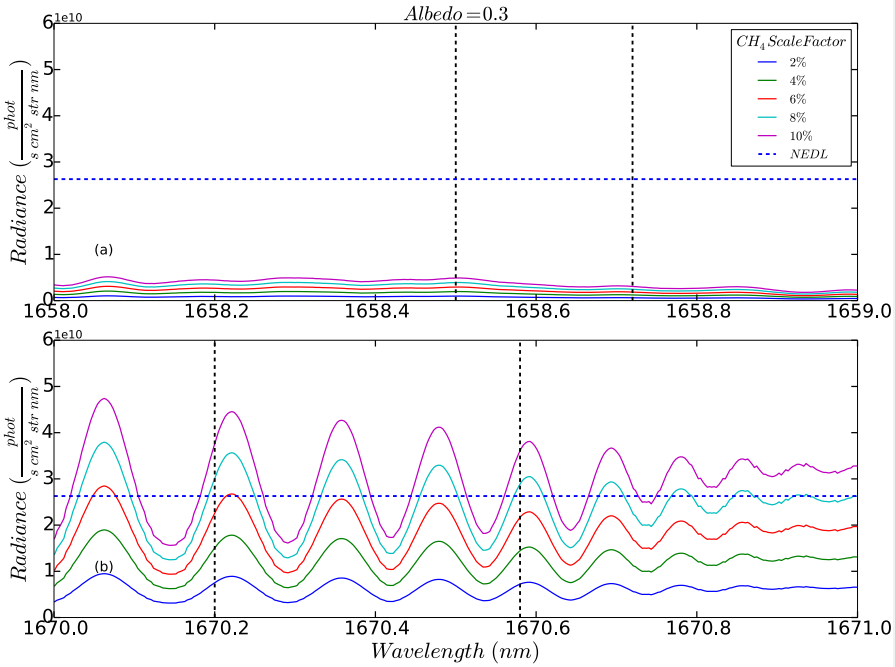

Figure 9. As Figure 7, and Figure 8, with surface albedo increased to 0.3, assuming the standard $\delta^{13}C$ value is -70‰ as opposed to 0‰.

Deleted: 8

Deleted: 6

Deleted: 7

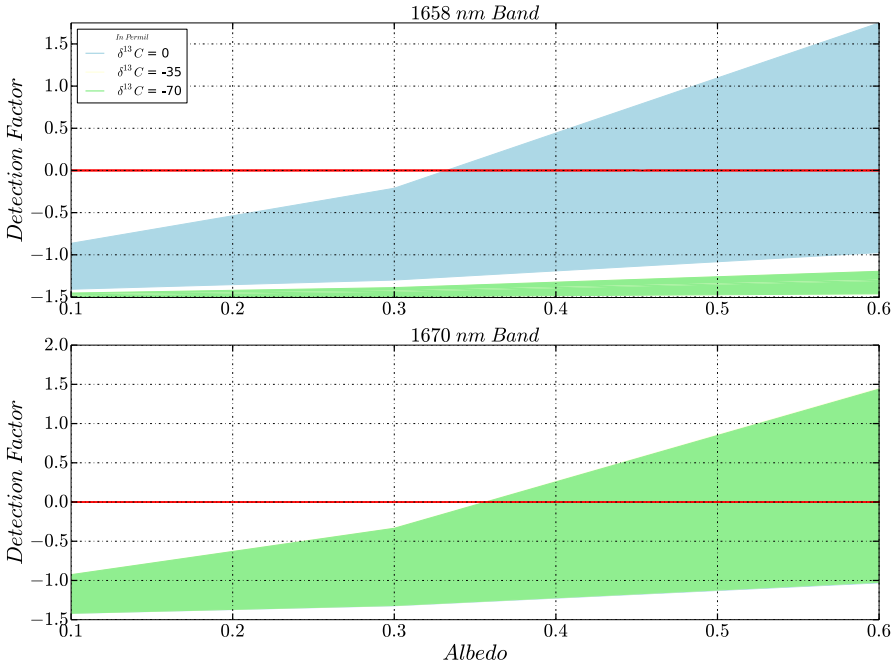

Figure 10. Plot indicating the surface conditions required to generate detection factors > 0, thus suggesting a positive detection of $\delta^{13}C$. The top panel shows results for the 1658 nm band, and the bottom panel shows results for the 1670 nm band. The light blue area indicates results assuming a $\delta^{13}C$ natural value of 0‰, light yellow -35‰ and light green -70‰, the solid red line indicates where the detection factor is zero.

Deleted: 9

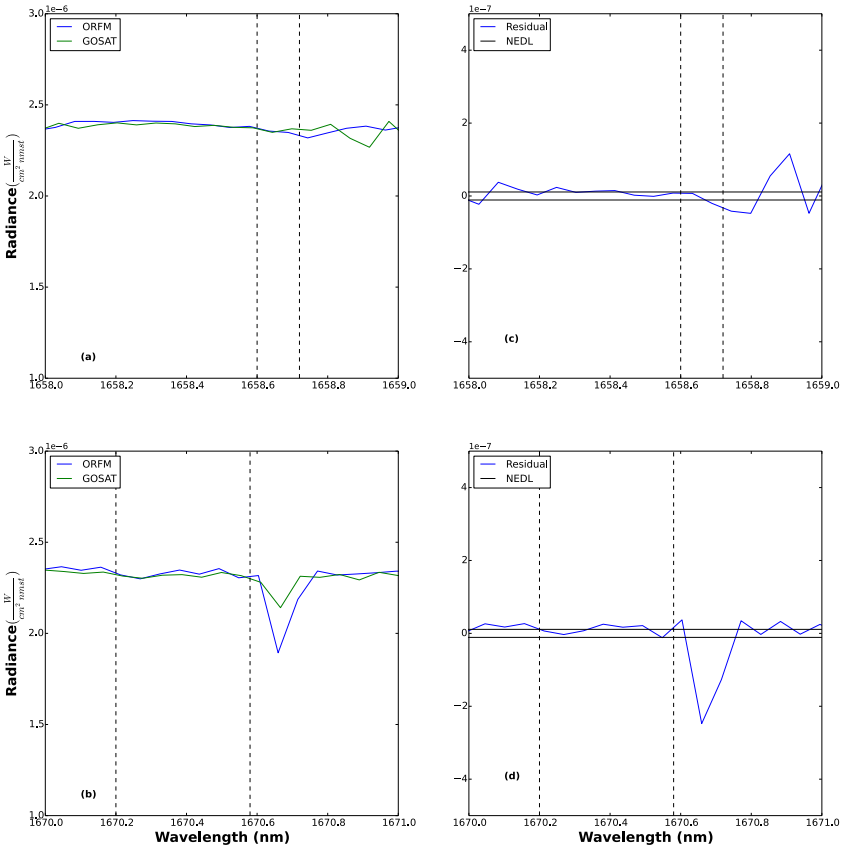

Figure 11. Comparison of simulated spectrum against GOSAT L1B data. In this particular example, the surface reflectance is 0.33, solar zenith angle is 46° and satellite view zenith angle is 24°, the L1B data was captured at a high latitude on 01/06/2016 at 61.7°N, 173°E: (a) highlights the 1658-1659 nm spectral region, where the two dashed lines highlight the exact region of $^{13}CH_4$ activity. The blue lines shows simulated ORFM data and the green line shows GOSAT L1B data; (b) highlights the 1670-1671 nm spectral region, where the two dashed lines highlight the exact region of $^{13}CH_4$ activity. The blue lines show simulated data and the green line shows GOSAT L1B data; (c) shows the residual radiance between the simulated spectrum and the L1B data in the 1658-1659 nm range, the horizontal solid lines represent the FTS NEDL and the two dashed lines highlight the exact region of $^{13}CH_4$ activity; (d) shows the residual radiance between the ORFM spectra and the L1B data in the 1670-1671 nm range, the horizontal solid lines represent the FTS NEDL and the two dashed lines highlight the exact region of $^{13}CH_4$ activity.

Formatted: Caption

A simple and quick sensitivity analysis method for methane isotopologues detection with GOSAT-TANSO-FTS

Edward Malina[1*], Jan-Peter Muller[1], David Walton[1]
[1]Imaging Group, Mullard Space Science Laboratory, Department of Space and Climate Physics, University College London, Holmbury St. Mary, Dorking, Surrey, RH5 6NT, UK.
** Currently at ESA/ESTEC, Noordwijk, The Netherlands.*

Keywords: Methane; Radiative transfer; GOSAT; Isotopologue; SWIR; Education; Outreach

1. Abstract

Measurements of methane isotopologues can differentiate between different source types, be they biogenic (e.g. marsh lands) or abiogenic (e.g. industry). Global measurements of these isotopologues would greatly benefit the current disconnect between "top-down" (knowledge from Chemistry Transport Models (CTMs) and satellite measurements) and "bottom-up" (in situ measurement inventories) methane measurements. However, current measurements of these isotopologues are limited to a small number of in situ studies and airborne studies. In this paper we investigate the potential for detecting the second most common isotopologue of methane ($^{13}CH_4$) from space using the Japanese Greenhouse Gases Observation Satellite (GOSAT) applying a quick and simple residual radiance analysis technique. The method allows for a rapid analysis of spectral regions, and can be used to teach University students or advanced school students about radiative transfer analysis. Using this method we find limited sensitivity to $^{13}CH_4$, with detections limited to total column methane enhancements of >6%, assuming a desert surface albedo of >0.3.

2. Statement of Robustness

The potential impact of methane and other greenhouse gases (GHGs) on the global environment is recognised at the highest levels of government, shown in the recent signing of the COP21 in Paris. Atmospheric methane is composed of differing isotopic concentrations, with $^{12}CH_4$ and $^{13}CH_4$ representing ~99% of total methane concentration. Previous studies have shown that the ratio of these two main 'isotopologues' can indicate if the measurement is from a biological or non-biological source. Therefore the exploitation of this known ratio using new measurement techniques on current GHG measuring satellites is timely as well as necessary; potentially allowing for source apportionment on a global scale. This paper demonstrates a unique assessment towards determining the feasibility of retrieving the main methane isotopologues concentrations in the Earth's atmosphere, using the nadir-sounding instrument Greenhouse Gases Observing Satellite – Thermal and near Infrared Sensor for Carbon Observations – Fourier Transform Spectrometer (GOSAT-TANSO-FTS). The methods used in this paper are designed so that advanced school students or

early University students can easily apply the methods, which is important in the context of science outreach and citizen engagement.

3. Introduction

3.1. Global context

The impact of methane on the environment and its potential for global warming is well documented (IPCC, 2014). Wuebbles and Hayhoe (2002) state that the increasing levels of methane in the atmosphere significantly affects levels of ozone, water vapour (in the stratosphere), hydroxyl radicals, and numerous other compounds in the atmosphere which result from the oxidation of methane (Bréas et al., 2001). All of these occurrences lead to detrimental effects on the chemistry of the atmosphere (for example the formation of tropospheric ozone, and the depletion of atmospheric methane sinks), as well as the absorption of Infra-red (IR) radiation causing atmospheric heating (Bréas et al., 2001). The total global methane budget is not currently well understood, exemplified by multiple contrasting theories for the stall of the global methane concentration between 2000 and 2006 after a century of increase, and then a subsequent rise from 2014 (Nisbet et al., 2016). Aydin et al. (2011) suggest that the drop in global methane output is due to a reduction in the fossil fuel sources of methane, through observations of global concentrations of ethane, which can be used as a global indicator of anthropogenic methane. However in a completely contrasting view, Kai et al. (2011) assert that the reduction in global methane output is in fact due to a reduction in microbial methane from the northern hemisphere; while Mcnorton et al. (2016); Rigby et al. (2012); Turner et al. (2017) suggest that fluctuating hydroxyl radical concentrations is a potential cause of global methane variations. It is therefore important to understand how and where methane is released, and to develop more sophisticated methods of methane detection that will allow for greater understanding of the processes behind methane generation, and how they will affect the global environment.

Methane gas may be formed through multiple natural and anthropogenic processes, including microorganism decomposition of cellulose in sediments under reducing conditions, the breakdown of gas hydrates including clathrates, and thawing permafrost in arctic and subarctic conditions. Melting of the permafrost is a topic of particular concern, with the Arctic warming faster than any other part of the Earth. The Arctic, currently a minor source of methane, could become a major source over the coming century due to warming (Nisbet et al., 2019). Methane emissions from the Arctic is a particularly complex issue, with up to 33% of the world's organic carbon stored within the Arctic permafrost (Schuur et al., 2015), and vast reserves of methane stored in crystalline clathrate structures (Myhre et al., 2016). Yet there is no consensus on how and when these carbon reserves will enter the atmosphere; new data and methods are required to address these uncertainties. Other important processes include, geological processes in the Earth's crust reaching the surface through features such as mud volcanoes or soil exhalation, catagenesis, metamorphism of coal and dispersed organic matter, as well as during petroleum maturation. Anthropogenic sources such as industry bi-products (e.g. leaks from gas plants) and agriculture (e.g. livestock or rice paddy fields) must also be considered as highly significant (Archer et al., 2009; Bréas et al., 2001). Industrial bi-products imply that fossil fuels can be detected by the type of

methane gas given off by their formation and exploitation (Kort et al., 2014; Rella et al., 2013). Towards this end many satellite missions have been focused on trying to measure fossil fuel sources by their methane emissions, including the Japanese Greenhouse Gases Observation Satellite (Kuze et al., 2009; Turner et al., 2015), which was designed specifically for this purpose.

Atmospheric methane consists of a number of different isotopologues (molecules that vary according to their isotopic composition), the main four being $^{12}CH_4$ accounting for roughly 98% of atmospheric methane, $^{13}CH_4$ making up roughly 1.1% of atmospheric methane and CH_3D, present in very small concentrations (roughly 0.06%), with all the other isotopologues present in tiny amounts. The ability to distinguish spectroscopically between the isotopologues of methane can potentially allow the determination of the nature of the source of methane emissions (either biogenic, thermogenic or abiogenic), by taking the ratio of the concentration of $^{12}CH_4$ and $^{13}CH_4$ isotopologues (Etiope and Ciccioli, 2009; Nisbet et al., 2016; Schwietzke et al., 2016). This method has been used effectively for *in situ* terrestrial studies previously and it is this relationship that is the focus of this study. Currently there are limited global measurements of separated methane isotopologues, the majority of measurement sites falling under the National Oceanic and Atmospheric Administration (NOAA) *(www.esrl.noaa.gov/gmd/ccgg/trends_ch4/)* as well as a small number of other independent organisations (Nisbet et al., 2016). Based on this limited spread of measurement sites, the existence of a satellite instrument that can differentiate between methane isotopologues would expand the global knowledge of methane distributions. It has been achieved in the upper troposphere and lower stratosphere with solar occultation limb viewing instruments (Buzan et al., 2016; Irion et al., 1996), and is hoped to be achieved with dedicated potential future instruments (Weidmann et al., 2017).

3.2. GOSAT and measuring radiance

GOSAT-TANSO-FTS measures solar backscatter radiance, such that solar irradiance passes through the atmosphere, is reflected off the surface of the Earth, and passes back through the atmosphere where GOSAT-TANSO-FTS measures the radiance (i.e light magnitude). As this light passes through the atmosphere, it is absorbed at specific frequencies determined by the gases the light passes through. Absorbing this light causing the atoms of the specific gas to change energy levels, these jumps are characterised by spectral lines of finite width. Knowledge of the position of spectral lines for methane (or other gases), means it is possible to calculate how much energy was absorbed by these gases, and therefore how much of this gas is in the path the light travelled through the atmosphere (Tennyson, 2005).

The radiance received at the instrument due to absorption in the Sun-Earth-GOSAT light path is determined by the following equation, known as the 'Beer-Lambert' law (Swinehart, 1962).

$$I(\lambda) = I_0(\lambda)e^{-\sigma C(\lambda)x}. \qquad (1)$$

Where I refers to the intensity of the incident radiation at wavelength λ, given an optical path of thickness x, and I_0 is the intensity of the initial incident light or radiation, C is the density of the light path (or concentration of molecules) and σ is the absorption cross section (or the likelihood of absorption by a given molecule).

A representation of the standard operations of GOSAT is identified in Figure 1, where $I(\lambda)$ is what is received at GOSAT-TANSO-FTS, and σ in the case of this paper refers to methane spectral lines. However, Equation 1 is not directly applicable to what GOSAT-TANSO-FTS measures, since Equation 1 assumes a constant density across the light path. The density of the atmosphere (C) is not constant, meaning Equation 1 must be separately applied for multiple atmospheric layers, in order to accurately measure absorption over a long distance. Larger particles in the atmosphere (e.g. aerosols) can scatter radiation away from the main light path, meaning the difference between I and I_0 is not purely due to absorption. These absorption and scattering properties vary depending on what region of the electromagnetic spectrum is observed. Meaning that prior to attempting to measure the concentration of trace gases in the atmosphere, the most optimum portion of the electromagnetic spectrum must be identified.

The aim of this paper is to identify spectral regions where the main methane isotopologues ($^{12}CH_4$ and $^{13}CH_4$) can be detected with the existing GOSAT-TANSO-FTS. Such studies are typically performed using the Information Content (IC) analysis method described in (Rodgers, 2000), examples of which are also reported in (Herbin et al., 2013; Malina et al., 2018; Yoshida et al., 2011). IC analysis is a powerful tool, but has several significant challenges associated with its use. Firstly, on its own the IC analysis cannot be used to estimate atmospheric trace gas concentration since it is an analysis method and not a full retrieval algorithm (such as (Parker et al., 2011; Schepers et al., 2012; Yoshida et al., 2011)). Secondly, there is a substantial step in effort required to convert the IC analysis method into a retrieval tool capable of trace gas estimation (in terms of computation, analysis methods etc). The current algorithms used to produce trace gas concentrations from instruments such as GOSAT-TANSO-FTS or the recently launched Sentinel-5P/Tropospheric Monitoring Instrument (TROPOMI) are the results of multi-year efforts, built on experience with older instruments (e.g. the SCanning Imaging Absorption SpectroMeter for Atmospheric CHartographY (SCIAMACHY) or similar). Therefore, new research into satellite trace gas retrieval must rely on one of these well-established algorithms, or embark on an expensive development program.

In this paper we propose to use a simple residual radiance analysis technique to identify the suitability of GOSAT-TANSO-FTS for detecting $^{13}CH_4$, and the ratio of $^{13}CH_4$ and $^{12}CH_4$ known as $\delta^{13}C$, which is based on the IC analysis method. Although the residual radiance analysis technique is not as sophisticated as the Optimal Estimation Method (OEM) of (Rodgers, 2000), it remains relevant in the context of trace gas detection/retrieval for its ease of use, and quick applicability. Fundamentally, the residual radiance technique is an excellent starting point for getting familiar with the OEM, and could be an important aspect of advanced school students or University students.

This paper is structured as follows:

- Section 1-3 – Abstract and Introduction.
- Section 4 – Describes the tools and methods used in this study.
- Section 5 – Outlines the results.

- Section 6 – Discusses the results and methods from sections 2 and 3.
- Section 7 – Concludes the findings.

4. Experimental Design and Starting Assumptions

4.1. Methane Source Isotopologue Composition

The isotopic composition of atmospheric background methane and methane sources has been studied at some length (Chanton, 2005; Nisbet et al., 2016; Rigby et al., 2012; Röckmann et al., 2011), especially the four key isotopologues $^{12}CH_4$, $^{13}CH_4$, $^{12}CH_3D$ and $^{13}CH_3D$. These papers effectively describe how the ratios of methane isotopologues (often referred to as "δ" values) can be used to identify the nature of the source. Normally the metrics $\delta^{13}C$ and δD are used to define the ratio of isotopologues at the source. The $\delta^{13}C$ ratio is defined as:

$$\boldsymbol{\delta^{13}C = \left(\frac{\left(\frac{13C}{12C}\right)sample}{\left(\frac{13C}{12C}\right)standard} - 1 \right) \times 1000‰} \quad \textbf{(2)}$$

$\delta^{13}C$ is generated by taking the ratio C13:C12 of the gas sample under investigation, and dividing it by a base ratio (or standard ratio) taken from the established literature known as the Vienna Pee Dee Belemnite, which then determines how far the sample in question deviates from the standard (Craig, 1957). A large negative value indicates that the sample is depleted in C13. Large negative values tend to be associated with biogenic sources of methane, while values closer to 0 are largely from industrial sources.
The methane to deuterium based methane ratio is known as δD is calculated using a similar method to the calculation of $\delta^{13}C$, this ratio divided by an established base ratio taken from the established literature known as the Vienna Standard Ocean Water. However as stated earlier, deuterium based methane is very rare in the atmosphere, and we decided early on to focus solely on $^{13}CH_4$ as opposed to CH_3D.

The main reason for the depletion of the heavier isotopologues in biogenic sources is due to the observation that microorganism formation of methane tends to discriminate against ^{13}C due to Kinetic Isotope Effects (KIEs), accounting for the low $\delta^{13}C$ values. Different forms of microorganisms will have different rates of KIEs, thus changing the $\delta^{13}C$ values with respect to the exact source, however the precise nature of these KIEs is still poorly understood. In addition, specific plants will vary in their ^{13}C signature due to differing photosynthetic enzymes, partially accounting for the range in $\delta^{13}C$ values noted in microbial sources (Schweizer et al., 1999; Whiticar, 1999).

4.2. Radiative Transfer Models – SCIATRAN and ORFM

Radiative Transfer Models (RTMs) are a fundamental aspect of this work, and a key aspect of this study is focused on providing trace gas investigation methods for independent research. It is difficult to perform trace gas research without the use of an

RTM. Developing an RTM from scratch for this project fulfils neither of the quick or simple goals, and we therefore decided to use an open source RTM.

In this study we use the SCIATRAN (Rozanov et al., 2014) RTM, developed by the SCIATRAN working group at the Institute of Environmental Physics and the University of Bremen, available from http://www.iup.uni-bremen.de/sciatran/index.html. SCIATRAN is an RTM capable of solving the radiative transfer equation using multiple numerical methods. SCIATRAN can simulate satellite solar backscatter radiative transfer in both clear-sky and aerosol loaded conditions. SCIATRAN is versatile and can simulate numerous atmospheric effects such as clouds, fluorescence, advanced bidirectional reflectance distribution functions and others for multiple geometry types. For this study the simulations from SCIATRAN are run at a spectral resolution of 0.01 cm^{-1} and are convolved with a TANSO-FTS type Gaussian Instrument Line Shape Function (ILSF) of 0.27 cm^{-1} full width half max (Kuze et al., 2009). All simulations include multiple scattering effects, where all Mie scattering effects assume spherical particles. SCIATRAN has a significant pedigree with previous instruments such as SCIAMACHY, and has been previously used in studies relating to GOSAT previously e.g. (Reuter et al., 2012).

SCIATRAN uses a climatological database derived from a 2D CTM described in (Sinnhuber et al., 2009). All gases, temperatures and pressures are provided in the altitude range 1-95 km for 10° latitudinal bins for all months in a given year. The isotopologue profiles in SCIATRAN are identical to the CH_4 profile included in the simulated atmosphere. The difference in abundance between CH_4 and $^{12/13}CH_4$ is accounted for in the HITRAN2016 database, which scales the isotopologue line strengths by abundance figures provided by (Biévre et al., 1984). The advantage of this method is that the complexity of adding an additional trace gas profile to the forward model is reduced, the disadvantage is that this scaling assumes that this abundance ratio is true for the whole globe (which is unlikely to be true).

Scattering is considered in SCIATRAN, both through Rayleigh scattering and aerosol induced Mie scattering. Rayleigh scattering is not considered in this study as it is minor in the SWIR. For aerosol related scattering SCIATRAN draws upon the LOWTRAN database (Kneizys et al., 1988), which can simulate multiple different aerosol types for different layers of the atmosphere. In this study we assume the standard SCIATRAN/LOWTRAN settings for aerosol loading in SCIATRAN.

The spectral line database used in this study is HITRAN2016 (Gordon et al., 2017). HITRAN2016 builds upon the HITRAN2012 database, but includes an increase in the number of assigned $^{13}CH_4$ spectral lines, with Brown et al (Brown et al., 2013) indicating a significant jump in the number of and accuracy of $^{13}CH_4$ (and $^{12}CH_4$) spectral lines in comparison to the previous HITRAN iteration (HITRAN 2008; (Rothman et al., 2009)). HITRAN2016 includes data from recent studies such as (Starikova et al., 2016), which contain numerous additional line assignments in the spectral range of GOSAT-TANSO-FTS band 2. However it is not suggested that there are any updates to the $^{13}CH_4$ line lists in band 4 of TANSO-FTS.

In addition to SCIATRAN, we also employ the Oxford Reference Forward Model (ORFM; (Dudhia, 2017)), developed at the University of Oxford, and available at http://eodg.atm.ox.ac.uk/RFM/. We do not use the ORFM in the residual radiance

calculations described in the sections below, but rather to simulate atmospheric transmittance and optical depth. This is because the ORFM allows for quick and easy transmission (and absorption) calculations in all of the wavelengths of interest in this study. ORFM is not used for the residual radiance study since a 'sun' is not included in the radiance calculations, and scattering is not included.

4.3. GOSAT-TANSO-FTS

The Japanese Aerospace Exploration Agency (JAXA) launched GOSAT in 2009; GOSAT was the first satellite specifically designed to measure GHG emissions around the globe. The GOSAT project is a joint effort between the Ministry of the Environment (MOE), the National Institute for Environmental Studies (NIES), and JAXA (Kuze et al., 2009; Yokota et al., 2009). GOSAT originally had a 6 year lifespan, but has since been extended. Its replacement was GOSAT-2 was launched in October of 2018, but data is as yet unavailable.

The key instrument on GOSAT is the TANSO-FTS, which measures the radiance of sunlight reflected from the Earth's surface through the atmosphere in three separate bands: the main band of interest in this study is band 2 which measures radiance in the wavenumber range 5814-6410 cm^{-1} (1.56-1.72 μm), with a sampling interval of 0.2 cm^{-1}. GOSAT-TANSO-FTS has a fourth band that measures emissions spectra in the Thermal Infrared (TIR) between 699 – 1799 cm^{-1} (5.56-14.3 μm) (Kuze et al., 2009; Yokota et al., 2009).

GOSAT has a history of providing reliable estimates of the global distributions of methane and carbon dioxide (Parker et al., 2015, 2016; Schepers et al., 2012; Yoshida et al., 2013) since its launch. With its high spectral resolution and high SNR, GOSAT was judged to be a good candidate for detecting methane isotopologues, and therefore prompted this investigation. There are other instruments for measuring methane isotopologues from orbit e.g. SCIAMACHY and TROPOMI. SCIAMACHY has a significantly lower spectral resolution (1.5 cm^{-1}) and has been found to have poor single sounding precision. Buchwitz et al (Buchwitz et al., 2017) state that SCIAMACHY registers a maximum single sounding measurement precision of 30 ppbv, which is unlikely to be sufficient for the retrieval of $^{13}CH_4$, where the total column concentration of $^{13}CH_4$ is roughly 20 ppbv. The recently launched TROPOMI is a possible candidate for methane isotopologues measurements, TROPOMI contains a push-broom spectrometer and sacrifices spectral resolution (0.45 cm^{-1}) for much increased SNR. TROPOMI is likely to be investigated in the future for methane isotopologue detection.

4.4. Study Structure and Methods

The following subsection discusses the structure of the research study. The key aims are to show the following under realistic atmospheric conditions:

a) The optimal regions in bands 2 and 4 of the GOSAT-TANSO-FTS for $^{13}CH_4$ detection.
b) Measurable changes in $^{13}CH_4$ spectral lines over and above the background contaminating gases, and GOSAT-TANSO-FTS instrument noise.

c) The effects of background contaminate gases on any measurable changes.

4.4.1. Spectral Region Identification

The first step of this study is to make an initial assessment as to where the least contaminated regions for $^{13}CH_4$ may be found in the SWIR and TIR. The strongest absorption lines for methane in the SWIR are present within the wavebands at 1.6 μm and 2.3 μm (Brown et al., 2013). However the GOSAT-TANSO-FTS sensitivity to methane is limited to 1.6 μm, in band 2. In the TIR region there is a broadband methane absorption feature at 7.7 μm, which is covered by band 4 of TANSO-FTS. We therefore set-up a simulation scenario with ORFM in order to pick out the maximum absorption points for the $^{13}CH_4$, outlined in Table 1.

The atmospheric model used in this assessment provides a high number of vertical levels and gas concentrations at more recent magnitudes (2002) than the standard mid-latitude model atmospheres (which were designed in the 1970's), and was originally designed to aid in Michelson Interferometer for Passive Atmospheric Sounding (MIPAS) retrievals (Remedios et al., 2007). An example of the atmospheric profiles of three gases from this model is shown in Figure 2.

GOSAT-TANSO-FTS measures the column average density of methane and carbon dioxide (XCH_4, XCO_2); therefore, using the pressure profiles captured in the UoL MIPAS profile, the column-averaged densities can be calculated.

The strongest absorption regions of the methane isotopologues are then investigated in order to gain further insight into the influence of contaminant gases on the isotopologues. The ORFM includes the options to simulate absorption as well as radiance, thus giving some insight into the presence of spectral lines of interest. The conditions required to calculate a typical $^{13}CH_4$ atmospheric absorption profile are specified in Table 1.

4.4.2. Detecting Changes in $^{13}CH_4$ Signal

Background simulated radiance values (containing radiance from the main contaminating gases,) are subtracted from the radiances generated from a scenario with elevated concentrations of methane. If this calculated residual difference is greater than the noise radiance known as the Noise Equivalent Delta Radiance (NEDL) then it suggests that GOSAT-TANSO-FTS could detect this change in methane concentration. This is known as the residual radiance technique, and has been demonstrated by both Roberts et al and Leifer et al (Leifer et al., 2006; Roberts et al., 2010) as an effective technique for assessing whether changes in concentrations of trace gases can be detected. Roberts et al (Roberts et al., 2010) states that spectral residuals are often the first step in full atmospheric inversions. Following the method proposed by (Roberts et al., 2010), the residual radiance technique is used to determine the atmospheric conditions when isotopologue retrieval may be possible. The key question to answer is which combination(s) of methane concentration, water vapour concentration and

surface reflectance allow for a residual radiance greater than the instrumental noise. This can be determined from the equation below.

$$F_d = |L_b(A, \lambda_m) - L_e(A, \lambda_m)| - NEDL, \quad (3)$$

where F_d is the detection factor, where any value above 0 suggests that some signal is detectable above the noise limit, and therefore constitutes a detection. L_b is the background radiance at the wavelength of the maximum radiance λ_m given reflectance A, L_e is the atmospheric radiance with elevated methane concentrations (see Table 3) at the wavelength of the maximum radiance λ_m given reflectance A and NEDL.

Typically NEDL can be calculated from knowledge of instrument parameters (dark current etc), however these parameters are often kept secret by instrument manufacturers. According to the GOSAT-TANSO-FTS instrument manufacturers at JAXA the GOSAT-TANSO-FTS L1B product (interferograms (L1A data) are converted into radiance spectra via a Fourier transform, including some data screening routines). They contain two separate elements: real spectra (equivalent to the radiance spectra of interest in trace gas retrieval), and imaginary spectra which are equivalent to noise from FTS theory. The implication of this is that the noise from the spectrum of a particular retrieval can be extracted from the L1B spectra. Therefore, we generate a relationship where the noise profile of GOSAT-TANSO-FTS is estimated given a radiance output from real spectra. The steps for generating this profile are as follows: Extract the real and imaginary spectra from several L1B data GOSAT-TANSO-FTS band 2 products, in order to get variation in radiance output based on the location and surface characteristics of the retrieval. Calculate the Root Mean Square (RMS) of the off-band imaginary spectrum radiance (where off band is the region where the Indium Gallium Arsenide detector is not sensitive to the incident radiation due to an optical band pass filter present in the instrument). This is equivalent to the inherent instrument noise, and the RMS of the on-band (which is where the detector is sensitive to measured radiance) real spectrum for multiple retrievals. This builds up a profile of how instrument noise varies with received radiance at the detector (dominated by shot noise). The square of the RMS imagery spectrum radiance values are then plotted against the RMS of the real spectrum radiance values; this builds up a profile of how the noise is dependent on the spectral radiance, as well as highlighting what the basic instrument noise is. This allows for a mathematical relationship to be generated, meaning that for any given particular retrieval radiance, a specific noise value can be attributed to it. Using a random selection of 400 GOSAT L1b spectra downloaded from the GOSAT Data Archive Service (https://data2.gosat.nies.go.jp/index_en.html), the following relationship was calculated.

$$\text{NEDL} = \sqrt{(1.76e^{-8}\text{L} + 1.358e^{-11})} \times C, \quad (4)$$

where, L is the received radiance (in $W/cm^2/str/cm^{-1}$) and C is a conversion factor from internal GOSAT units into radiance units. The value of C is available on the GOSAT data archive website in the TANSO-FTS Radiometric Conversion for Band 1-3 document (https://data2.gosat.nies.go.jp/doc/document.html#Document). In this study the NEDL is assumed to be a constant value over the whole spectral range, and we assume that the GOSAT spectra are captured under high gain conditions.

Equation 3 is based on using individual measurements, which will most likely suffer significantly from noise levels. However as suggested by (Roberts et al., 2010) the NEDL can be reduced by averaging multiple spectral measurements focusing on the spectral positions with the most $^{13}CH_4$ information. In such a case the NEDL reduces with √n, where n is the number of spectral sampling points, described by Equation 5 (modified from (Roberts et al., 2010)), below.

$$F_d = \frac{\sum_{\lambda=b}^{\lambda=a}(L_b(A,\lambda_m) - L_e(A,\lambda_m))}{n} - \frac{NEDL}{\sqrt{n}}, \quad (5)$$

where Fd is the detection factor over an averaged number of spectral bands, n is the number of spectral bands for combination, between wavelengths a and b. In the normal operation of GOSAT there is no oversampling of measurement points, until the satellite returns to the same orbital path (i.e. only one spectrum is captured per sample point). In this case the method proposed in Equation 5 cannot be used, since repeat measurements are captured under different conditions. However, Kuze et al. (2012) describe non-standard operational modes, one of which includes 3 repeat measurements of the same point for "sun glint and limited calibration and validation site observations". Although not all GOSAT data will be captured in this way, for simulation purposes, it is justified to investigate the effects of averaging 3 concurrently captured spectra. Indeed, GOSAT has a 'targeted observations' mode, where registered researchers can request observations of specific sites, implying that a large number of concurrently captured spectra could be obtained with this method. The exact details of this mode are not published, and are therefore not modelled in this study. Note that the method described in Equation (5) assumes that errors between spectral points are uncorrelated.

The sensitivity of any $^{12}CH_4$ and $^{13}CH_4$ absorption bands to interfering trace gases and different reflectance conditions must also be considered; the methane absorption windows in the SWIR are typically heavily influenced by water vapour, and therefore any absorption by $^{13}CH_4$ is likely to be affected. The influence of water vapour on specific $^{13}CH_4$ absorption peaks can be determined from the simple ratio factor as described below (modified from (Roberts et al., 2010)).

$$S_f = \frac{\frac{\sum_{\lambda=b}^{\lambda=a} L_{res}(W_s,A)}{n}}{\frac{\sum_{\lambda=b}^{\lambda=a} L_{res}(W_e,A)}{n}}. \quad (6)$$

Where S_f is the sensitivity factor, $L_{res}(W_s,A)$ is the residual radiance between background and elevated methane conditions at standard atmospheric conditions between wavelengths, a and b, $L_{res}(W_e,A)$ is the residual radiance between background and elevated methane conditions with elevated water vapour concentrations between the wavelengths, a and b, and n is the number of spectral measurements considered. Note that this method applies to any desired target and interfering species.

It is important to define appropriate atmospheric scenarios in order to determine feasible detection factors, with the key factors being methane concentration in the atmospheric profile and surface reflectance. Numerous total column retrieval methods

are based on the 'scale' method, where the total column concentration is scaled rather than individual atmospheric layer concentrations modified. Therefore, a range of total column scale factors on which to calculate residuals are specified, appropriate to real world scenarios. The maximum total column XCH_4 values observed from GOSAT tend to be roughly 1900 ppb (Parker et al., 2016), equating to a column scaling of 10% (w.r.t to the MIPAS profile). Very large methane values (>1900 ppb) have been observed by GOSAT in fire affected regions (Parker et al., 2016), suggesting that although >1900 ppb values are possible, they will be found in unique circumstances.

The second key factor, reflectance, can be determined using the online database created by UCL and Noveltis under contract to ESA called "A surface reflectance Database for ESA's earth observation Missions (ADAM)" available at http://adam.noveltis.com/ (Muller et al., 2013). ADAM predicts that the expected Earth surface reflectance values at 1600 nm range from 0.1 for densely vegetated areas, to 0.6 for desert regions (e.g. in the USA or the Sahara).

Based on this range of values, a series of simulation conditions and scenarios were generated as specified in Table 2.

4.4.3. Applying to GOSAT-TANSO-FTS L1B Spectra

The final step in this process is to determine whether or not the changes shown in the results from section 4.4.2 are observable in real L1B spectra. Towards that end, GOSAT L1B spectra were downloaded from the GOSAT Data Archive Service (https://data2.gosat.nies.go.jp/index_en.html), and compared against synthetic spectra, in order to determine what levels of $^{13}CH_4$ variation can be expected over real scenes as opposed to synthetic scenes. Unlike in section 4.4.2, direct comparisons of L1B spectra and synthetic spectra are not quite as simple, since all L1B spectra are captured under a wide range of atmospheric, surface reflectance and instrument geometry conditions. But close conditions are required in order to make any comparisons valid. Therefore, we matched the conditions in real spectra as closely as possibly by 1) Using solar zenith angles and instrument angles identified in the L1B data, 2) Using the geolocation of data capture to inform as to which UoL MIPAS model atmosphere to use. 3) Identify surface reflectance values by fitting reflectance values in 0.001 steps linearly to the synthetic spectra sections until the RMSE difference between the synthetic spectra and the L1B spectra were at a minimum. 4) Convolved the synthetic spectra with the GOSAT instrument line shape model available on the data archive service, and resampled to a 0.2 cm^{-1} grid using a 'Matlab' spline interpolation function. 5) Applied a linear shift to the x axis of the L1B spectra, since the wavenumber axis on TANSO-FTS is variable. The magnitude of the linear shift is defined by wavelength differences between large spectral peaks found in both simulated and measured spectra.

Based on these conditions, direct comparisons between synthetic spectra and L1B spectra were made over known regions of $^{13}CH_4$ activity in the SWIR spectrum. Several hundred L1B data points from June in 2016 were used in order to provide a wide range of atmospheric and surface conditions.

5. Results

5.1. Absorption Assessment

5.1.1. SWIR

Using the atmospheric conditions specified in Table 1, ORFM was used to focus on the 1600-1700nm region. Figure 3 indicates that it will be challenging to resolve $^{13}CH_4$ absorption lines in this spectral region, suggesting that pinpointing $^{13}CH_4$ absorption above background gases will be difficult. The strongest/most dense $^{13}CH_4$ lines appear to be at 1658-1659nm and 1670-1671nm. Focusing on these two spectral regions, the optical depth is explored to determine the effect of background absorbers at these specific wavelengths. Figure 4 makes clear that both of the $^{13}CH_4$ spectral regions indicated have similar optical depth values to those of all of the remaining gases, implying that the majority of absorption in these spectral regions is due to $^{13}CH_4$. However, the spectral line in the 1658-1659nm wavelength range clearly shows the least interference from background contaminating gases, therefore suggesting that it is more suited for retrieval. In spite of this, it is obvious that the optical depth of the $^{13}CH_4$ lines in this region is very low, and it will therefore be challenging to detect any changes to $^{13}CH_4$ in this wavelength range.

5.1.2. TIR

Focusing on the TIR band of GOSAT, we perform a repeat analysis of 4.1.1. Comparing the strength of $^{13}CH_4$ absorption in the TANSO-FTS TIR wavelength range shown in Figure 5 against that in the SWIR shows a number of striking differences, primarily in the magnitude of the absorption. With the strongest of the $^{13}CH_4$ TIR lines having absorption strengths x40 of their SWIR equivalents. Despite this, background interference is still strong, dominated by water vapour continuum absorption. We now focus on the optical depth of two regions, the 7700-7800 nm region due to the strength of $^{13}CH_4$ absorption in this region, and the 8050-8150 nm range due to the lower background absorbance.

The optical depth survey shown in Figure 6 demonstrates magnitudes far in excess of the SWIR optical depth in Figure 4 (especially Figure 6(a), where the atmosphere is opaque), but as shown in Figures 5 and 6, the background interference on the $^{13}CH_4$ signal is significant, with only minor impacts from the $^{13}CH_4$ spectral lines. This leaves us with the unenviable position of small optical depth but low background interference in the SWIR, and high optical depth but high levels of interference in the TIR.

Figure 6 suggests that $^{12}CH_4$ and other background gases will dominate the residual radiance method for the TIR. Therefore for this reason, and that measurements in the TIR are often more uncertain than SWIR measurements, exemplified in multiple studies (Holl et al., 2016; Ohyama et al., 2013, 2017), we decided to focus on the SWIR in this study. In addition it has been shown that the SNR on the methane absorption regions in GOSAT are significantly lower than in the SWIR (Holl et al., 2016; Zou et al., 2016), suggesting that the TIR is not ideal for methane retrieval with GOSAT. TIR instruments are heavily based on measuring thermal contrast between atmospheric layers, and because of the lack of such contrast in the lower troposphere, therefore have limited sensitivity near the surface (Clerbaux et al., 2009; Worden et al., 2015). This suggests that measurements in the SWIR are far more likely to capture methane fractionation at the surface than in the TIR. There are cases with global scenes with high thermal contrast, which will allow for sensitivity to the surface for TIR instruments, however we believe that the low SNR of TANSO-FTS band 4 is the more important issue, as opposed to surface sensitivity.

5.2. $^{13}CH_4$ Detectability under Standard Conditions

Based on the simulation conditions specified in Table 2, consideration is given as to whether or not the individual peaks highlighted in Figure 4 will exceed the NEDL. Figures 5 and 8 show example results for two different surface albedos, for all the proposed methane concentration levels.

The results in Figures 7 and 8 suggest that detecting changes in concentration of $^{13}CH_4$ using individual peaks is unlikely to succeed, with only the highest methane concentrations at the highest albedo levels giving a positive detection and all other residual radiance calculations falling below the NEDL line. However, if we assume the GOSAT sampling pattern which takes three concurrent measurements of the same area (Kuze et al., 2012), by applying Equation 5, and using the mean of $^{13}CH_4$ residual radiance peaks, the NEDL is reduced by $\sqrt{3}$. These are summarised in Table 3.

Considering the results outlined in Table 3 it is clear that the feasibility of detecting any change in $^{13}CH_4$ concentration above the NEDL is going to be difficult. The results indicate that the minimum requirements for measuring $^{13}CH_4$ concentration with any certainty are a methane source of at least 10% higher concentration than background total column value, with a high surface albedo of 0.3. Although such a combination of conditions is possible, it would likely be limited to wildfire regions such as (Parker et al., 2016). Note that the detection factors between the two regions of interest are very similar.

We note in section 3.2 that HITRAN2016 includes an intensity adjustment for methane isotopologues that accounts for natural atmospheric abundance. We now investigate if the detection factors indicated in Table 3 change, if we assume the standard $\delta^{13}C$ value is -70‰ as opposed to 0‰. To achieve this, we modified the isotopologues intensity in HITRAN2016, by assuming Vienna Pee Dee Belemnite is 0.0010326 as opposed to

0.0011031. Then we reran the scenarios shown in Table 2; the results for the albedo = 0.3 case are shown in Figure 9.

Figure 9 is interesting because it shows that the $^{13}CH_4$ peak at 1658.6 nm is highly sensitive to changes in the assumed $\delta^{13}C$ value, to the point where changes of the methane column concentration has practically no impact on the residual radiance. While the spectral lines at 1670.4 is not as sensitive to the change in $\delta^{13}C$ value, and as indicated in Table 4, actually shows an increase in the magnitude of the detection factors.

The HITRAN2016 database suggests that the $^{13}CH_4$ spectral lines in the 1670.2-1670.6 nm are made up of a number of different transitions, which exhibit a range of lower state energy values. A number of which are of similar magnitude to those for the main methane isotopologue $^{12}CH_4$. While the lower state energy levels for $^{12}CH_4$ are significantly larger than those for the $^{13}CH_4$ lines in the 1658 – 1659 nm range, which explains this difference in reactions to changes in the standard $\delta^{13}C$ values.

In addition to the simulations for the $\delta^{13}C$ values of 0‰ and -70‰, we also performed an analysis for $\delta^{13}C$ values of -35‰. Based on the detection factors for the range of $\delta^{13}C$ value shown in this study, we can plot these variables and determine the conditions where GOSAT can detect differences in $\delta^{13}C$ values.

Based on the detection values indicated in Tables 3, and 4, and given similar results from an analysis of $\delta^{13}C$ values of -35‰. We can plot a relationship between the detection values and the surface albedo for a given $\delta^{13}C$ value.

Figure 10 is interesting since it shows that the 1658 nm band has more sensitivity to changes in surface reflectance, and total column methane concentration than the 1670 nm band. But only in the case where $\delta^{13}C$ is assumed to be equal to zero. For the other $\delta^{13}C$ cases shown in Figure 10, there are no examples where the detection factor is greater than 0. For the 1670 nm band, although the detection factors are lower in magnitude, the sensitivity to changes in the $\delta^{13}C$ are minor. These results imply (focusing on the 1670 nm band), that given a significant enhancement in the total methane column, and a high enough surface reflectance, it may be possible to detect changes in the $\delta^{13}C$ of the measurement. Since the detection factor can be related back to a total methane column value, $\delta^{13}C$ values could be directly estimated. Assuming some knowledge of $^{12}CH_4$. Figure 10 suggests that the lowest possible surface albedo of 0.35, requires an enormous methane enhancement of 8% in order to achieve a detection of $^{!3}CH_4$, while the highest surface albedo of 0.6 requires an enhancement of 5 or 6%.

The required surface conditions to achieve the above values are not common. Using the aforementioned ADAM dataset (http://adam.noveltis.com/), we can indicate how much of the Earth's land surface has surface albedo values of at least 0.3. The database suggests that a significant proportion of the Earth has >0.3 surface albedo. Significantly the biomass burning regions indicated in (Parker et al., 2016) have the required surface albedo, thus suggesting that in the scenarios observed in (Parker et al., 2016) it would be possible to detect $^{13}CH_4$ signals with GOSAT using the methods described in this paper.

5.3. $^{13}CH_4$ Detectability under High Water Vapour Conditions

Using Equation 6 we can interpret the potential effects of varying water vapour concentration on the spectral averaging factor, given the high water vapour concentration conditions specified in Table 3. Based on the sensitivity factors indicated in Table 5, it is clear that both of the spectral bands we investigate in this paper are affected by the increase in loading of water vapour to some degree. The 1658 nm band is affected to a far less extent than the 1670 nm band (~10%). Most likely because the 1658 nm band is narrower than the 1670 nm band. For both bands the scaling of the methane column has a negligible effect, meaning that the high methane scenarios required to detect $^{13}CH_4$ will not be subject to water vapour errors, any more than high surface albedo scenarios. The loading of the water vapour column by 100% is not an unreasonable scenario when considering the difference between mid-latitude scenes and tropical scenes.

5.4. Comparisons with GOSAT-TANSO-FTS L1B Data

The assessments outlined above are predominately based on using synthetic data; it is therefore important to determine if variations in $^{13}CH_4$ can occur in real measured GOSAT-TANSO-FTS L1B spectra. Based on the method described in section 4.4.3, direct comparisons can be made between the synthetic data and L1B data. Figure 11 represents an interesting counter perspective to the results shown in the previous sections. Figure 11(a) shows largely good agreement between the ORFM and L1B spectra, aside from two spectral line absorption points in the L1B data, not present in the ORFM simulation (highlighted in Figure 11(b)), possibly due to residuals not captured in the ORFM simulations. Despite this, there is very little difference between the radiances of the ORFM and L1B spectra in the highlighted portion.
However, considering Figure 11(c), the closely matching spectra indicate a reasonable fit from the method discussed in section 2.4.3. Focusing on the highlighted region in Figure 11(c) and (d) show a variation in the radiance of the $^{13}CH_4$ region, suggesting potential for GOSAT measuring changes in $^{13}CH_4$ over background concentrations. An important point to consider is the water vapour spectral line peak at 1670.68 nm; the ORFM simulations suggest a higher concentration of water vapour in the atmosphere based on the depth of the spectral line than the L1B data. Section 3.3 shows that the methane isotopologue spectral lines are heavily influenced by water vapour; therefore the lower concentrations of water vapour in the L1B spectrum, combined with the high reflectance value may allow for variation in the $^{13}CH_4$ concentration to become more obvious than suggested in the simulation studies. Therefore, in some scenarios, a high surface reflectance of at least 0.6 may not be necessary.

6. Discussion

The range of scenarios where $^{13}CH_4$ can be detected is very small. We acknowledge that this method is not as sophisticated or as accurate as a full sensitivity analysis using

Rodgers optimal estimation method. However we argue that the benefits of the method shown in this study is its simplicity, such that a quick analysis can be performed by a lay person interested in the subject area, or it could be used to teach advanced school students, or early year University students. Indeed scientists interested in quickly determining the sensitivity of a trace gas species could use this method as a quick first step, before committing to further analysis. The most complex part of this study is the RTM, and here we use two well established RTMs to achieve the goals of this study. RTM development is a far more complex task than developing a retrieval algorithm, and independently developing an RTM would no longer make this study simple or quick. There are significantly more open source RTMs available than retrieval algorithms, this variety in RTMs mean that there should be sufficient ranges in solutions and methods that allow for characterisation of any errors in the forward models.

The detection analysis outlined in section 4.4.2 is based on the total column of methane detection of $\delta^{13}C$, this method is potentially limiting to a degree since this does not take into account KIEs in the upper troposphere and lower stratosphere due to the destruction of methane. However, since $^{13}CH_4$ concentration is low, and the KIE factors are less than those at the surface, such factors are unlikely to have a significant impact on the results. In addition atmospheric air currents interfere with the total column and thus will dampen the signal of $\delta^{13}C$ in the total column, as opposed to in situ measurements. There are currently no studies that investigate this effect, but we can assume that the $\delta^{13}C$ differences between source types will be even smaller.

Other error sources include the spectroscopy and the forward model. The HITRAN2016 database in combination with the SCIATRAN forward model assumes a Voigt profile for all methane lines in the GOSAT spectral sensitivity ranges. The Voigt profile has been generally assumed for methane spectral regions in the past, however this shape is now acknowledged to be no longer sufficient (Gordon et al., 2017). The current HITRAN2016 database does not include the parameters necessary to estimate non-Voigt line shapes for methane; however it is anticipated that future updates will include these. We therefore accept that there will be spectroscopic errors present in this study. Following on from the HITRAN database, the next largest error sources are likely to arise from SCIATRAN, generated from inaccuracies in recreating the absorption or radiance spectra from a given set of atmospheric inputs.

The metrics F_d and S_f give a useful indication of the feasibility of detecting $^{13}CH_4$, and can be used to further inform a user about the feasibility of detection over a wider variety of atmospheric and surface conditions than shown in this study. However, caution must be applied since as highlighted in Table 5, the influence of water vapour on the $^{13}CH_4$ peaks might well lead to false positive values of F_d, and therefore create an incorrect inference of isotopologues detection.

Although we briefly looked at methane isotopologues absorption in the GOSAT TIR band, we did not investigate this in depth. This is despite the fact that the isotopologues indicated much larger optical depth than their equivalent in the SWIR. However there is significant evidence to suggest that the spectroscopy of methane in the TIR is not nearly as advanced as that in the SWIR (De Lange and Landgraf, 2018), which is important given the short wavebands used in this study. In addition to the high levels of background interference on the $^{13}CH_4$ spectral lines observed in Figure 6.

An obvious next or alternative step would is to perform retrievals of the methane isotopologues using the Total Column Carbon Observing Network (TCCON, (Wunch et al., 2011)). TCCON relies on solar occultation measurements as opposed to solar backscatter, and operates at a much higher SNR and spectral resolution than GOSAT. The key disadvantage to TCCON is that it is limited to a small number of sites all over the globe, and cannot be as beneficial to global studies as satellites such as GOSAT. This work has been shown in a separate study, indicating that even with the improved SNR of the TCCON instruments, there are still significant challenges with retrievals of methane isotopologues (Malina et al., 2020)

7. Conclusions

In this paper we investigated the potential to detect the second most common methane isotopologue ($^{13}CH_4$) using the GOSAT-TANSO-FTS instrument. The ratio of the main methane isotopologues has been shown to be able to differentiate between different methane source types, and could be a useful tool in linking global bottom-up emissions with top-down emissions.

We use a simple and quick residual radiance method in order to investigate the benefit of such techniques, in the wider context of the more sophisticated methods based on Rodgers' optimal estimation techniques. We argue that the residual radiance technique is useful as a simple and quick method for analysing spectral regions for sensitivity to specific trace gases.

The results of this study generally suggest that detecting the second most important methane isotopologue is difficult in most circumstances, apart from unique circumstances such as large biomass burning events. Using these techniques we find that detections of $^{13}CH_4$ with GOSAT can only occur with surface albedos of >0.3, assuming at least an 8% enhancement in the methane total column. This total column requirement is reduced with increasing surface albedo. In the context of a world where El Nino events are likely to become more frequent, it is possible that the required conditions for $^{13}CH_4$ detection using this technique, may become more common.

We perform the assessment using the general assumption of $\delta^{13}C = 0$ globally as this is built into the HITRAN databases. However we also investigate the effects of detecting the $^{13}CH_4$ isotopologue using different values of $\delta^{13}C$, ranging up to -70‰. We find that the spectral lines in the 1670 nm waveband are unaffected by the change in $\delta^{13}C$, while other spectral regions are significantly affected by this change.

We also assess the suitability of the TIR region for methane isotopologues, and find that although the optical depth of $^{13}CH_4$ is greater than that in the SWIR region, the dominance of background trace gases, and the unknowns in the spectroscopy of the region make this region less attractive than the SWIR.

Acknowledgments
We would also like to acknowledge Anu Dudhia at Oxford University for the ORFM, the SCIATRAN working group at the Institute of Environmental Physics at the University of

Bremen for SCIATRAN, HITRAN for HITRAN2016 and JAXA/NIES/MOE for GOSAT-TANSO-FTS L1B data.

Funding Statement
This research has been funded under a PhD grant (award number 157550) from the National Centre for Earth Observation (NCEO) through the Natural Environment Research Council (NERC) based in the UK.

Data Accessibility

HITRAN2016 data is available from https://hitran.org/. The OFRM is available through the website http://eodg.atm.ox.ac.uk/RFM/. SCIATRAN is available through http://www.iup.uni-bremen.de/sciatran/index.html. The GOSAT L1B data is available through the GOSAT Data Archive Service https://data2.gosat.nies.go.jp/index_en.html.

The ORFM and SCIATRAN simulations used in this paper are fully reproducible given the input parameters provided in this paper.

Competing Interests
'There are no competing interests.'

Authors' Contributions
E.M., J-P. M. and D.W. conceived and designed the experiments; E.M. performed the experiments, analysed the data and wrote the paper; D.W. contributed code for initial HITRAN line survey analysis. JPM contributed the reflectance analysis.

8. Glossary

This section provides a table of key terms and acronyms.

9. References

Archer, D., Buffett, B., Brovkin, V. and Schellnhuber, H. J.: Ocean methane hydrates as a slow tipping point in the global carbon cycle, PNAS, 106(49), 20596–20601, doi:10.1073/pnas.0800885105, 2009.
Aydin, M., Verhulst, K. R., Saltzman, E. S., Battle, M. O., Montzka, S. A., Blake, D. R., Tang, Q. and Prather, M. J.: Recent decreases in fossil-fuel emissions of ethane and methane derived from firn air, Nature, 476(7359), 198–201, doi:10.1038/nature10352, 2011.
Biévre, P., Gallet, M., Holden, N. E. and Barnes, I. L.: Isotopic Abundances and Atomic Weights of the Elements, J. Phys. Chem. Ref. Data, 13(3), 809–891, doi:10.1063/1.555720, 1984.
Bréas, O., Guillou, C., Reniero, F. and Wada, E.: The Global Methane Cycle: Isotopes and Mixing Ratios, Sources and Sinks, Isotopes Environ. Health Stud., 37(4), 257–379,

doi:10.1080/10256010108033302, 2001.
Brown, L. R., Sung, K., Benner, D. C., Devi, V. M., Boudon, V., Gabard, T., Wenger, C., Campargue, A., Leshchishina, O., Kassi, S., Mondelain, D., Wang, L., Daumont, L., Régalia, L., Rey, M., Thomas, X., Tyuterev, V. G., Lyulin, O. M., Nikitin, A. V, Niederer, H. M., Albert, S., Bauerecker, S., Quack, M., O'Brien, J. J., Gordon, I. E., Rothman, L. S., Sasada, H., Coustenis, A., Smith, M. A. H., Carrington, T., Wang, X. G., Mantz, A. W. and Spickler, P. T.: Methane line parameters in the HITRAN2012 database, J. Quant. Spectrosc. Radiat. Transf., 130, 201–219, doi:10.1016/j.jqsrt.2013.06.020, 2013.
Buchwitz, M., Schneising, O., Reuter, M., Heymann, J., Krautwurst, S., Bovensmann, H., Burrows, J. P., Boesch, H., Parker, R. J., Somkuti, P., Detmers, R. G., Hasekamp, O. P., Aben, I., Butz, A., Frankenberg, C. and Turner, A. J.: Satellite-derived methane hotspot emission estimates using a fast data-driven method, Atmos. Chem. Phys., 17(9), 5751–5774, doi:10.5194/acp-17-5751-2017, 2017.
Buzan, E. M., Beale, C. A., Boone, C. D. and Bernath, P. F.: Global stratospheric measurements of the isotopologues of methane from the Atmospheric Chemistry Experiment Fourier transform spectrometer, Atmos. Meas. Tech, 9, 1095–1111, doi:10.5194/amt-9-1095-2016, 2016.
Chanton, J. P.: The effect of gas transport on the isotope signature of methane in wetlands, , doi:10.1016/j.orggeochem.2004.10.007, 2005.
Clerbaux, C., Boynard, A., Clarisse, L., George, M., Hadji-Lazaro, J., Herbin, H., Hurtmans, D., Pommier, M., Razavi, A., Turquety, S., Wespes, C. and Coheur, P. F.: Monitoring of atmospheric composition using the thermal infrared IASI/MetOp sounder, Atmos. Chem. Phys., 9(16), 6041–6054, doi:10.5194/acp-9-6041-2009, 2009.
Craig, H.: Isotopic standards for carbon and oxygen and correction factors for mass-spectrometric analysis of carbon dioxide, Geochim. Cosmochim. Acta, 12(1–2), 133–149, doi:10.1016/0016-7037(57)90024-8, 1957.
Dudhia, A.: The Reference Forward Model (RFM), J. Quant. Spectrosc. Radiat. Transf., 186, 243–253, doi:10.1016/j.jqsrt.2016.06.018, 2017.
Etiope, G. and Ciccioli, P.: Earth's Degassing: A Missing Ethane and Propane Source, Science (80-.)., 323(5913), 478–478, doi:10.1126/science.1165904, 2009.
Gordon, I. E., Rothman, L. S., Hill, C., Kochanov, R. V., Tan, Y., Bernath, P. F., Birk, M., Boudon, V., Campargue, A., Chance, K. V., Drouin, B. J., Flaud, J.-M., Gamache, R. R., Hodges, J. T., Jacquemart, D., Perevalov, V. I., Perrin, A., Shine, K. P., Smith, M.-A. H., Tennyson, J., Toon, G. C., Tran, H., Tyuterev, V. G., Barbe, A., Császár, A. G., Devi, V. M., Furtenbacher, T., Harrison, J. J., Hartmann, J.-M., Jolly, A., Johnson, T. J., Karman, T., Kleiner, I., Kyuberis, A. A., Loos, J., Lyulin, O. M., Massie, S. T., Mikhailenko, S. N., Moazzen-Ahmadi, N., Müller, H. S. P., Naumenko, O. V., Nikitin, A. V., Polyansky, O. L., Rey, M., Rotger, M., Sharpe, S. W., Sung, K., Starikova, E., Tashkun, S. A., Auwera, J. Vander, Wagner, G., Wilzewski, J., Wcisło, P., Yu, S. and Zak, E. J.: The HITRAN2016 Molecular Spectroscopic Database, J. Quant. Spectrosc. Radiat. Transf., doi:10.1016/j.jqsrt.2017.06.038, 2017.
Herbin, H., -Labonnote, L. C. and Dubuisson, P.: Multispectral information from TANSO-FTS instrument – Part 1: Application to greenhouse gases (CO 2 and CH 4) in clear sky conditions, Atmos. Meas. Tech, 6, 3301–3311, doi:10.5194/amt-6-3301-2013, 2013.
Holl, G., Walker, K. A., Conway, S., Saitoh, N., Boone, C. D., Strong, K. and Drummond, J. R.: Methane cross-validation between three Fourier transform spectrometers: SCISAT ACE-FTS, GOSAT TANSO-FTS, and ground-based FTS measurements in the Canadian high Arctic, Atmos. Meas. Tech., 9(5), 1961–1980, doi:10.5194/amt-9-1961-2016, 2016.
IPCC: Fifth Assessment Report - Impacts, Adaptation and Vulnerability, [online]

Available from: http://www.ipcc.ch/report/ar5/wg2/ (Accessed 12 June 2017), 2014.
Irion, F. W., Moyer, E. J., Gunson, M. R., Rinsland, C. P., Yung, Y. L., Michelsen, H. A., Salawitch, R. J., Chang, A. Y., Newchurch, M. J., Abbas, M. M., Abrams, M. C. and Zander, R.: Stratospheric observations of CH_3D and HDO from ATMOS infrared solar spectra: Enrichments of deuterium in methane and implications for HD, Geophys. Res. Lett., 23(17), 2381–2384, doi:10.1029/96GL01402, 1996.
Kai, F. M., Tyler, S. C., Randerson, J. T. and Blake, D. R.: Reduced methane growth rate explained by decreased Northern Hemisphere microbial sources, Nature, 476(7359), 194–197, doi:10.1038/nature10259, 2011.
Kneizys, F. X., Anderson, G. P., Shettle, E. P., Gallery, W. O., Abreu, L. W., Selby, J. E. A., Chetwynd, J. H. and Clough, S. A.: Users guide to LOWTRAN 7. [online] Available from: https://apps.dtic.mil/dtic/tr/fulltext/u2/a206773.pdf (Accessed 12 January 2019), 1988.
Kort, E. A., Frankenberg, C., Costigan, K. R., Lindenmaier, R., Dubey, M. K. and Wunch, D.: Four corners: The largest US methane anomaly viewed from space, Geophys. Res. Lett., 41(19), 6898–6903, doi:10.1002/2014GL061503, 2014.
Kuze, A., Suto, H., Nakajima, M. and Hamazaki, T.: Thermal and near infrared sensor for carbon observation Fourier-transform spectrometer on the Greenhouse Gases Observing Satellite for greenhouse gases monitoring, Appl. Opt., 48(35), 6716, doi:10.1364/AO.48.006716, 2009.
Kuze, A., Suto, H., Shiomi, K., Urabe, T., Nakajima, M., Yoshida, J., Kawashima, T., Yamamoto, Y., Kataoka, F. and Buijs, H.: Level 1 algorithms for TANSO on GOSAT: processing and on-orbit calibrations, Atmos. Meas. Tech, 5, 2447–2467, doi:10.5194/amt-5-2447-2012, 2012.
De Lange, A. and Landgraf, J.: Methane profiles from GOSAT thermal infrared spectra, Atmos. Meas. Tech., 11(6), 3815–3828, doi:10.5194/amt-11-3815-2018, 2018.
Leifer, I., Roberts, D., Margolis, J. and Kinnaman, F.: In situ sensing of methane emissions from natural marine hydrocarbon seeps: A potential remote sensing technology, Earth Planet. Sci. Lett., 245(3–4), 509–522, doi:10.1016/j.epsl.2006.01.047, 2006.
Malina, E., Yoshida, Y., Matsunaga, T. and Muller, J. P.: Information content analysis: The potential for methane isotopologue retrieval from GOSAT-2, Atmos. Meas. Tech., 11(2), 1159–1179, doi:10.5194/amt-11-1159-2018, 2018.
Malina, E., Veihelmann, B., Feist, D. and Morino, I.: On the consistency of methane isotopologue retrievals using TCCON and multiple spectroscopic databases, Atmos. Meas. Tech. Discuss., 1–44, doi:10.5194/amt-2020-86, 2020.
Mcnorton, J., Chipperfield, M. P., Gloor, M., Wilson, C., Feng, W., Hayman, G. D., Rigby, M., Krummel, P. B., O 'doherty, S., Prinn, R. G., Weiss, R. F., Young, D., Dlugokencky, E. and Montzka, S. A.: Role of OH variability in the stalling of the global atmospheric CH 4 growth rate from 1999 to 2006, Atmos. Chem. Phys, 16, 7943–7956, doi:10.5194/acp-16-7943-2016, 2016.
Muller, J.-P., Lewis, P., Bréon, F.-M., Bacour, C., Price, I., Chaumat, L., Prunet, P., Gonzales, L., Schlundt, C., Vountas, M., Burrows, J., von Hoyningen-Huene, W., Guanter, L., Fischer, J., North, P., Heckel, A. and Straume-Lindner, A. G.: A Surface Reflectance Database for ESA's Earth Observation Missions (ADAM), ESA Living Planet Symposium , Edinburgh. [online] Available from: http://www.livingplanet2013.org/abstracts/849688.htm (Accessed 13 June 2017), 2013.
Myhre, C. L., Ferré, B., Platt, S. M., Silyakova, A., Hermansen, O., Allen, G., Pisso, I., Schmidbauer, N., Stohl, A., Pitt, J., Jansson, P., Greinert, J., Percival, C., Fjaeraa, A. M., O'Shea, S. J., Gallagher, M., Le Breton, M., Bower, K. N., Bauguitte, S. J. B., Dalsøren, S.,

Vadakkepuliyambatta, S., Fisher, R. E., Nisbet, E. G., Lowry, D., Myhre, G., Pyle, J. A., Cain, M. and Mienert, J.: Extensive release of methane from Arctic seabed west of Svalbard during summer 2014 does not influence the atmosphere, Geophys. Res. Lett., 43(9), 4624–4631, doi:10.1002/2016GL068999, 2016.
Nisbet, E. G., Dlugokencky, E. J., Manning, M. R., Lowry, D., Fisher, R. E., France, J. L., Michel, S. E., Miller, J. B., White, J. W. C., Vaughn, B., Bousquet, P., Pyle, J. A., Warwick, N. J., Cain, M., Brownlow, R., Zazzeri, G., Lanoisellé, M., Manning, A. C., Gloor, E., Worthy, D. E. J., Brunke, E.-G., Labuschagne, C., Wolff, E. W. and Ganesan, A. L.: Rising atmospheric methane: 2007-2014 growth and isotopic shift, Global Biogeochem. Cycles, 30(9), 1356–1370, doi:10.1002/2016GB005406, 2016.
Nisbet, E. G., Manning, M. R., Dlugokencky, E. J., Fisher, R. E., Lowry, D., Michel, S. E., Myhre, C. L., Platt, S. M., Allen, G., Bousquet, P., Brownlow, R., Cain, M., France, J. L., Hermansen, O., Hossaini, R., Jones, A. E., Levin, I., Manning, A. C., Myhre, G., Pyle, J. A., Vaughn, B. H., Warwick, N. J. and White, J. W. C.: Very Strong Atmospheric Methane Growth in the 4 Years 2014–2017: Implications for the Paris Agreement, Global Biogeochem. Cycles, 33(3), 318–342, doi:10.1029/2018GB006009, 2019.
Ohyama, H., Kawakami, S., Shiomi, K., Morino, I. and Uchino, O.: Atmospheric Temperature and Water Vapor Retrievals from GOSAT Thermal Infrared Spectra and Initial Validation with Coincident Radiosonde Measurements, SOLA, 9(0), 143–147, doi:10.2151/sola.2013-032, 2013.
Ohyama, H., Kawakami, S., Shiomi, K., Morino, I. and Uchino, O.: Intercomparison of XH2O data from the GOSAT TANSO-FTS (TIR and SWIR) and ground-based FTS measurements: Impact of the spatial variability of XH2O on the intercomparison, Remote Sens., 9(1), 64, doi:10.3390/rs9010064, 2017.
Parker, R., Boesch, H., Cogan, A., Fraser, A., Feng, L., Palmer, P. I., Messerschmidt, J., Deutscher, N., Griffith, D. W. T., Notholt, J., Wennberg, P. O. and Wunch, D.: Methane observations from the Greenhouse Gases Observing SATellite: Comparison to ground-based TCCON data and model calculations, Geophys. Res. Lett., 38(15), doi:10.1029/2011GL047871, 2011.
Parker, R. J., Boesch, H., Byckling, K., Webb, A. J., Palmer, P. I., Feng, L., Bergamaschi, P., Chevallier, F., Notholt, J., Deutscher, N., Warneke, T., Hase, F., Sussmann, R., Kawakami, S., Kivi, R., Griffith, D. W. T. and Velazco, V.: Assessing 5 years of GOSAT Proxy XCH 4 data and associated uncertainties, Atmos. Meas. Tech, 8, 4785–4801, doi:10.5194/amt-8-4785-2015, 2015.
Parker, R. J., Boesch, H., Wooster, M. J., Moore, D. P., Webb, A. J., Gaveau, D., Murdiyarso, D. and Parker, R.: Atmospheric CH 4 and CO 2 enhancements and biomass burning emission ratios derived from satellite observations of the 2015 Indonesian fire plumes, Atmos. Chem. Phys, 16, 10111–10131, doi:10.5194/acp-16-10111-2016, 2016.
Rella, C. W., Crosson, E., Jacobson, G., Karion, A., Petron, G. and Sweeney, C.: Quantifying the relative contribution of natural gas fugitive emissions to total methane emissions in Colorado and Utah using mobile d 13 CH 4 analysis, pp. 12–1, EGU, Vienna. [online] Available from: https://www.picarro.com/sites/default/files/Rella IG4 - S4.12 - BG1.4 - 20130411 - 0845.pdf (Accessed 12 June 2017), 2013.
Remedios, J. J., Leigh, R. J., Waterfall, A. M., Moore, D. P., Sembhi, H., Parkes, I., Greenhough, J., Chipperfield, M. P. and Hauglustaine, D.: MIPAS reference atmospheres and comparisons to V4.61/V4.62 MIPAS level 2 geophysical data sets, Atmos. Chem. Phys. Discuss. Eur. Geosci. Union, 7(4), 9973–10017, doi:10.5194/acpd-7-9973-2007, 2007.
Reuter, M., Bovensmann, H., Buchwitz, M., Burrows, J. P., Deutscher, N. M., Heymann, J.,

Rozanov, A., Schneising, O., Suto, H., Toon, G. C. and Warneke, T.: On the potential of the 2041-2047nm spectral region for remote sensing of atmospheric CO 2 isotopologues, J. Quant. Spectrosc. Radiat. Transf., 113(16), 2009–2017, doi:10.1016/j.jqsrt.2012.07.013, 2012.
Rigby, M., Manning, A. J. and Prinn, R. G.: The value of high-frequency, high-precision methane isotopologue measurements for source and sink estimation, J. Geophys. Res. Atmos., 117(12), doi:10.1029/2011JD017384, 2012.
Roberts, D. A., Bradley, E. S., Cheung, R., Leifer, I., Dennison, P. E. and Margolis, J. S.: Mapping methane emissions from a marine geological seep source using imaging spectrometry, Remote Sens. Environ., 114(3), 592–606, doi:10.1016/j.rse.2009.10.015, 2010.
Röckmann, T., Brass, M., Borchers, R. and Engel, A.: The isotopic composition of methane in the stratosphere: High-altitude balloon sample measurements, Atmos. Chem. Phys., 11(24), 13287–13304, doi:10.5194/acp-11-13287-2011, 2011.
Rodgers, C. D.: Inverse Methods for Atmospheric Sounding - Theory and Practice, World Scientific., 2000.
Rothman, L. S., Gordon, I. E., Barbe, A., Benner, D. C., Bernath, P. F., Birk, M., Boudon, V., Brown, L. R., Campargue, A., Champion, J.-P., Chance, K., Coudert, L. H., Dana, V., Devi, V. M., Fally, S., Flaud, J.-M., Gamache, R. R., Goldman, A., Jacquemart, D., Kleiner, I., Lacome, N., Lafferty, W. J., Mandin, J.-Y., Massie, S. T., Mikhailenko, S. N., Miller, C. E., Moazzen-Ahmadi, N., Naumenko, O. V., Nikitin, A. V., Orphal, J., Perevalov, V. I., Perrin, A., Predoi-Cross, A., Rinsland, C. P., Rotger, M., Šimečková, M., Smith, M. A. H., Sung, K., Tashkun, S. A., Tennyson, J., Toth, R. A., Vandaele, A. C. and Vander Auwera, J.: The HITRAN 2008 molecular spectroscopic database, J. Quant. Spectrosc. Radiat. Transf., 110(9–10), 533–572, doi:10.1016/j.jqsrt.2009.02.013, 2009.
Rozanov, V. V., Rozanov, A. V., Kokhanovsky, A. A. and Burrows, J. P.: Radiative transfer through terrestrial atmosphere and ocean: Software package SCIATRAN, J. Quant. Spectrosc. Radiat. Transf., 133, 13–71, doi:10.1016/j.jqsrt.2013.07.004, 2014.
Schepers, D., Guerlet, S., Butz, A., Landgraf, J., Frankenberg, C., Hasekamp, O., Blavier, J. F., Deutscher, N. M., Griffith, D. W. T., Hase, F., Kyro, E., Morino, I., Sherlock, V., Sussmann, R. and Aben, I.: Methane retrievals from Greenhouse Gases Observing Satellite (GOSAT) shortwave infrared measurements: Performance comparison of proxy and physics retrieval algorithms, J. Geophys. Res. Atmos., 117(10), doi:10.1029/2012JD017549, 2012.
Schuur, E. A. G., McGuire, A. D., Schädel, C., Grosse, G., Harden, J. W., Hayes, D. J., Hugelius, G., Koven, C. D., Kuhry, P., Lawrence, D. M., Natali, S. M., Olefeldt, D., Romanovsky, V. E., Schaefer, K., Turetsky, M. R., Treat, C. C. and Vonk, J. E.: Climate change and the permafrost carbon feedback, Nature, 520(7546), 171–179, doi:10.1038/nature14338, 2015.
Schweizer, M., Fear, J. and Cadisch, G.: Isotopic (13C) fractionation during plant residue decomposition and its implications for soil organic matter studies, Rapid Commun. Mass Spectrom., 13(13), 1284–1290, doi:10.1002/(SICI)1097-0231(19990715)13:13<1284::AID-RCM578>3.0.CO;2-0, 1999.
Schwietzke, S., Sherwood, O. A., Bruhwiler, L. M. P., Miller, J. B., Etiope, G., Dlugokencky, E. J., Michel, S. E., Arling, V. A., Vaughn, B. H., White, J. W. C. and Tans, P. P.: Upward revision of global fossil fuel methane emissions based on isotope database, Nature, 538(7623), 88–91, doi:10.1038/nature19797, 2016.
Sinnhuber, B. M., Sheode, N., Sinnhuber, M., Chipperfield, M. P. and Feng, W.: The contribution of anthropogenic bromine emissions to past stratospheric ozone trends: A

modelling study, Atmos. Chem. Phys., 9(8), 2863–2871, doi:10.5194/acp-9-2863-2009, 2009.
Starikova, E., Nikitin, A. V., Rey, M., Tashkun, S. A., Mondelain, D., Kassi, S., Campargue, A. and Tyuterev, V. G.: Assignment and modeling of the absorption spectrum of13CH4at 80 K in the region of the 2ν3band (5853-6201 cm-1), J. Quant. Spectrosc. Radiat. Transf., 177, 170–180, doi:10.1016/j.jqsrt.2015.12.023, 2016.
Swinehart, D. F.: The Beer-Lambert Law, J. Chem. Educ., 39(7), 333, doi:10.1021/ed039p333, 1962.
Tennyson, J.: Astronomical spectroscopy : an introduction to the atomic and molecular physics of astronomical spectra, Imperial College Press. [online] Available from: https://books.google.co.uk/books/about/Astronomical_Spectroscopy.html?id=A4BBfuJPqOAC&redir_esc=y (Accessed 13 June 2017), 2005.
Turner, A. J., Jacob, D. J., Wecht, K. J., Maasakkers, J. D., Lundgren, E., Andrews, A. E., Biraud, S. C., Boesch, H., Bowman, K. W., Deutscher, N. M., Dubey, M. K., Griffith, D. W. T., Hase, F., Kuze, A., Notholt, J., Ohyama, H., Parker, R., Payne, V. H., Sussmann, R., Sweeney, C., Velazco, V. A., Warneke, T., Wennberg, P. O. and Wunch, D.: Estimating global and North American methane emissions with high spatial resolution using GOSAT satellite data, Atmos. Chem. Phys., 15(12), 7049–7069, doi:10.5194/acp-15-7049-2015, 2015.
Turner, A. J., Frankenberg, C., Wennberg, P. O. and Jacob, D. J.: Ambiguity in the causes for decadal trends in atmospheric methane and hydroxyl., Proc. Natl. Acad. Sci. U. S. A., 114(21), 5367–5372, doi:10.1073/pnas.1616020114, 2017.
Weidmann, D., Hoffmann, A., Macleod, N., Middleton, K., Kurtz, J., Barraclough, S. and Griffin, D.: The Methane Isotopologues by Solar Occultation (MISO) Nanosatellite Mission: Spectral Channel Optimization and Early Performance Analysis, Remote Sens., 9(10), 1073, doi:10.3390/rs9101073, 2017.
Whiticar, M. J.: Carbon and hydrogen isotope systematics of bacterial formation and oxidation of methane, Chem. Geol., 161(1–3), 291–314, doi:10.1016/S0009-2541(99)00092-3, 1999.
Worden, J. R., Turner, A. J., Bloom, A., Kulawik, S. S., Liu, J., Lee, M., Weidner, R., Bowman, K., Frankenberg, C., Parker, R. and Payne, V. H.: Quantifying lower tropospheric methane concentrations using GOSAT near-IR and TES thermal IR measurements, Atmos. Meas. Tech, 8, 3433–3445, doi:10.5194/amt-8-3433-2015, 2015.
Wuebbles, D. and Hayhoe, K.: Atmospheric methane and global change, Earth-Science Rev., 57(3–4), 177–210, doi:10.1016/S0012-8252(01)00062-9, 2002.
Wunch, D., Toon, G. C., Blavier, J.-F. L., Washenfelder, R. A., Notholt, J., Connor, B. J., Griffith, D. W. T., Sherlock, V. and Wennberg, P. O.: The Total Carbon Column Observing Network, Phil. Trans. R. Soc. A, 369, 2087–2112, doi:10.1098/rsta.2010.0240, 2011.
Yokota, T., Yoshida, Y., Eguchi, N., Ota, Y., Tanaka, T., Watanabe, H. and Maksyutov, S.: Global Concentrations of CO2 and CH4 Retrieved from GOSAT: First Preliminary Results, SOLA, 5, 160–163, doi:10.2151/sola.2009-041, 2009.
Yoshida, Y., Ota, Y., Eguchi, N., Kikuchi, N., Nobuta, K., Tran, H., Morino, I. and Yokota, T.: Retrieval algorithm for CO 2 and CH 4 column abundances from short-wavelength infrared spectral observations by the Greenhouse gases observing satellite, Atmos. Meas. Tech, 4, 717–734, doi:10.5194/amt-4-717-2011, 2011.
Yoshida, Y., Kikuchi, N., Morino, I., Uchino, O., Oshchepkov, S., Bril, A., Saeki, T., Schutgens, N., Toon, G. C., Wunch, D., Roehl, C. M., Wennberg, P. O., Griffith, D. W. T., Deutscher, N. M., Warneke, T., Notholt, J., Robinson, J., Sherlock, V., Connor, B., Rettinger, M., Sussmann, R., Ahonen, P., Heikkinen, P., Kyrö, E., Mendonca, J., Strong, K., Hase, F., Dohe, S. and Yokota, T.: Improvement of the retrieval algorithm for GOSAT SWIR XCO2 and XCH4 and their

validation using TCCON data, Atmos. Meas. Tech., 6(6), 1533–1547, doi:10.5194/amt-6-1533-2013, 2013.
Zou, M., Xiong, X., Saitoh, N., Warner, J., Zhang, Y., Chen, L., Weng, F. and Fan, M.: Satellite observation of atmospheric methane: intercomparison between AIRS and GOSAT TANSO-FTS retrievals, Atmos. Meas. Tech, 9, 3567–3576, doi:10.5194/amt-9-3567-2016, 2016.

Tables

Table 1. The conditions used by ORFM in generating SWIR Absorption from an assumed GOSAT-TANSO-FTS like instrument. All conditions are taken from MIPAS Model atmospheres (Remedios et al., 2007)**.**

Condition Variables	Value
Wavelength Range	1600-1700 nm 7600 – 8300 nm
Background Gases	H_2O, CO_2 and N_2O at standard model concentrations
Instrument Altitude	666km
Solar Zenith Angle	30°
Atmospheric Model	University of Leicester MIPAS Model
Spectral Line Database	HITRAN 2016
Spectral Resolution	0.01cm^{-1}
Viewing Profile	Nadir

Table 2. SCIATRAN Simulation conditions for detection study.

Sensor	Surface/Atmosphere	Notes
Solar Zenith: 30° Altitude: 666 km	<u>Background Conditions</u>	
	Reflectance: 0.1, 0.3 - 0.6	
	H_2O: As SCIATRAN CTM (November, Latitude 45°)	
	CH_4: As SCIATRAN CTM (November, Latitude 45°)	
	Aerosols: As LOWTRAN SCIATRAN standard settings	Maritime/tropospheric in the boundary layer. Background in the stratosphere.
	<u>Elevated Conditions</u>	
	Reflectance: 0.1, 0.3, 0.6	Vegetation to Desert.
	H_2O: As background x2	Not necessarily realistic, but indicates sensitivity to water vapour.
	CH_4 Scale Factor: 1.02, 1.04, 1.06, 1.08, 1.10	XCH_4 values, minimum 1.78 ppm, maximum 1.94 ppm.

Table 3. Spectral average F_d (Equation 5) values summarised for the standard conditions expressed Table 2. The F_d values are shown for each CH_4 scale given the range of reflectances indicated in Table 1.

CH_4 Total Column Scale Factor	F_d Albedo = 0.1 ($x10^{-10}$)	F_d Albedo = 0.3 ($x10^{-10}$)	F_d Albedo = 0.4 ($x10^{-10}$)	F_d Albedo = 0.5 ($x10^{-10}$)	F_d Albedo = 0.6 ($x10^{-10}$)
1658.6 – 1658.65 nm					
x1.02	-1.41	-1.19	-1.08	-0.975	-0.864
x1.04	-1.30	-0.87	-0.652	-0.432	-0.211
x1.06	-1.19	-0.546	-0.219	0.110	0.444

x1.08	-1.08	-0.223	0.213	0.652	1.10
x1.10	-0.974	0.0999	0.644	1.19	1.75
1670.35 – 1670.55 nm					
x1.02	-1.42	-1.23	-1.13	-1.03	-0.931
x1.04	-1.32	-0.938	-0.742	-0.545	-0.346
x1.06	-1.23	-0.648	-0.355	-0.0582	0.241
x1.08	-1.13	-0.358	0.0327	0.428	0.827
x1.10	-1.03	-0.0688	0.420	0.913	1.41

Table 4. Spectral average F_d (Equation 5) values summarised for the standard conditions expressed Table 2, assuming a global standard $\delta^{13}C$ value of -70. The F_d values are shown for each CH_4 scale given the range of reflectances indicated in Table 2.

CH_4 Total Column Scale Factor	F_d Albedo = 0.1 ($x10^{-10}$)	F_d Albedo = 0.3 ($x10^{-10}$)	F_d Albedo = 0.4 ($x10^{-10}$)	F_d Albedo = 0.5 ($x10^{-10}$)	F_d Albedo = 0.6 ($x10^{-10}$)
1658.6 – 1658.65 nm					
x1.02	-1.51	-1.49	-1.47	-1.46	-1.45
x1.04	-1.50	-1.45	-1.43	-1.41	-1.39
x1.06	-1.48	-1.42	-1.39	-1.35	-1.32
x1.08	-1.47	-1.39	-1/34	-1.30	-1.25
x1.10	-1.46	-1.36	-1.30	-1.25	-1.19
1670.35 – 1670.55 nm					
x1.02	-1.42	-1.22	-1.12	-1.03	-0.924
x1.04	-1.32	-0.93	-0.733	-0.535	-0.330
x1.06	-1.22	-0.636	-0.341	-0.043	0.263
x1.08	-1.12	-0.343	0.0512	0.448	0.857
x1.10	-1.02	-0.0494	0.443	0.939	1.450

Table 5. Sensitivity factor for the 1658 nm and 1670 nm wavebands, assuming the low and high water vapour conditions, and a surface albedo of 0.3 specified in Table 2.

Waveband/Methane scale	Scale = 2%	Scale = 4%	Scale = 6%	Scale = 8%	Scale = 10%
1658.6 nm S_f	1.00121	1.00126	1.00127	1.00125	1.00125
1670.35 nm S_f	1.0113	1.00113	1.0113	1.0112	1.0112

1

2 **Table 6. Glossary of key terms and acronyms used in this paper.**

Term	Details
ADAM	A surface reflectance Database for ESA's earth observation Missions; Database of surface reflectance.
CTM	Chemistry Transport Model; Mathematical model simulating the transport of trace gases in the atmosphere.
$\delta^{13}C$	Ratio of $^{13}CH_4$ to $^{12}CH_4$ compared to the Vienna Pee Dee Belemnite standard.
ESA	European Space Agency
FTS	Fourier Transform Spectrometer; Sensor on GOSAT designed to measure trace gases.
GHG	Greenhouse Gas(es)
GOSAT	Greenhouse Gases Observing Satellite; Satellite launched in 2009.
HITRAN	High Resolution Transmission; Database of spectroscopic parameters.
L1B	Level 1B data; first stage processed data from the instrument, representing the spectral response.
IC	Information Content; Mathematical technique to assess quality of trace gas retrievals.
Isotopologue	Molecule with at least one atom containing non-periodic table number of neutrons.
JAXA	Japanese Aerospace Exploration Agency.
KIE	Kinetic Isotope Effects; Determines the rate of reactions based on isotopic make up of molecule.
MIPAS	Michelson Interferometer for Passive Atmospheric Sounding; Instrument on ENVISAT.
NEDL	Noise Equivalent Radiance; Instrument noise represented as radiance values.
NIES	National Institute for Environmental Studies.
ORFM	Oxford Reference Forward Model; Radiative transfer model developed at the University of Oxford.
RTM	Radiative Transfer Model; Model designed to simulate radiation transfer through a medium.

SCIAMACHY	SCanning Imaging Absorption SpectroMeter for Atmospheric CHartographY; Instrument on ENVISAT,
SCIATRAN	Name of radiative transfer model developed at the University of Bremen.
SNR	Signal to Noise Ratio.
SWIR	Shortwave Infrared; Portion of the electromagnetic spectrum ~1-3 µm.
TANSO	Thermal and near Infrared Sensor for Carbon Observations; Instrument onboard GOSAT.
TCCON	Total Column Carbon Observing Network; Series of upwards viewing FTSs located around the world.
TIR	Thermal Infrared; Portion of the electromagnetic spectrum ~>5 µm to microwave.
TROPOMI	Tropospheric Monitoring Instrument; Instrument based on Sentinel-5P.

Figures

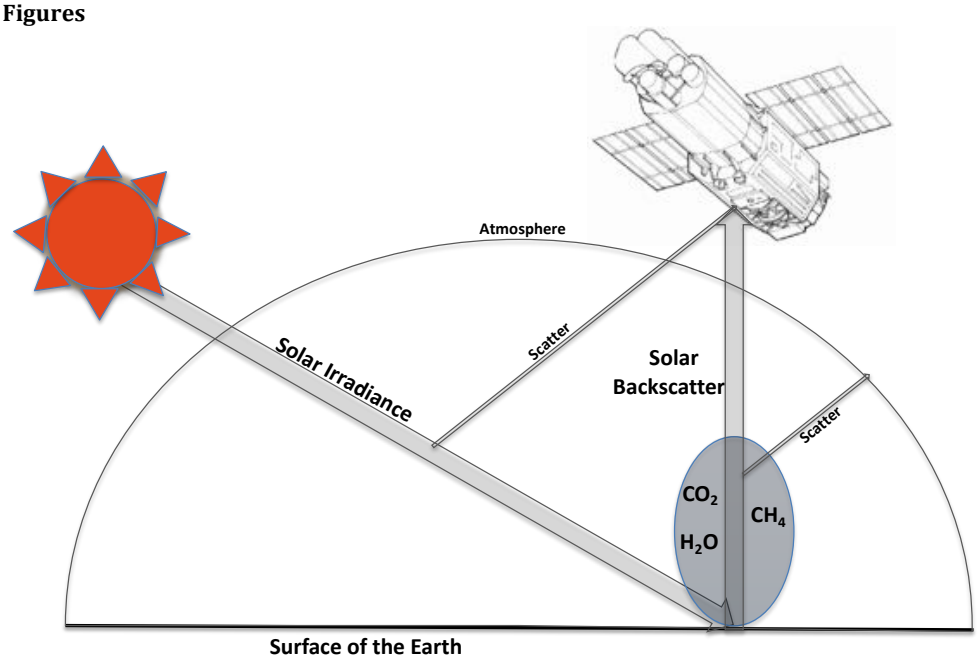

Figure 1. Schematic representation of GOSAT measuring solar backscatter light.

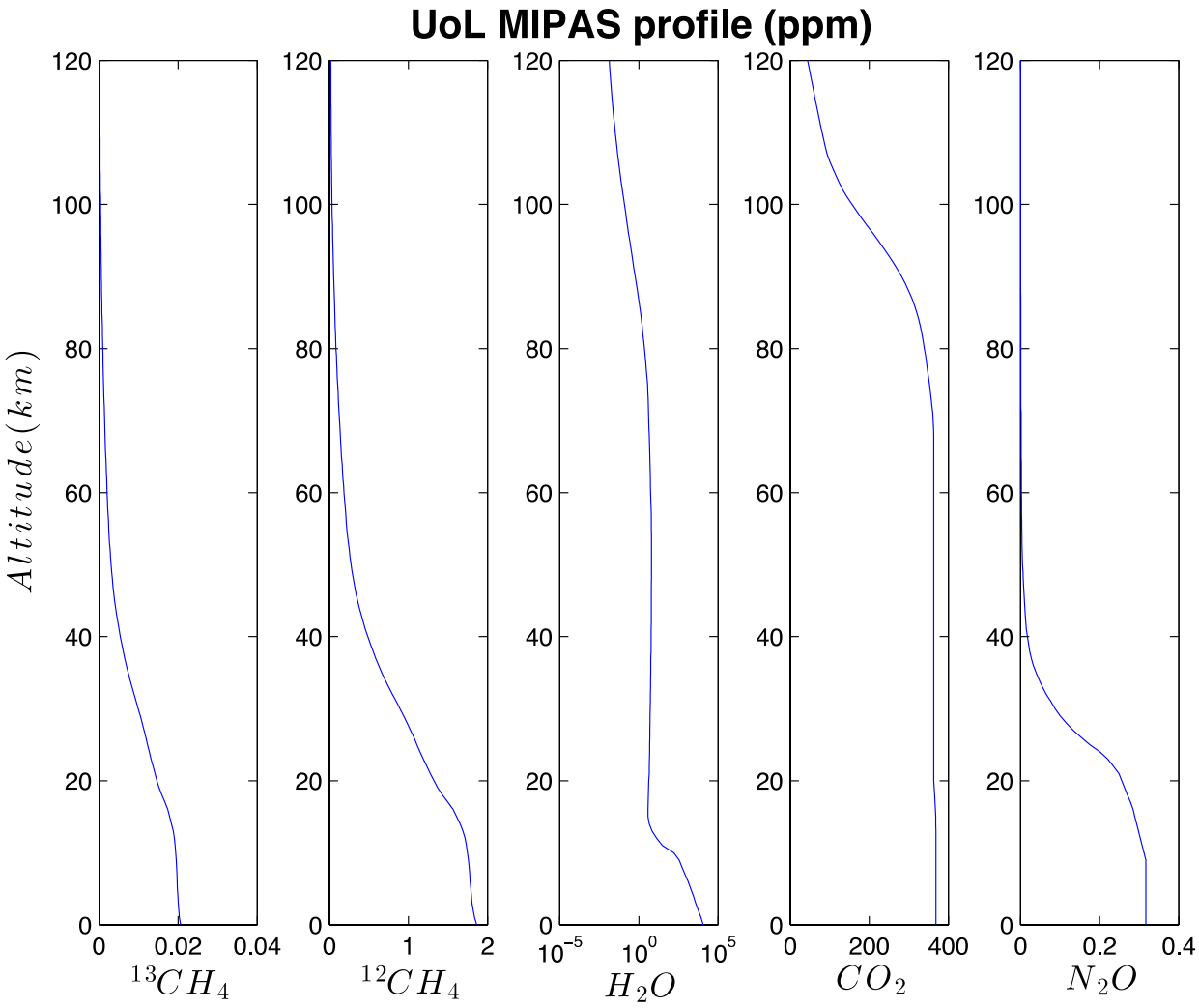

Figure 2. Volume Mixing Ratio profiles of the main gases of interest CH_4, H_2O and CO_2 in ppm from 0-120km altitude, (Remedios et al., 2007)**, adapted from** (Malina et al., 2018)**.**

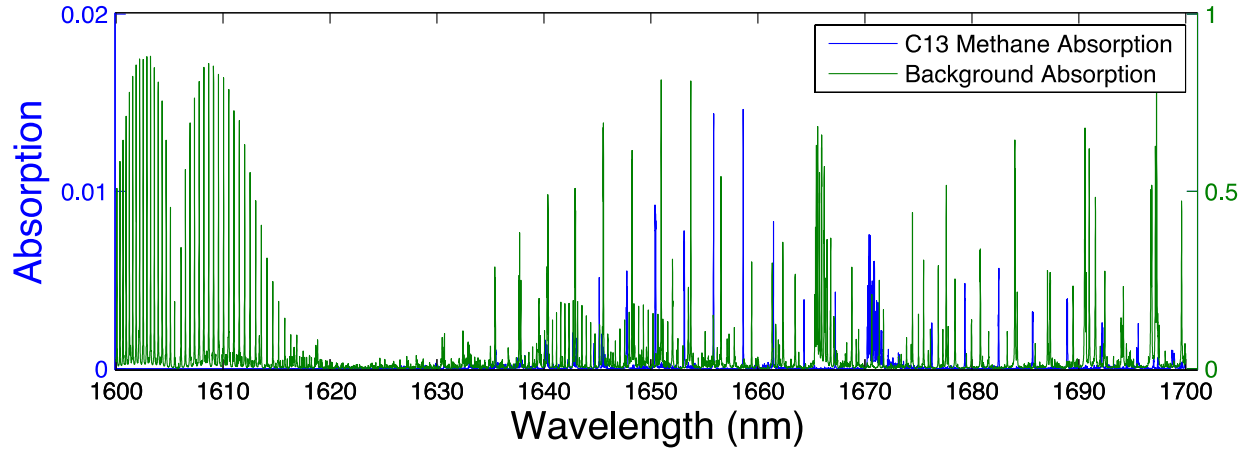

Figure 3. Simulated absorption spectrum from ORFM in the wavelength range 1600-1700nm, the y scale represents the fraction of radiation absorbed by the molecules under investigation. The blue line represents absorption by $^{13}CH_4$ (left hand scale) and green represents all other key absorbing background gases (CO_2, H_2O and $^{12}CH_4$) (right hand scale).

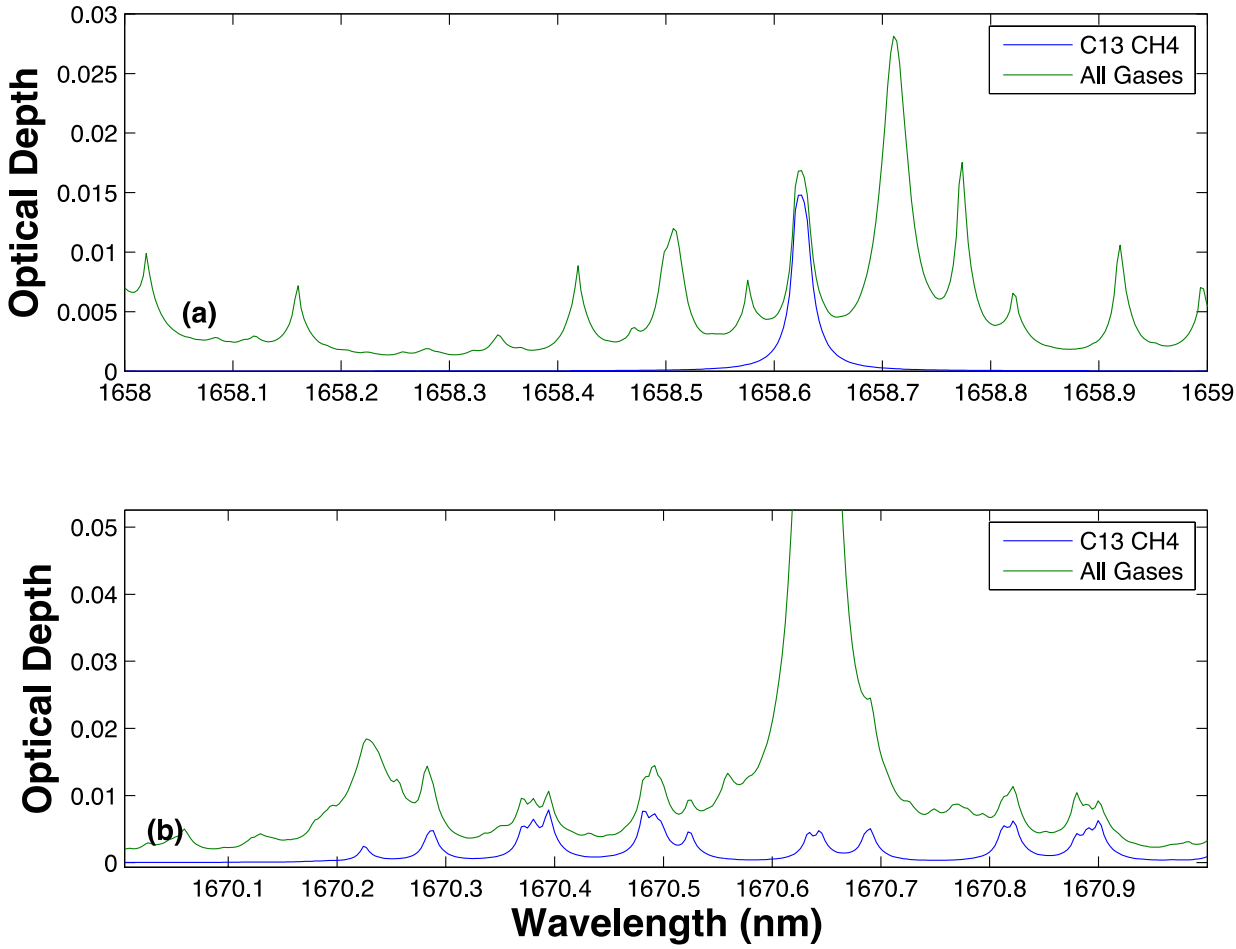

Figure 4. Optical depth covering $^{13}CH_4$ absorption points of interest, the green line represents optical depth of all gases present in this portion of the spectrum (CH_4, CO_2 and H_2O), whilst the blue line shows optical depth of purely the methane isotopologue $^{13}CH_4$: (a) indicates optical depth in the wavelength range 1658-1659nm; (b) shows optical depth in the wavelength range 1670-1671nm. This figure is as figure 5 in (Malina et al., 2018)**, but has been updated to reflect the use of HITRAN2016.**

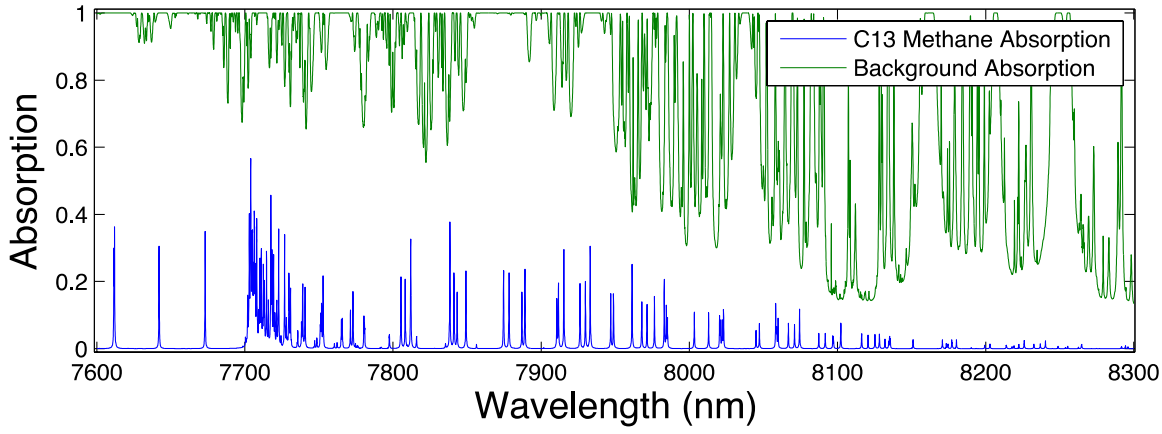

Figure 5. Simulated absorption spectrum from ORFM in the wavelength range 7600-8300 nm, the y scale represents the fraction of radiation absorbed by the molecules under investigation. The blue line represents absorption by $^{13}CH_4$ and green represents all other key absorbing background gases (CO_2, H_2O, N_2O and $^{12}CH_4$).

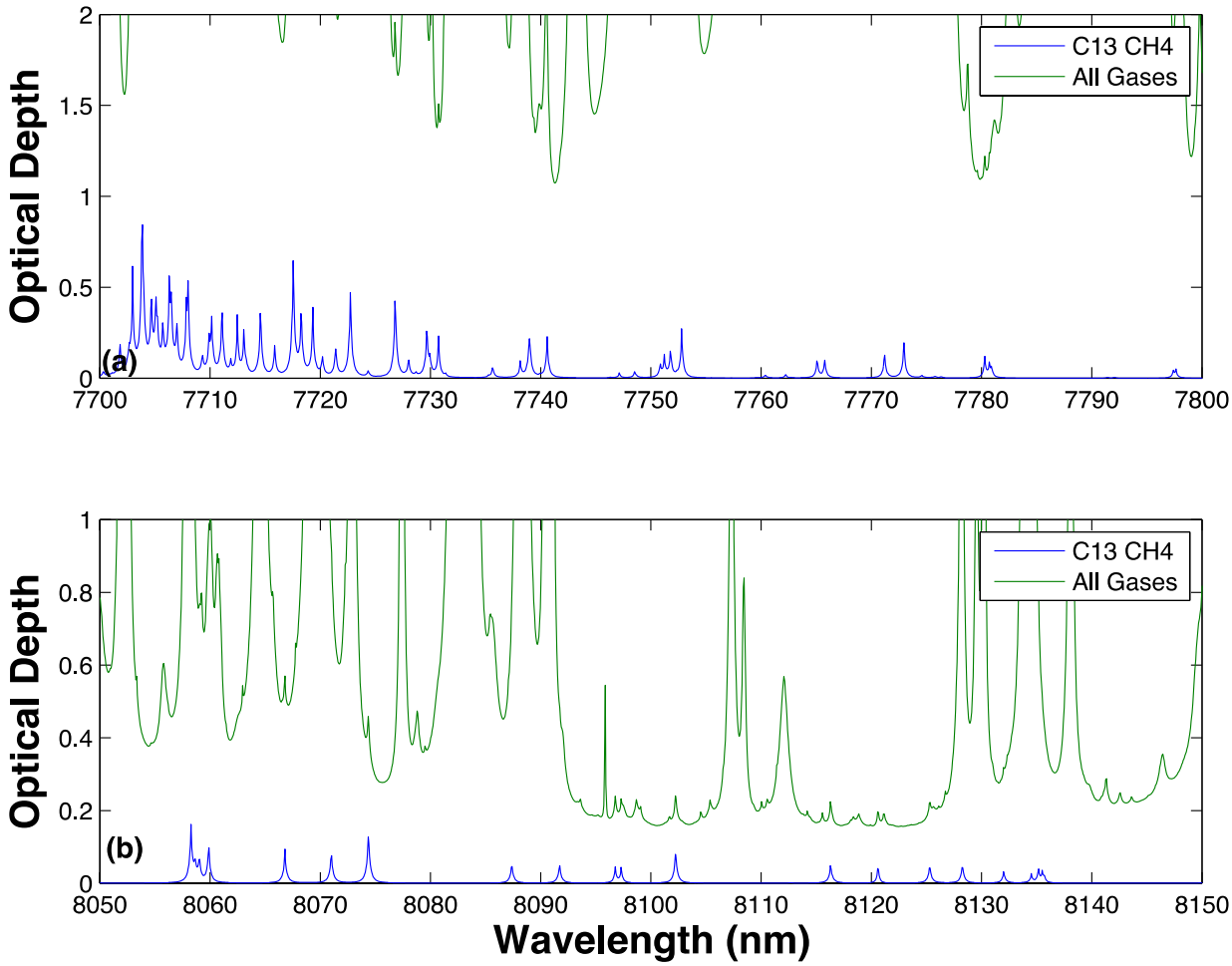

Figure 6. As figure 4, but focused on the wavelength ranges 7700-7800 nm and 8050-8150 nm.

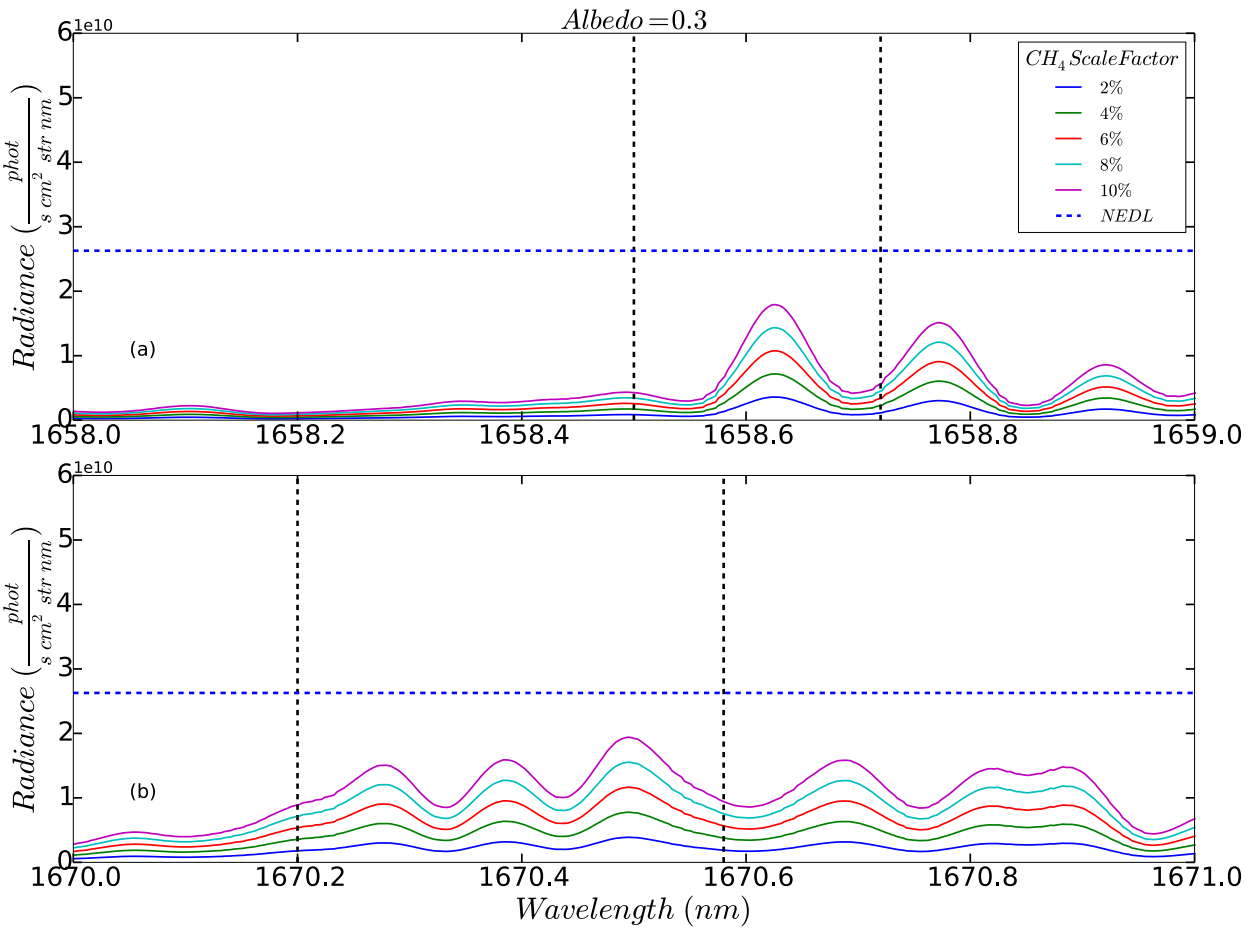

Figure 7. Residual Radiance plots based on the simulation conditions highlighted in Table 3, where simulated radiance from the background conditions under the standard 'day' scene with a reflectance of 0.3 are subtracted from elevated methane conditions. The residual radiance values are represented by the lines indicated in the legend. The Blue dashed line represents the NEDL. The solid vertical dashed lines identify the regions where $^{13}CH_4$ spectral lines are prevalent: (a) highlights the $^{13}CH_4$ spectral line in the 1658-1659 nm range; (b) focuses on the $^{13}CH_4$ spectral line in the 1670-1671 nm range.

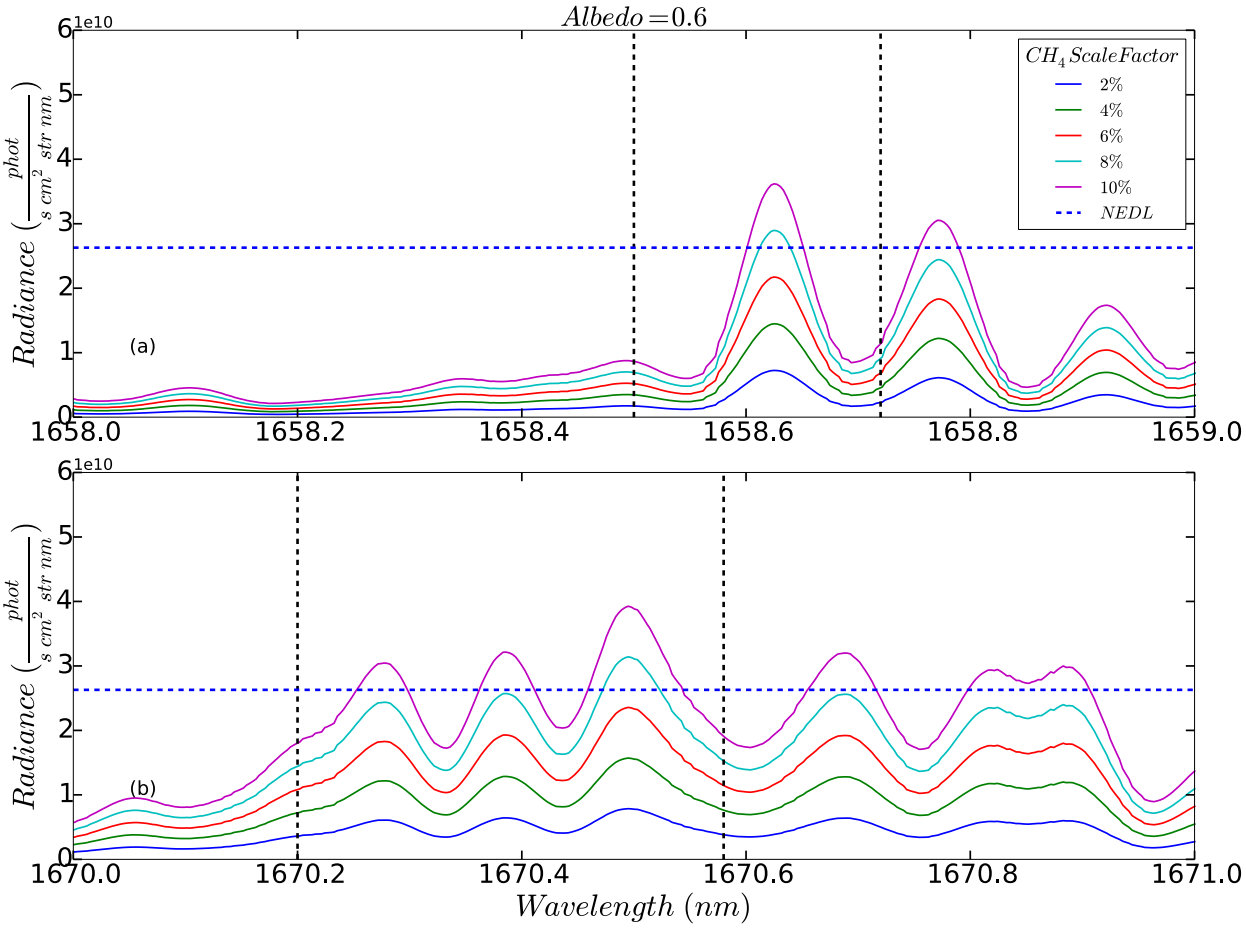

Figure 8. As Figure 7, with surface albedo increased to 0.6.

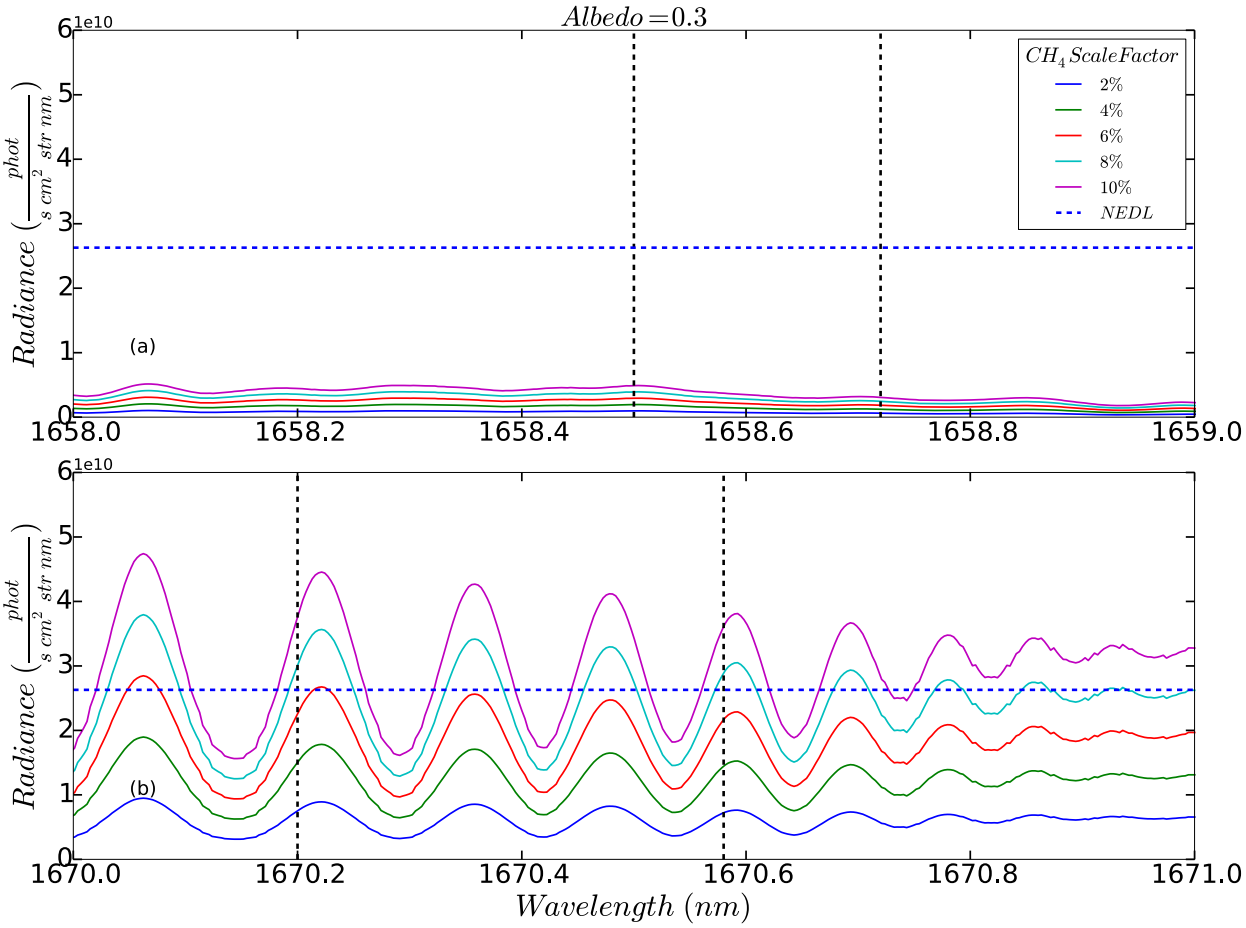

Figure 9. As Figure 7 and Figure 8, with surface albedo increased to 0.3, assuming the standard $\delta^{13}C$ value is -70‰ as opposed to 0‰.

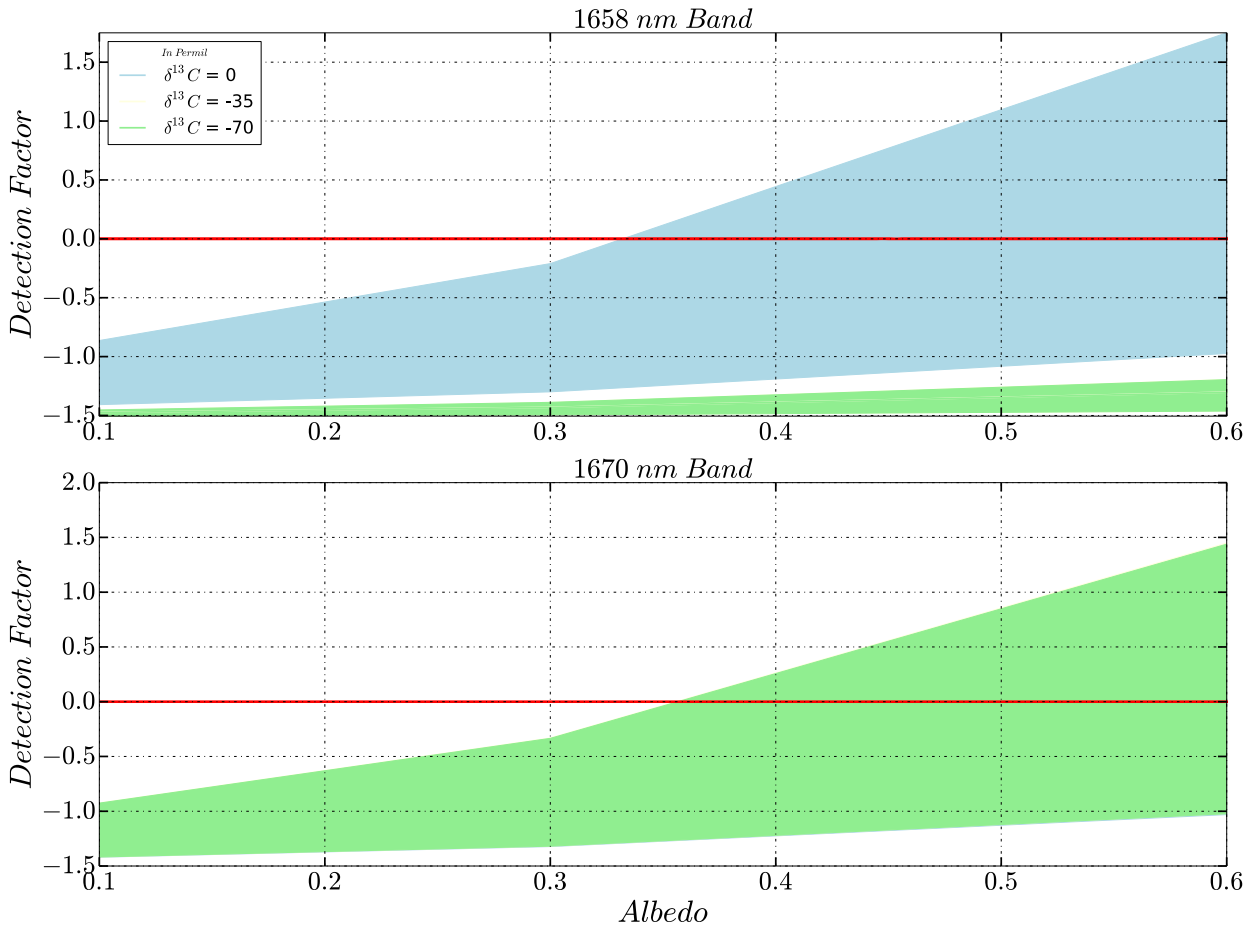

Figure 10. Plot indicating the surface conditions required to generate detection factors > 0, thus suggesting a positive detection of $\delta^{13}C$. The top panel shows results for the 1658 nm band, and the bottom panel shows results for the 1670 nm band. The light blue area indicates results assuming a $\delta^{13}C$ natural value of 0‰, light yellow -35‰ and light green -70‰, the solid red line indicates where the detection factor is zero.

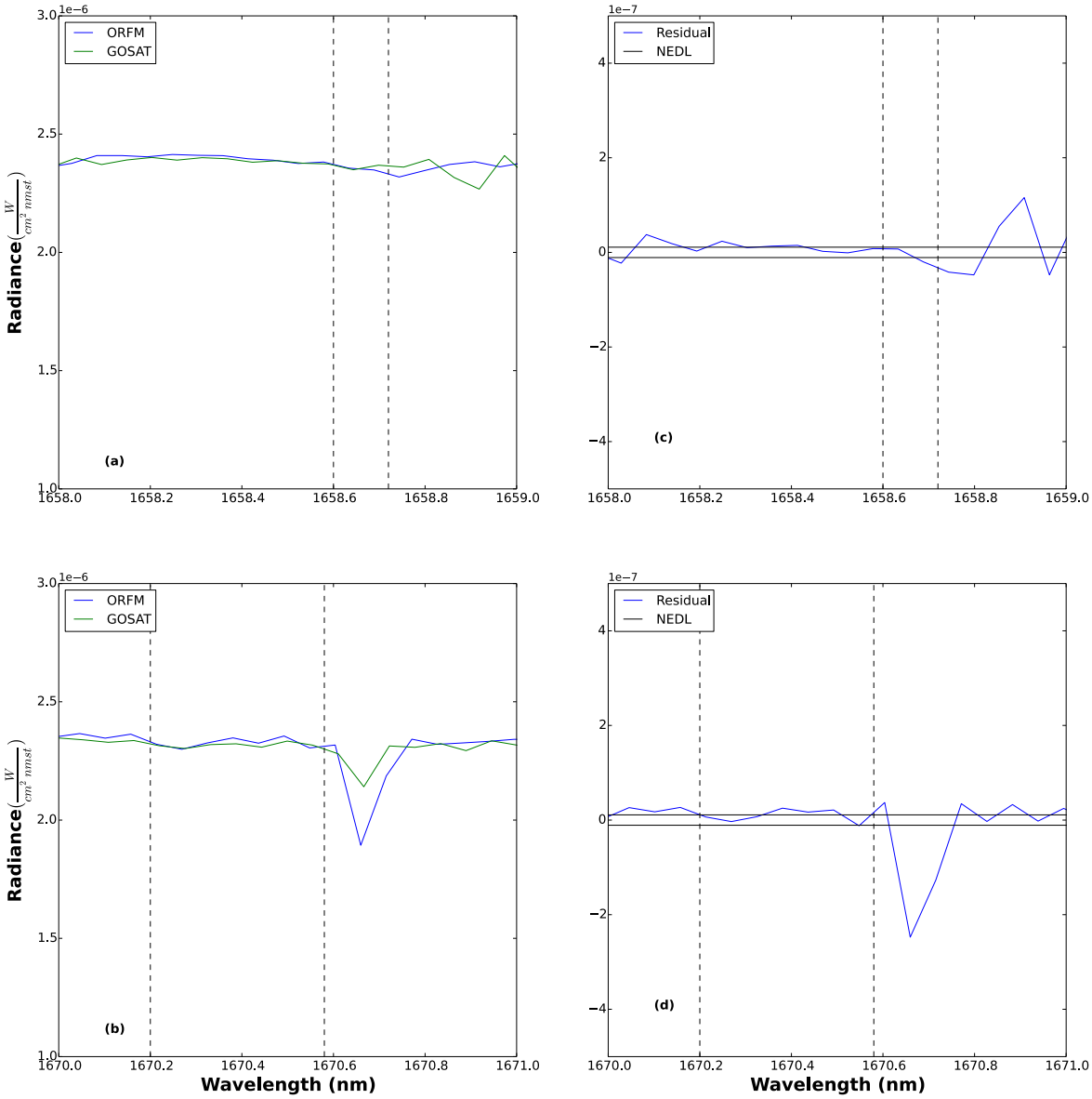

Figure 11. Comparison of simulated spectrum against GOSAT L1B data. In this particular example, the surface reflectance is 0.33, solar zenith angle is 46° and satellite view zenith angle is 24°, the L1B data was captured at a high latitude on 01/06/2016 at 61.7°N, 173°E: (a) highlights the 1658-1659 nm spectral region, where the two dashed lines highlight the exact region of $^{13}CH_4$ activity. The blue lines shows simulated ORFM data and the green line shows GOSAT L1B data; (b) highlights the 1670-1671 nm spectral region, where the two dashed lines highlight the exact region of $^{13}CH_4$ activity. The blue lines show simulated data and the green line shows GOSAT L1B data; (c) shows the residual radiance between the simulated spectrum and the L1B data in the 1658-1659 nm range, the horizontal solid lines represent the FTS NEDL and the two dashed lines highlight the exact region of $^{13}CH_4$ activity; (d) shows the residual radiance between the ORFM spectra and the L1B data in the 1670-1671 nm range, the horizontal solid lines represent the FTS NEDL and the two dashed lines highlight the exact region of $^{13}CH_4$ activity.

1